

# *Mechanisms of interannual variability of deep convection in the Greenland Sea*

Article

Accepted Version

Creative Commons: Attribution-Noncommercial-No Derivative Works 4.0

Bashmachnikov, I. L., Fedorov, A. M., Golubkin, P. A., Vesman, A. V., Selyuzhenok, V. V., Gnatiuk, N. V., Gnatiuk, L. P., Hodges, K. I. ORCID: <https://orcid.org/0000-0003-0894-229X> and Dukhovskoy, D. S. (2021) Mechanisms of interannual variability of deep convection in the Greenland Sea. *Deep Sea Research Part I: Oceanographic Research Papers*, 174. 103557. ISSN 0967-0637 doi: <https://doi.org/10.1016/j.dsr.2021.103557> Available at <https://centaur.reading.ac.uk/97608/>

It is advisable to refer to the publisher's version if you intend to cite from the work. See [Guidance on citing](#).

To link to this article DOI: <http://dx.doi.org/10.1016/j.dsr.2021.103557>

Publisher: Elsevier

All outputs in CentAUR are protected by Intellectual Property Rights law, including copyright law. Copyright and IPR is retained by the creators or other copyright holders. Terms and conditions for use of this material are defined in the [End User Agreement](#).

[www.reading.ac.uk/centaur](http://www.reading.ac.uk/centaur)

**CentAUR**

Central Archive at the University of Reading

Reading's research outputs online

# Mechanisms of Interannual Variability of Deep Convection in the Greenland Sea

Igor L. Bashmachnikov<sup>1,2</sup>, Aleksandr M. Fedorov<sup>1,2,3</sup>, Pavel A. Golubkin<sup>2</sup>, Anna V. Vesman<sup>1,2,3</sup>, Valeria V. Selyuzhenok<sup>1,2</sup>, Natalia V. Gnatiuk<sup>2</sup>, Leonid P. Bobylev<sup>2</sup>, Kevin I. Hodges<sup>4</sup>, Dmitry S. Dukhovskoy<sup>5</sup>

<sup>1</sup>St. Petersburg State University, SPbSU, 7/9 Universitetskaya nab., St. Petersburg, 199034, Russia

<sup>2</sup>Nansen International Environmental and Remote Sensing Centre, 14 Line V.O., 7, St.Petersburg, 199034, Russia

<sup>3</sup>Arctic and Antarctic Research Institute, Bering str., 38, St.Petersburg, 199397, Russia

<sup>4</sup>Department of Meteorology, University of Reading, Reading, United Kingdom

<sup>5</sup>Florida State University, Tallahassee, Florida, USA.

**Corresponding author:** i.bashmachnikov@spbu.ru

## Highlights

- The upper ocean salinity governs the interannual change of the convection intensity
- Interannual change of the upper ocean advection is of the primarily importance
- Interannual change of the sea ice melt is of the secondary importance
- The ocean-atmosphere heat release is only of the tertiary importance

## Keywords

deep convection, the Greenland Sea, oceanic freshwater advection, winter ice conditions

## Acknowledgments

The research was funded by the Saint Petersburg State University (project N 75295423). D.S. Dukhovskoy was funded by the DOE (award DE-SC0014378).

## Abstract

This study investigates the physical processes and mechanisms driving the interannual variability of deep convective intensity in the Greenland Sea from 1993 to 2016. The intensity of deep convection is derived using the traditional Maximum Mixed Layer Depth, the total surface area with the monthly-mean mixed layer depth exceeding 800 m and various indices. All metrics show that the intensity of convection increased during the 2000s.

The analysis demonstrates that observed increases of the deep convective intensity in the Greenland Sea is associated with an increase in the upper ocean salinity. The long-term interannual variability of deep convection is mainly linked to the variation of the water salinity during the preceding summer and the current winter. In turn, the variability of the upper-ocean salinity is primarily related to the variability in the advection of Atlantic water into the region with the re-circulating branches of the West Spitsbergen Current and to a lesser degree, to the local sea ice melt. For only two winters during the study period did the sea ice contribute significantly to a weakening of the intensity of deep convection by substantially reducing oceanic heat loss to the atmosphere. The variability in the advected heat is effectively abated by the concurrent variations of oceanic heat release to the atmosphere. The interplay between the interannual variability of the oceanic heat advection and the winter air-sea net heat flux leads to a noticeable reduction of the interannual variability of both fluxes over the convective regions. As a result, the direct effect of the varying air-sea heat exchange did not have a

48 pronounced direct effect on the interannual variation in the intensity of deep convection in the  
49 Greenland Sea, at least during the study period.

50

## 51 **1. Introduction**

52

53 In this paper, we investigate the mechanisms driving the interannual variability of the intensity  
54 of Deep Convection (DC) in the Greenland Sea. The process of deep convection is affected by  
55 a number of linked and interacting processes. However, the leading mechanisms governing the  
56 interannual variability of deep convection in the region remain a subject of discussion. We show  
57 that the oceanic heat release to the atmosphere is of secondary importance for the long-term  
58 interannual variability of the DC. This is due to the relatively small interannual variability of  
59 the heat flux compared to other factors. The intensity of DC during the study period (1993-  
60 2016) was found to be primarily controlled by the long-term variations in the volume transport  
61 and the thermohaline characteristics of the Re-circulating Atlantic Water (RAW) reaching the  
62 central Greenland Sea. This acts together with a possible positive feedback mechanism between  
63 the Atlantic Meridional Overturning Circulation (AMOC) and the deep convection that may  
64 govern the system on interdecadal or longer time scales (Stommel et al., 1958; Levermann and  
65 Born, 2007).

66

### 67 **1.1 Deep convection in the Greenland Sea and its variability**

68

69 The AMOC is an essential component of the global conveyor belt (Lappo, 1984; Broecker,  
70 1987, 1991), as well as of the global climate system. The AMOC links the circulation in the  
71 Atlantic and the Southern oceans in a unified system of two semi-closed interacting multilevel  
72 circulation cells (Lumpkin and Speer, 2007; Garzoli and Matano, 2011; Johnson et al., 2019).  
73 The observed faster change of the surface air temperature in polar regions (Gulev et al., 2008;  
74 Johannessen et al., 2016) is argued to be associated with the AMOC intensity (Lockwood, 2001;  
75 Drijfhout, 2015). The atmospheric conditions, as well as the direct oceanic advection to the  
76 subpolar and polar regions affects the DC (Buckley and Marshall, 2016; Gladyshev et al., 2016;  
77 Lozier et al., 2019). In turn, among other factors, the variability of the DC in the North Atlantic,  
78 linking its upper and deep branches of its upper circulation cell and assuring its continuity, is  
79 considered to be one of the mechanisms forcing the AMOC variability (Buckley and Marshall,  
80 2016; Johnson et al., 2019; Volkov et al., 2020).

81 We define DC as the vertical mixing of water driven by gravitational instability that results in  
82 a renewal of intermediate and/or deep water masses participating in the formation of the deep  
83 branch of the AMOC. In the Greenland Sea, such water masses are the Greenland Sea  
84 Intermediate Water (the typical depth range is 500-1000 m) with a temperature of  $-0.44 \sim -0.8$   
85  $^{\circ}\text{C}$  and a salinity around 34.90 and the Greenland Sea Deep Water (below 1000 m) with a  
86 temperature of  $-0.8 \sim -1.2$   $^{\circ}\text{C}$  and a salinity  $\sim 34.90$  (Nagurny and Popov 1985; Alekseev et al.,  
87 1989; Moretsky and Popov, 1989; Johannessen et al., 1991, 2005; Korablev, 2001). Both water  
88 masses are formed as a mixture of the Re-circulating Atlantic Water with the Arctic  
89 Intermediate and Deep water, regularly modified during winter convection events (Rudels et  
90 al., 2002; Jeansson et al., 2008; Langehaug and Falck, 2012).

91 The DC in the Greenland Sea has been extensively studied during several comprehensive  
92 international projects since the 1980s (see reviews by Killworth, 1983; GSP Group 1990; Chu  
93 and Gascard, 1991; Marshall and Schott, 1999). A series of field experiments (GSP Group in  
94 1990; Drange et al., 2005; Bashmachnikov et al., 2018) and theoretical models (Chu and

95 Gascard, 1991; Visbeck et al., 1996; Marshall and Schott, 1999; Kovalevsky et al., 2020) have  
96 revealed typical patterns of evolution of the areas of DC.

97 DC “chimneys” represent deeply mixed regions (often reaching 1500- 2000 m depth) which are  
98 relatively small in diameter (typically of 20-50 km), each composed of a number of high-density  
99 negatively buoyant DC plumes (GSP Group, 1990; Johannessen et al., 1991; Kovalevsky 2002;  
100 Yashayaev et al., 2007). The latter structures have typical horizontal scales of order of 100 m  
101 (Marshall and Schott, 1999; Johannessen et al., 2005). The sea-level and the water density  
102 gradients turn the chimneys into mesoscale heton structures, with cyclonic circulation in the  
103 upper ocean and anticyclonic circulation at depth (Marshall and Schott, 1999; Kovalevsky,  
104 2002). The resulting potential vorticity anomalies inhibit fluid exchange across the boundaries  
105 of the structure, adding stability to the chimneys.

106 A stable DC chimney is a result of the balance between the ocean buoyancy release to the  
107 atmosphere and the horizontal turbulent buoyancy exchange through the side-walls of the DC  
108 region. The latter is a result of the dynamic instability developed along the “walls” of the  
109 chimney, which leads to the water exchange with sub-mesoscale eddies (Chu and Gascard,  
110 1991; Jones and Marshall, 1993). The eddy-like structures with radii 7-15 km, which are of the  
111 order of the first baroclinic Rossby deformation radius (Nurser and Bacon, 2014), have  
112 previously been detected at the boundary of a DC region in the Boreas basin of the Greenland  
113 Sea (Johannessen et al., 2005).

114 The dynamical processes regulating the vertical and horizontal buoyancy fluxes in DC regions,  
115 range from sub-mesoscale to mesoscale. Only very high resolutions (less than 1 km) non-  
116 hydrostatic hydrodynamic models are able to reproduce the approximate dynamics of physical  
117 processes during formation and decay of a DC chimney (Jones and Marshall, 1993;  
118 Paluszkiwicz and Romea, 1997; Androsof et al., 2005; Kovalevsky et al., 2020). Even in eddy-  
119 resolving models with the spatial resolution of 2-4 km, the DC dynamics are parameterized  
120 (Dukhovskoy et al., 2019). Depending on the parameterization used in a model the DC intensity  
121 can vary within wide limits (Timmerman et al., 2004). The analysis of in situ observations  
122 remains critical for progress to be made in further understanding and modelling this climatically  
123 important phenomenon.

124

## 125 **1.2 Factors governing interannual variability of DC in the Greenland Sea**

126

127 In spite of the fact that a number of mechanisms controlling DC intensity in the subpolar North  
128 Atlantic have been suggested (Glessmer et al., 2014; Moore et al., 2015; Boning et al., 2016;  
129 Luo et al., 2016; Yang et al., 2016), the principal factors driving the observed interannual  
130 variability of the DC intensity remain unclear. It is generally accepted that the intensity of DC  
131 is a function of the air-sea heat and freshwater fluxes and stratification of the upper water  
132 column at the beginning of the convective event (Visbeck et al., 1996). Factors controlling  
133 interannual and interdecadal variability of DC in the Greenland Sea discussed in previous  
134 studies can be divided into three major groups:

- 135 1) the air-sea buoyancy (heat and/or freshwater) fluxes,
- 136 2) the buoyancy variability due to oceanic heat and/or freshwater advection,
- 137 3) the intensity of the cyclonic circulation in the central Greenland Sea.

138 These factors are reviewed in the following sections.

139 The variability in the upper ocean stratification is mostly governed by changes in the upper  
140 ocean temperature and salinity, as the thermohaline characteristics of the deep layers vary at  
141 significantly smaller amplitudes and over longer time scales. The Upper Greenland Sea water

142 is observed in the upper 200-500 m layer. Its temperature typically varies from 0 to 3 °C and  
143 salinity – from 34.4 to 34.9. Most of the results suggest that in the central part of the Greenland  
144 Sea, the sea-surface salinity declined in the late 1970s and did not recover until the end of the  
145 1990s (Johannessen et al., 1991; Alekseev et al., 2001; Glessmer et al., 2014). There are  
146 indications that this tendency has reversed since the beginning of the 2000s (Yashayaev and  
147 Seidov, 2015; Dukhovskoy et al., 2016; Lauvset et al., 2018). A tendency for warming of the  
148 Greenland Sea at all depths has also been noted (Lauvset et al., 2018; Selyuzhenok et al., 2020).

149

### 150 *1.2.1. Heat and freshwater fluxes through the sea surface*

151

152 Since the work of Nansen (1912), the ocean-atmosphere buoyancy flux has been considered the  
153 principal reason for triggering DC development in the subpolar seas (Marshall and Schott, 1999;  
154 Bailey et al., 2005; Falina and Safronov, 2015; Yang et al., 2016). The typical sea-surface heat  
155 loss in the central Greenland Sea of 120-160 W m<sup>-2</sup> leads to a moderate convective deepening,  
156 while its episodic increase to greater than 200 W m<sup>-2</sup> may lead to a substantial increase in the  
157 deepening rate and a formation of a deep chimney within a week (Moore et al., 2015;  
158 Kovalevsky et al., 2020). In particular, the magnitude of the air-sea fluxes may drastically  
159 increase when atmospheric cyclones are crossing the region (Zolina and Gulev, 2003; Dickson  
160 et al., 2008; Skagseth et al., 2008; Tilinina et al., 2016; Dukhovskoy et al., 2017). Thus,  
161 variations in the cyclonic activity should also be considered as a factor contributing to the  
162 interannual variability of the DC intensity.

163 Sea ice cover affects the intensity of DC by hampering the heat and freshwater exchange with  
164 the atmosphere. It has been seen that, with sea ice extending into the central Greenland Sea, DC  
165 does not occur (Mysak et al., 1990; Moore et al., 2015; Vage et al., 2018). On the other hand,  
166 formation of sea ice might trigger haline convection through brine rejection (Meincke et al.,  
167 1997). The sea ice retreat observed during 1980 through 2015 is believed to have induced the  
168 winter air warming over the Greenland Sea, which resulted in a decrease of the ocean-  
169 atmosphere heat release by 20% and limited DC (Moore et al., 2015; Vage et al., 2018). The  
170 reliability of the these hypotheses remains unproven because observations demonstrating the  
171 link between long-term variability of the ice area and the DC intensity is absent. As over 65%  
172 of the sea-ice of the Greenland Sea is imported from the Arctic (Mironov, 2004), the inter-  
173 annual variability of the ice extent in the Greenland Sea is also linked to ice dynamics in the  
174 Arctic and to the atmospheric circulation over the Fram Strait (Vinje and Finnekasa, 1986;  
175 Gudkovich and Nikolaev, 2001; Koenigk et al., 2007; Giles et al., 2012; Kohl and Serra, 2014).

176 The interannual variability of the net precipitation over the Greenland Sea is not the primary  
177 source of the interannual variability of the freshwater content of the upper Greenland Sea  
178 (Peterson et al., 2006). While the major influence of the sea ice and freshwater advected from  
179 the Arctic Ocean is attributed to the western Greenland Sea (see Supplement 7.4), net  
180 precipitation directly affects its central areas (DC sites). Net precipitation decreased during the  
181 1990s-2000s, linked to changes in the North Atlantic and Arctic Oscillations, when both indices  
182 shifted from being mostly positive to a mostly negative phase (Peterson et al., 2006).

183

### 184 *1.2.2. Horizontal buoyancy fluxes*

185

186 The Upper Greenland Sea water is the mixture of the Polar Water (with temperature below zero  
187 and salinity from 33 to 34) exported from the Arctic Ocean and the Re-circulating Atlantic  
188 Water (with temperature over 3 °C and salinity around 34.9) originating from the West

189 Spitsbergen Current (WSC) in the eastern Fram Strait (Rudels et al., 2002; Jeansson et al.,  
190 2008). The water then joins the East Greenland Current (EGC) and enters the central Greenland  
191 Sea through re-circulation patterns (Fig. 1). Several studies have speculated that freshening  
192 events in the upper Greenland Sea in the 1960s, the early 1980s and the late 1990s were due to  
193 an increased influence of the Polar Water, whereas salinity variations in the 1970s and from the  
194 late 1980s to the early 1990s were due to the stronger RAW influence (Johannessen et al. 1991;  
195 Alekseev et al., 2001; Glessmer et al., 2014). The detected 2-3-year and 6-7-year periodicities  
196 in the upper ocean salinity correspond to the same periodicities in the oceanic meridional heat  
197 fluxes into the region (Dukhovskoy et al., 2004; Proshutinsky et al., 2015; Bashmachnikov et  
198 al., 2016a).

199 The Polar water from the Arctic Ocean forms approximately half of the freshwater storage in  
200 the Nordic Seas (Peterson et al., 2006). The volumes of liquid freshwater and ice transported  
201 through the Fram Strait are of the same order of magnitude (Vinie, 1986; Serreze et al., 2006;  
202 Maslowski et al., 2008; Rabe et al., 2013; Glessmer et al., 2014). Both fluxes have increased in  
203 recent decades (Kwok, 2004; Selyuzhenok et al., 2020). However, most of this freshwater  
204 passes through the Greenland Sea, following its continental margin (Curry et al., 2005; Peterson  
205 et al., 2006; Serreze et al., 2006; Koenigk et al., 2007; Boning et al., 2016). Only a small portion  
206 of the freshwater becomes trapped by the re-circulation along the Jan Mayen ridge (Björk et al.,  
207 2001; Peterson et al., 2006; Dukhovskoy et al., 2019). Winds and eddies may episodically  
208 transport the freshwater and ice in the central areas (Johannessen et al., 1987; Gascard et al.,  
209 2002; Gerdes et al., 2005; Koenigk et al., 2008; Proshutinsky et al., 2015; von Appen et al.,  
210 2018), but it is not known whether these fluxes are of any significance.

211 Over the past 20 years, the freshwater discharge from the Greenland Ice Sheet has increased by  
212 50%. The surplus of freshwater discharge forms about half of the freshwater volume fluxed into  
213 the North Atlantic during the Great salinity anomaly of the 1970s (Box et al., 2004; Bamber et  
214 al., 2012; Swingedouw et al., 2014; Lenaerts et al., 2015; Boning et al., 2016). On the other  
215 hand, model results suggest that Greenland meltwater does not leave the northeast Greenland  
216 shelf therefore having a very small direct influence on the convective areas in the central  
217 Greenland Sea (Dukhovskoy et al., 2019).

218 The relatively warm and salty Atlantic water, re-circulating in the southern Fram Strait, can  
219 strongly influence the buoyancy of the upper Greenland Sea (Johannessen et al., 1991; Alekseev  
220 et al., 2001; Furevik et al., 2002; Yashayaev, 2007; Dickson et al., 2008; Beszczynska- Möller  
221 et al., 2012; Marnela et al., 2013; Glessmer et al., 2014; Deshayes et al., 2014; Yang et al.,  
222 2016; Boning et al., 2016; Luo et al., 2016; Lauvset et al., 2018; Ferreira et al., 2018). Strongly  
223 modified in the Fram Strait by mixing with the Polar Water and with the modified Atlantic  
224 Water returning from the Arctic (Langehaug and Falck, 2012), the long-term variations in RAW  
225 properties conserve the original anomalies of the Atlantic water in the Faroe-Shetland Channel  
226 (Lauvset et al., 2018). According to some estimates, the RAW forms up to 90% of the upper  
227 ocean water in the central Greenland Sea, while only 1-2% is formed by the Arctic Polar water  
228 (Johannessen et al., 1991; Alekseev et al., 2001; Marnela et al., 2013). Although the interannual  
229 variability along the Atlantic Water pathway shows clear differences linked to various  
230 atmospheric forcing mechanisms (Lien et al., 2013; Chafik et al., 2015; Raj et al., 2018; Vesman  
231 et al., 2020), since the 1990s the Atlantic Water inflow shows a clear decadal tendency to  
232 increase along the whole pathway from the Faroe-Shetland Channel to the Fram Strait  
233 (Lumpkin, Speer, 2007; Schauer et al., 2008; Hakkinen, Rhines, 2009; Piechura, Walczowski,  
234 2009; Srokosz et al., 2012; Beszczynska-Möller et al., 2012; Walkzowski, 2014; Yashayaev,  
235 Seidov 2015; Lauvset et al., 2018). Consistently, observations from the recent decades show  
236 that, despite some increase in the freshwater flux from the Arctic, the upper layer salinity has  
237 been increasing in the central Greenland Sea (Dickson et al., 2008; Dukhovskoy et al., 2016,  
238 Lauvset et al., 2018; Selyuzhenok et al., 2020), suggesting lower stratification and favouring a

239 stronger DC. The weaker haline stratification might yet be partly mitigated by an observed  
240 increase of the temperature of the Atlantic Water at the end of the 1990s (Johannessen et al.,  
241 1991; Alekseev et al., 2001; Dickson et al., 2008).

242

### 243 *1.2.3. Intensity of cyclonic circulation*

244

245 The cyclonic circulation in the Greenland Sea (Greenland Gyre) causes Ekman pumping that  
246 brings dense weakly stratified water closer to the surface and results in a doming of isopycnals  
247 in the central Greenland Sea (Rossby et al., 2009). This decreases the depth-integrated heat and  
248 freshwater content above the weakly stratified mid-depth ocean and facilitates development of  
249 DC during winter. Therefore, the intensity of the Greenland Gyre might be another factor  
250 controlling the variability of DC in the Greenland Sea (Clarke and Gascard, 1983; Jonsson,  
251 1991; Meincke et al., 1992; Malmberg and Jonsson, 1997; Marshall and Schott, 1999).

252

253 In summary, Sections 1.2.1-1.2.3 show that previous studies have presented a number of  
254 plausible, sometimes contradictory, hypotheses explaining some of the variability of DC in the  
255 Greenland Sea. In this paper, we employ observational-based hydrographic data-sets to perform  
256 a comprehensive analysis of the most plausible mechanisms affecting the intensity of DC during  
257 the period covering an intense observational effort in the region, from 1993 to 2016. We will  
258 show that the buoyancy input due to horizontal advection plays the principal role in the  
259 interannual variability of DC, whereas the air-sea fluxes and the variability of the sea-ice extent  
260 are of secondary importance.

261

## 262 **2. The data-sets**

263

### 264 *2.1 Oceanic data*

265

266 To compute the current velocity and the mean relative vorticity, the AVISO14 altimetry data-  
267 set is used (<https://www.aviso.altimetry.fr/en/my-aviso.html>). The data are available since 1993  
268 with a horizontal resolution of  $0.25^\circ \times 0.25^\circ$  (28 km x 7 km in the central Greenland Sea). The  
269 current velocity and relative vorticity are computed from the sea-level data using the 7-point  
270 stencil width formulae to minimize the noise level (Arbic et al 2012).

271 The 3D fields of water density and ocean currents are obtained from the ARMOR3D data-set,  
272 a relatively new global ocean state product combining in situ and satellite ocean observations.  
273 The data are available since 1993, limited to the beginning of the satellite altimetry (Rosmorduc  
274 and Hernandez, 2003; Muller et al., 2019). A relatively robust estimate of oceanic advective  
275 fluxes is possible since 1993, as well.

276 In ARMOR3D, “synthetic” temperature and salinity at different water levels are first derived  
277 from altimeter and sea surface temperature (SST) anomalies through a multiple regression  
278 (Guinehut et al., 2004). The regression coefficients are regionally obtained by combining the  
279 satellite and all available sub-satellite historical data. The synthetic thermohaline fields are  
280 combined with in situ historical data in the optimal interpolation procedure to obtain the final  
281 product (Guinehut et al., 2012). Geostrophic currents are then computed by extrapolating the  
282 sea surface altimetry currents downwards, using the thermal wind equations (Mullet et al.  
283 2012). As a result, the ARMOR3D data-set contains monthly 3D fields of temperature, salinity,  
284 and geostrophic currents, gridded to the standard depth levels with  $0.25^\circ \times 0.25^\circ$  spatial



285 resolution (Verbrugge et al. 2017). The use of satellite information results in more robust  
286 thermohaline and current velocity fields, available with a higher spatial and temporal resolution  
287 than the results of interpolation of in situ data only (Larnicol et al., 2006). The stated maximum  
288 RMS error is 0.3°C in temperature and 0.02 in salinity in the upper 100-m layer (Verbrugge et  
289 al. 2017). Below 1500 m, the data-set is replaced with the WOA13 climatology modified by  
290 available in situ profiles. This makes values of interannual variability of temperature and  
291 salinity profiles below 1500 m less reliable. Comparison of the interannual variability of the  
292 DC intensity derived from ARMOR3D with that from the GLORYS reanalysis shows a high  
293 correlation between the results (see Supplement 7.2). We also develop alternative metrics,  
294 which do not use these deep levels (see Section 3.2)

295 To verify the volume and heat fluxes derived from ARMOR3D in the Greenland Sea,  
296 independent data from moorings deployed in the southern Fram Strait along 77.8°N  
297 (Beszczynska-Möller et al., 2012; Beszczynska-Möller, 2015) are used. The data set consists  
298 of the temperature, salinity, and current velocity information at 10 moorings from 1997 to 2011  
299 (PANGAEA: <https://doi.pangaea.de/10.1594/PANGAEA.845938>). In addition, pre-computed  
300 oceanic heat fluxes from the Hornbanki mooring in the northern Denmark Strait (the NAACLIM  
301 project, Jonsson and Valdimarsson, 2012) are also used. The comparison shows that  
302 ARMOR3D reproduces the main seasonal cycle, as well as the interannual variability, with  
303 sufficient accuracy in spite of a somewhat lower interannual variability (Vesman et al., 2020).  
304 In areas with frequent ice cover and with increasing depth, the accuracy of the ARMOR3D heat  
305 fluxes decrease. Nevertheless, ARMOR3D reproduces well the interannual variability of heat  
306 and freshwater fluxes in the upper 500-m layer, which encompasses the main core of the  
307 Atlantic water re-circulation in the Greenland Sea (Rudels et al., 2002; Jeansson et al., 2008).

308

## 309 *2.2 Atmospheric data*

310

311 The ocean-atmospheric freshwater and heat exchange are computed from the 6-hourly ERA-  
312 Interim reanalysis data (Dee et al., 2011) on a 0.75°×0.75° grid  
313 (<https://apps.ecmwf.int/datasets/data/interim-full-daily/levtype=sfc/>), obtained from the  
314 European Centre for Medium-range Weather Forecasts (ECMWF). Reanalysis wind speed, air  
315 and sea surface temperatures, relative humidity, and surface pressure fields are used for surface  
316 turbulent flux calculation employing the COARE 3.5 algorithm (Fairall et al., 2003). The results  
317 are further averaged to the monthly means.

318 Sea-surface net solar radiation derived from ERA-Interim reanalysis data represents the sum of  
319 the shortwave (solar, direct and diffuse) radiation ([https://apps.ecmwf.int/codes/grib/param-  
db?id=176](https://apps.ecmwf.int/codes/grib/param-db?id=176)) and net longwave (downwards minus upwards) radiation  
320 ([https://apps.ecmwf.int/codes/grib/param-  
db?id=177](https://apps.ecmwf.int/codes/grib/param-db?id=177)).

322

## 323 *2.3. Ice data*

324

325 The variability of the ice volume in the Greenland Sea is derived from the PIOMAS reanalysis.  
326 The reanalysis is based on the Parallel Ocean Program model coupled with a thickness and  
327 enthalpy distribution (TED) sea ice model. The reanalysis assimilates NSIDC near-real time  
328 satellite passive microwave sea ice concentrations and NCEP/NCAR sea surface temperature  
329 in the ice-free areas (Zhang and Rothrock, 2003). Validation of the PIOMAS sea-ice thickness  
330 with in situ, submarine, and satellite observations for the Arctic suggests that the PIOMAS  
331 uncertainty in the monthly mean sea-ice thickness is below 80 cm (Schweiger et al., 2011).  
332 Similar to the Arctic Ocean, the model tends to overestimate thickness of thin ice and

333 underestimate thickness of thick ice in the Greenland Sea (Selyuzhenok et al., 2020). However,  
 334 deduced from PIMAS the interannual variability of the ice volume flux through the Fram Strait  
 335 and the interannual ice volume variation integrated over the Greenland Sea show high  
 336 correlations with independent in situ and satellite-derived Cryosat observations (Selyuzhenok  
 337 et al., 2020).

338 In this study, monthly mean Greenland freshwater discharge rates include solid (ice) discharge,  
 339 tundra runoff and the ice sheet meltwater in Greenland Sea (between the Fram Strait and 73°N)  
 340 ([https://www.bodc.ac.uk/data/published\\_data\\_library/catalogue/10.5285/643aa9bc-bcd6-45ad-e053-6c86abc07da0/](https://www.bodc.ac.uk/data/published_data_library/catalogue/10.5285/643aa9bc-bcd6-45ad-e053-6c86abc07da0/), Bamber et al, 2018). Approximately half of the freshwater flux  
 342 integrated along the eastern Greenland coast enters the Greenland shelf, onshore of the study  
 343 region shown in Figure 1(a) (Dukhovskoy et al. 2016, 2019).

344

### 345 **3. Methods**

346

347 All notations used throughout the text are summarised in Supplement 7.1

348

#### 349 *3.1 Variability of the mixed layer depth in the Greenland Sea*

350

351 The interannual variation of the DC intensity is typically obtained as the maximum mixed layer  
 352 depth (*MMLD\**). Hydrographic ship observations reveal notable interannual variability in the  
 353 maximum MLD in the Greenland Sea (Table 1 and Fig. 1).

354

355 Table 1. Interannual variability of the maximum MLD (m) in the Greenland Sea. The range of  
 356 values of the *MMLD\** come from different sources.

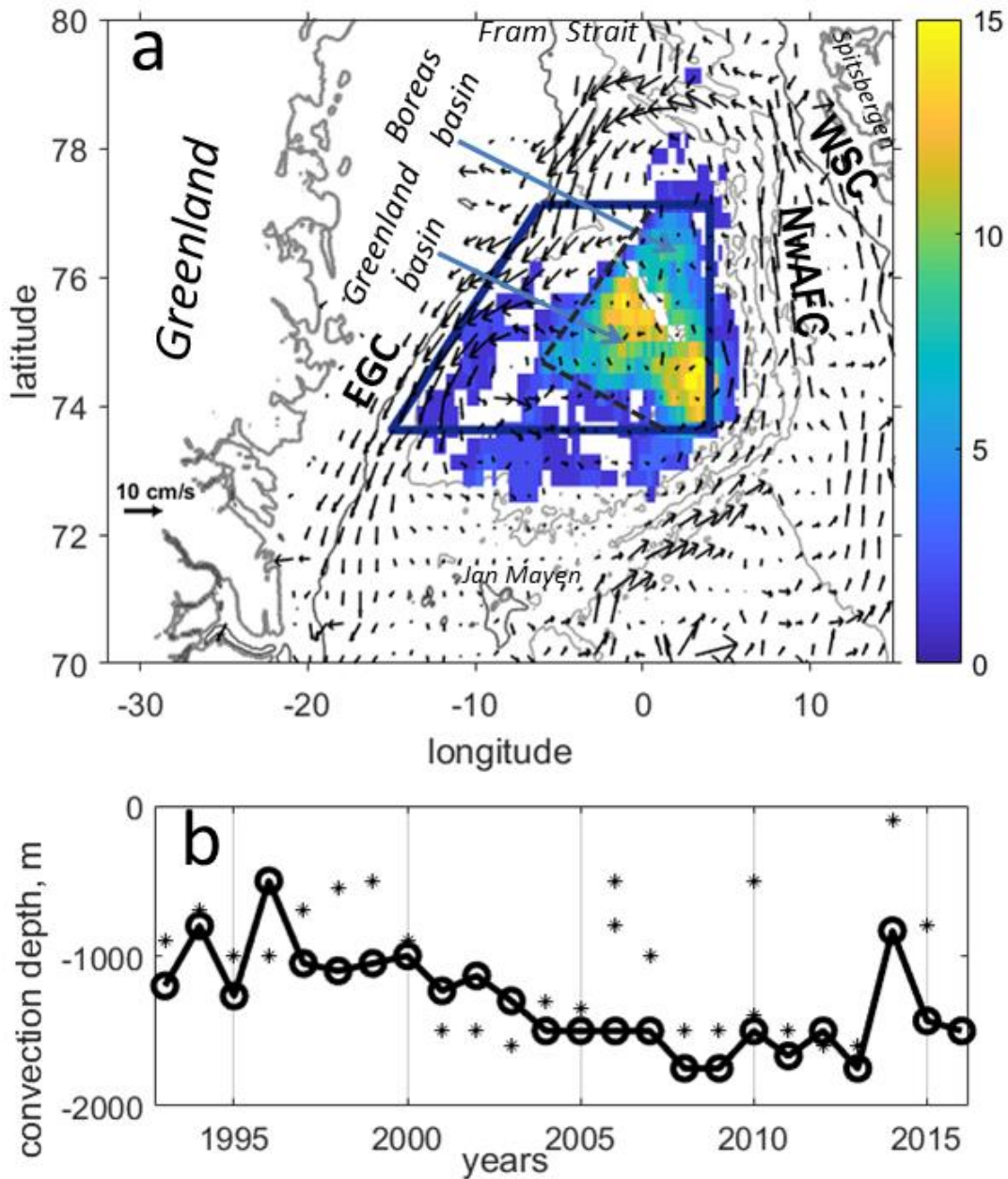
year	<i>MMLD*</i> (m)	Reference
1970/71	3500	Malmberg, 1983
1981/82	500	Clarke et al., 1990
1983/84	3500	Nagurny and Popov, 1985
1986/87	200	GSP-Group, 1990; Fischer et al., 1995; Lauvset et al., 2018; Somavilla, 2019; Brakstad et al., 2019
1987/88	1300	GSP-Group, 1990; Fischer et al., 1995
1988/89	1400-2000	GSP-Group, 1990; Fischer et al., 1995
1989/90	550	Somavilla, 2019
1990/91	500	Somavilla, 2019
1991/92	550	Somavilla, 2019
1992/93	800-1000	Fischer et al., 1995; Buderus et al., 1998; Lauvset et al., 2018; Brakstad et al., 2019
1993/94	700	Fischer et al., 1995; Buderus et al., 1998; Lauvset et al., 2018; Brakstad et al., 2019
1994/95	>1000	Fischer et al., 1995; Buderus et al., 1998; Lauvset et al., 2018; Brakstad et al., 2019
1995/96	>1000	Fischer et al., 1995; Buderus et al., 1998; Brakstad et al., 2019

1996/97	700	Somavilla, 2019
1997/98	550	Somavilla, 2019
1998/99	500	Somavilla, 2019
1999/00	900	Somavilla, 2019
2000/01	1500	Lauvset et al., 2018; Brakstad et al., 2019
2001/02	1500	Lauvset et al., 2018; Brakstad et al., 2019
2002/03	1600	Latarius and Quadfase, 2016
2003/04	1300	Somavilla, 2019
2004/05	1350	Somavilla, 2019
2005/06	500-800	Latarius and Quadfase, 2016; Lauvset et al., 2018; Somavilla, 2019; Brakstad et al., 2019
2006/07	1000	Latarius and Quadfase, 2016; Lauvset et al., 2018; Brakstad et al., 2019
2007/08	1500	Lauvset et al., 2018; Somavilla, 2019; Brakstad et al., 2019
2008/09	1500	Latarius and Quadfase, 2016
2009/10	500-1400	Latarius and Quadfase, 2016; Lauvset et al., 2018; Somavilla, 2019; Brakstad et al., 2019
2010/11	1500	Lauvset et al., 2018; Brakstad et al., 2019
2011/12	1600	Latarius and Quadfase, 2016
2012/13/	1600	Lauvset et al., 2018; Brakstad et al., 2019
2013/14	100	Lauvset et al., 2018; Brakstad et al., 2019
2014/15	800	Lauvset et al., 2018; Brakstad et al., 2019

357

358 It is noteworthy that for the same years, various authors give different maximum winter MLD.  
359 This stems from the limited spatial and temporal coverage of in situ observations analysed in  
360 the previous studies, as well as from inconsistencies in the definition of the MLD and the  
361 different methodologies for the MLD detection. This is discussed in more detail in the following  
362 sections.

363 Analysis of ARMOR3D hydrographic fields and individual vertical profiles (from EN4 Hadley  
364 Center data-set, <https://www.metoffice.gov.uk/hadobs/en4/>) show that at any point in the  
365 central Greenland Sea the DC may exceed 1000 m, at least once during the last two decades  
366 (Fedorov et al., 2018; Bashmachnikov et al., 2018). However, the most frequent DC is localized  
367 in a limited region of the central Greenland Basin (Fig. 1a). Strong DC in other regions is  
368 relatively rare. Thus, in the Boreas basin, DC was observed to penetrate down to 2000 m  
369 (Johannessen et al., 1991, 2005), but much less frequently than in the Greenland basin (Fig. 1,  
370 Fedorov et al., 2018; Bashmachnikov et al., 2018).



371

372 *Fig. 1. (a). The study region. Colour represents the number of winter months (January to April*  
 373 *of 1993-2016) in a grid-point with MLD over 1000 m divided by the total number of winter*  
 374 *months; derived from ARMOR3D data-set (see Bashmachnikov et al., 2018). Vectors are the*  
 375 *mean currents derived from AVISO altimetry. The region of deep convection is contoured with*  
 376 *the dark-blue line designating the study domain discussed in the text; the region with the most*  
 377 *frequent deep convection is limited by the dashed blue line from the west. Grey lines mark 500*  
 378 *m and 2500 m isobaths. EGC is the East Greenland Current, NwAFC is the Norwegian Atlantic*  
 379 *Front Current, WSC is the West Spitsbergen Current. (b) Maximum winter convection depth*  
 380 *(MMLD\*, m), derived from ARMOR3D data-set (line with empty circles) and from various*  
 381 *literature sources (Table 1, stars).*

382

### 383 3.2 Estimation of the intensity of DC

384

385 For the calculation of MLD, the small-scale noise is removed using a moving average filter on  
 386 the ARMOR3D vertical profiles with a 10-m window. Only profiles over the deep Greenland

387 Sea (with water depth exceeding 800 m) are considered. The gravitationally unstable segments  
388 of the profiles are artificially mixed until neutral stratification is achieved at all levels. If the  
389 artificially mixed layer exceeds half the local ocean depth, the profile is excluded as unreliable.

390 The MLD is detected using three different algorithms previously used by de Boyer Montegut  
391 et al. (2004), Kara et al. (2000), and Dukhovskoy (first presented in Bashmachnikov et al.,  
392 2018). The method of de Boyer Montegut et al. (2004) detects MLD as the upper level, where  
393 the potential density difference ( $\Delta\sigma$ ) between the tested and the fixed near sea surface level  
394 ( $z_b=10$  m) exceeds a pre-defined critical value ( $\Delta\sigma_c$ ):  $\Delta\sigma > \Delta\sigma_c$ . Tests of the algorithm  
395 performance shows  $\Delta\sigma_c = 0.01 \text{ kg m}^{-3}$  to be optimal for the Greenland Sea. The algorithm of  
396 Kara et al. (2000) is similar, except that the critical temperature difference  $\Delta T_c$  is now fixed.  
397 The density difference is derived from the equation of state using temperature at the upper level  
398  $z_b$ ,  $T(z_b)$ , while salinity is fixed to  $S(z_b)$ . Due to the nonlinearity of the equation of state, for a  
399 lower  $T(z_b)$ , we get smaller  $\Delta\sigma_c$  for the same  $\Delta T_c$  and a fixed salinity, which allows a more  
400 accurate detection of the MLD in smoother winter density profiles compared to de Boyer  
401 Montegut et al. (2004). Tests showed  $\Delta T_c = 0.1 \text{ }^\circ\text{C}$  to be optimal for the study region.  
402 Dukhovskoy suggests fixing MLD at the uppermost level where the vertical density gradient  
403 exceeds its local standard deviation (within the  $\pm 50$  m window). This algorithm does not depend  
404 on a pre-defined critical value and takes into account the intensity of the vertical density  
405 variations in each profile. This algorithm is sensitive to changes in the vertical density gradients,  
406 which characterizes the transition from the upper mixed layer to the pycnocline. As the upper  
407 “mixed” layer of the measured vertical profiles is often not completely homogeneous in the real  
408 ocean, this method provides a good balance between avoiding false detection of the MLD at  
409 relatively small density fluctuations within the MLD and the ability to detect even a weak  
410 pycnocline at large depths, which is often missed by the  $\Delta\sigma_c$  threshold methods. A similar  
411 methodology has been used by Pickart et al. (2002), but applied to vertical variations of density  
412 instead of variations of density gradients. Analysis shows that, in most cases, the results  
413 obtained by the three algorithms are similar (Fedorov et al., 2018; Bashmachnikov et al., 2018).  
414 However, the method of Dukhovskoy, is more accurate and robust, in particular for a weak  
415 pycnocline. It is selected as the principle method used in this study.

416 Due to the small area of the chimneys (Marshall and Scott, 1999; Johannessen et al., 1991,  
417 2005; Wadhams et al., 2004), the interannual variations of the DC intensity, based on the  
418 maximum MLD, has obvious limitations. With a typically low number of in situ profiles and  
419 the small area of a DC chimney, the observations may easily miss the deepest DC point,  
420 resulting in a bias in the estimate of the DC intensity (see Table 1 and the related discussion).  
421 Regular sampling by Argo profiling floats, available in the Greenland Sea since 2002 (Latarius  
422 and Quadfase, 2016; Brakstad et al., 2019), has improved the situation. With 5 to 20 profiles  
423 per month, Argo alone still gives an insufficient number of observations for obtaining the  
424 interannual variability of the maximum MLD, but together with other in situ profiles this forms  
425 a sufficient observational basis for correct derivation of the interannual tendencies  
426 (Bashmachnikov et al., 2018; Fedorov and Bashmachnikov, 2020). Previous studies also  
427 suggest a robust detection of the interannual DC variability with the use of the ARMOR3D  
428 data-set, available since 1993 (Bashmachnikov et al., 2019). This restricts the time interval of  
429 our analysis.

430 Another drawback is that assessing the intensity of DC as the maximum MLD, one uses an  
431 observation at a single point. However, the main result of the DC, the renewal of the Greenland  
432 Sea Deep Water, depends also on the area integral of the chimneys. In this study, the accuracy  
433 of the interannual variability of DC (from ARMOR3D data-set) is further confirmed by a  
434 second metric, which is the area where the vertical mixing exceeds a certain depth level. We  
435 use 800 m as the threshold depth level ( $S_{800}^*$ ) because this is the upper boundary of the  
436 Greenland Sea Deep Water (Rudels et al., 2002; Bashmachnikov et al., 2018). This metric is  
437 less dependent on the degradation of the gridded data-set accuracy with depth (see Section 2.1),

438 but it does require using gridded data. A nonlinear relationship between  $S_{800}^*$  and  $MMLD^*$  is  
 439 presented in Supplement 7.2. Next in this study we also use  $S_{800}$  and the  $MMLD$  notations for  
 440 the normalised values. Normalization is done by subtracting the mean and dividing by the  
 441 standard deviation.

442 In addition to the direct estimates, several proxy indices of the intensity of DC have been  
 443 suggested. These indices quantify changes in the thermohaline or hydrochemical properties of  
 444 sea water (temperature, salinity, oxygen, CFC, etc.), variability of which are supposed to be  
 445 governed by variations in the intensity of DC (Meincke et al., 1992; Johannessen et al., 1991;  
 446 Schlosser et al., 1991; Rhein 1996; Bonisch et al., 1997; Alekseev et al., 2001; Azetsu-Scott et  
 447 al., 2005; Yashayaev, 2007; Rhein et al., 2011; Gladyshev et al., 2016; Bashmachnikov et al.,  
 448 2019). As the renewed deep water masses spread their properties over the deep areas of the DC  
 449 basins within a few months, observing such changes in the deep water properties requires  
 450 substantially fewer observations than one would need for a robust detection of the  $MMLD$   
 451 variations via direct estimates. In the Greenland Sea, the variability of the  $MMLD$  shows high  
 452 a correlation with the depth-integrated (100-1500 m) water density averaged over the deep part  
 453 of the Greenland Basin (Bashmachnikov et al., 2019).

454

### 455 3.3 Oceanic advective fluxes

456

457 Following the divergence theorem, we estimate divergence of oceanic fluxes of heat ( $Q_{adv}$ ),  
 458 freshwater ( $FW_{adv}$ ) and density ( $DF_{adv}$ ), integrated over the study region (Fig. 1), as a surface  
 459 integral of the fluxes across its lateral boundaries:

$$460 \quad Q_{adv} = \oint_{\tilde{S}} \vec{V} \cdot \vec{n} C_p \rho_{ref} (T - T_{ref}) d\tilde{S}, \quad (1)$$

$$461 \quad FW_{adv} = \oint_{\tilde{S}} \vec{V} \cdot \vec{n} \left( \frac{S_{ref} - S}{S_{ref}} \right) d\tilde{S}, \quad (2)$$

$$462 \quad DF_{adv} = DF_{T,adv} + DF_{S,adv} = \rho_{ref} \left( -\frac{\alpha}{C_p \rho_{ref}} Q_{adv} - \beta S_{ref} FW_{adv} \right)$$

$$463 \quad = \rho_{ref} \oint_{\tilde{S}} \vec{V} \cdot \vec{n} (-\alpha(T - T_{ref}) + \beta(S - S_{ref})) d\tilde{S}. \quad (3)$$

464 Here the fluxes are integrated over the surface  $\tilde{S}$  bounding the study region (positive norm  
 465 vector  $\vec{n}$  is into the study region),  $V$  is the current velocity,  $T$  and  $S$  are the seawater temperature  
 466 and salinity, respectively,  $C_p = 3900 \text{ J kg}^{-1} \text{ °C}^{-1}$  is the specific heat capacity. The coefficients of  
 467 the thermal expansion ( $\alpha = 0.37 \cdot 10^{-4} \text{ °C}^{-1}$ ) and of the salt contraction ( $\beta = 7.74 \cdot 10^{-4}$ ) are set to the  
 468 reference temperature  $T_{ref} = -1 \text{ °C}$  and the reference salinity  $S_{ref} = 34.9$ , while  $\rho_{ref} =$   
 469  $\rho(T_{ref}, S_{ref}, 0) = 1028 \text{ kg m}^{-3}$ . The reference temperature and salinity are taken equal to their  
 470 typical values in the Greenland Sea Deep Water. The  $T_{ref}$  and  $S_{ref}$  correspond to the climatic  
 471 characteristics of the Greenland Sea Deep Water (Nagurniy and Popov, 1985; Alekseev et al.,  
 472 1989; Moretsky and Popov, 1989; Johannessen et al., 1991; Korablev, 2001). The  $\frac{\beta}{\alpha}$  ratio is 21,  
 473 five times higher than in tropical regions, and shows the strong relative effect of salinity  
 474 variation on water density in the subpolar waters.

475 The oceanic meridional advective fluxes are computed across the 73.5°N and 77.0°N sections,  
 476 extending from the Greenland shelf break across the Greenland Sea and encompassing the  
 477 region of the most frequent DC (Fig. 1, see also Supplement 7.6). The fluxes are integrated over  
 478 the whole length of a section and from the sea surface to 500 m depth (after reaching this level  
 479 the convective renewal of the Greenland Sea Intermediate Water begins).

480

### 481 3.4 Air-sea heat and freshwater fluxes

482

483 The net surface heat flux includes surface turbulent (sensible and latent) heat fluxes ( $Q_{atm}$ ,  
484 positive to the ocean) and net shortwave (solar) and longwave radiative fluxes ( $RB$ ). The net  
485 shortwave radiation is the difference between the incoming and outgoing (reflected) shortwave  
486 radiative fluxes. Similarly, the net longwave radiation is the difference between the incoming  
487 and outgoing surface longwave radiative fluxes, comprising the longwave (infrared) surface  
488 emissivity and reflected back atmospheric longwave radiation. The net freshwater flux (net  
489 precipitation) at the ocean surface is the difference between precipitation and evaporation.

490 In the following discussion, we will primarily use net surface heat flux and net precipitation for  
491 the DC analysis. In the ice-covered regions  $Q_{atm}$  depends on the ice concentration. Whenever  
492 the ice concentration is below 15%, the ocean is considered ice-free. For larger ice  
493 concentrations,  $Q_{atm}$  is integrated only over the ice-free fraction of the grid cell. Adding heat  
494 fluxes through the sea ice (Lecomte, 2013), using as an input the ice thickness from the  
495 PIOMAS dataset and the climatic snow thickness from Shalina and Sandven (2018), shows  
496 practically no effect, neither on seasonal nor on the interannual variability of  $Q_{atm}$ . The effect  
497 of the ice lid on the surface turbulent heat fluxes ( $dQ_{ilid}$ ) is computed as the difference between  
498 the turbulent heat fluxes over the ocean with no sea ice and over the ocean with the observed  
499 ice cover ( $Q_{atm}$ ). In the regions, where the sea ice is artificially removed, calculation of the  
500 sensible heat flux uses the water freezing temperature of  $-1.8^{\circ}\text{C}$ .

501 To determine the role of cyclones in the variation of the DC intensity, ocean heat and freshwater  
502 exchange with the atmosphere are also computed only inside cyclones, detected over the study  
503 region. The positions and size of the cyclones were obtained from a data-base of cyclone tracks,  
504 derived from the 6-hourly ERA-Interim reanalysis fields (Hoskins and Hodges, 2002; Hodges  
505 et al., 2011), which yields higher number of cyclones than when using mean sea level pressure  
506 fields (Vessey et al., 2020). In the data-base the cyclones are detected from the relative vorticity  
507 fields at 850hPa. The data are spatially filtered to focus on synoptic scale cyclones by spectrally  
508 filtering the data in the T5-42 (triangular truncation, total wavenumbers) band, the cyclones are  
509 identified as vorticity maxima on a polar stereographic grid and the locations refined using B-  
510 splines and steepest ascent maximization (Hodges, 1995). The identified points are then initially  
511 linked together over consecutive time steps using a nearest neighbour method and then are  
512 refined by minimising a cost function for track smoothness subject to adaptive constraints on  
513 the track smoothness and displacement distance in a time step. The tracks are further filtered to  
514 retain only those that travel more than 1000 km and last for more than 2 days. This methodology  
515 is described in detail in Hodges (1995, 1999). The cyclone size was estimated from the ERA-  
516 Interim mean sea level pressure fields as the last closed air pressure contour.

517 The density flux through the sea-surface ( $DF_{oa}$ ) is calculated as a sum of the corresponding net  
518 thermal ( $DF_{atm}$  and  $DF_{RB}$ ) and freshwater ( $DF_{PE}$  and  $DF_{ice}$ ) fluxes:

$$519 \quad DF_{oa} = (DF_{atm} + DF_{RB}) + (DF_{PE} + DF_{ice})$$
$$520 \quad = \rho_{ref} \left( -\frac{\alpha}{C_p \rho_{ref}} (Q_{atm} + RB) - \beta S_{ref} (FW_{PE} + FW_{ice}) \right), \quad (4)$$

521 where  $FW_{PE}$  is the precipitation minus evaporation and  $FW_{ice}$  is the freshwater flux from the  
522 sea ice formation/melting.

523 For the purpose of the following analysis, we also distinguish between the density fluxes solely  
524 determined by the heat fluxes ( $DF_T$ ) and solely by the freshwater fluxes ( $DF_S$ ) as

$$525 \quad DF_T = DF_{T.adv} + DF_{atm} + DF_{RB}, \quad (5)$$

$$526 \quad DF_S = DF_{S.adv} + DF_{ice} + DF_{PE}. \quad (6)$$

527

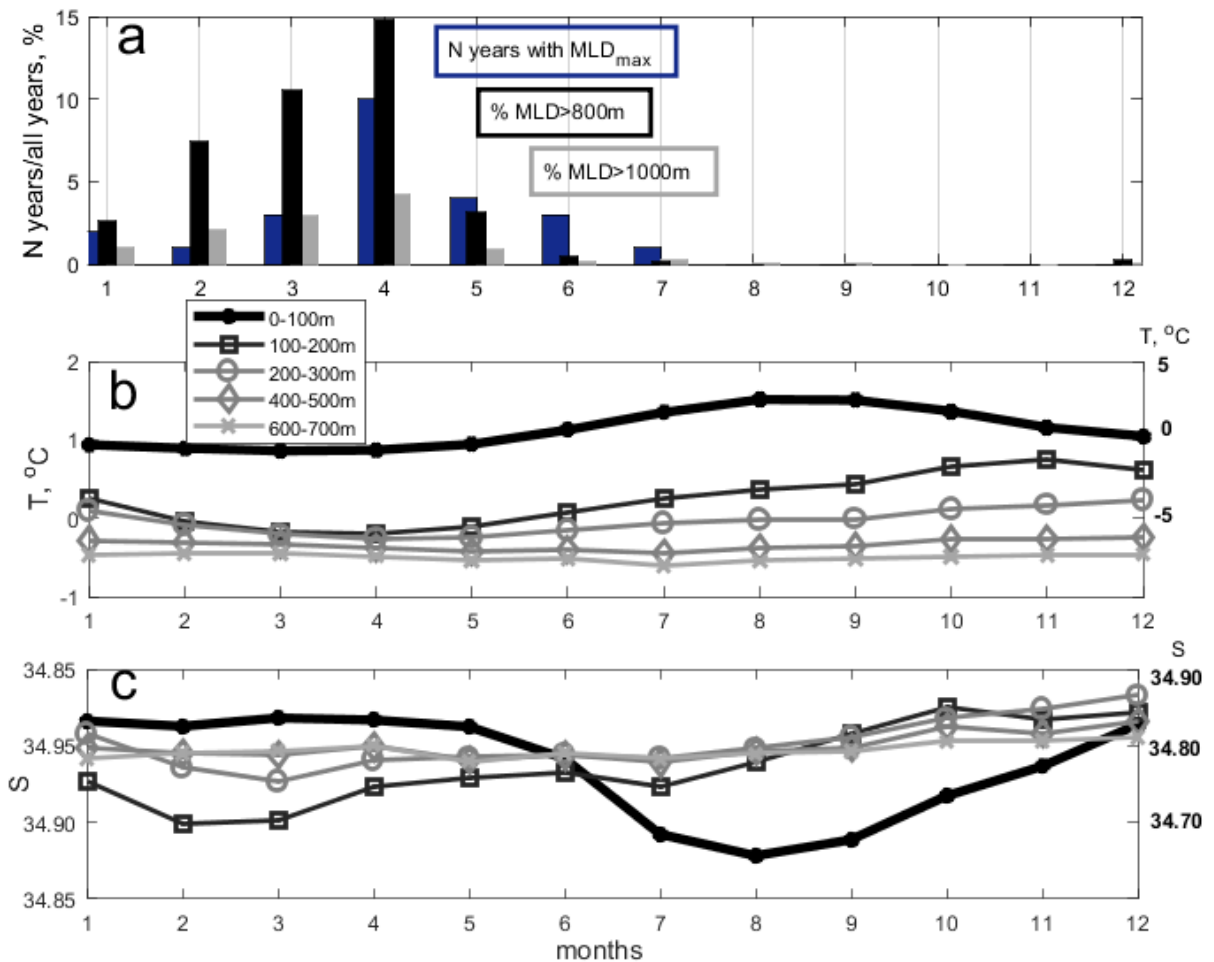
## 528 4. Results

529

### 530 4.1 Seasonal variability of the DC intensity

531

532 In the Greenland Sea, the deepening of the upper mixed layer typically begins in October and  
 533 continues until April. During October-December the MLD is still shallow, though it deepens  
 534 and re-stratifies intermittently. Consistent MLD deepening starts in January (Fig. 2a). The  
 535 month, when the *MMLD* is reached, varies from year to year. For about 50% of the years (since  
 536 1993) the *MMLD* is observed in April (see also Marshall and Schott, 1999; Kovalevsky, 2002;  
 537 Fedorov et al., 2018; Bashmachnikov et al., 2018). In late spring, the buoyancy fluxes restore  
 538 the upper ocean stratification preventing the formation of the DC chimneys (Marshall and  
 539 Schott, 1999; Kovalevsky, 2002; Kawasaki and Hasumi, 2014; Kovalevsky and  
 540 Bashmachnikov, 2019). However, observations show that even several months after a DC  
 541 chimney loses its connection with the sea-surface, water stability in the deep parts of the water  
 542 column in the Greenland Sea stay low (Wadhams et al., 2004) or may continue to decrease  
 543 (Kovalevsky, 2002). The percent of the area in the Greenland Sea with DC over 800 m (as well  
 544 as with DC over 1000 m) shows the same mean seasonal variability (Fig. 2a).



545

546 *Fig. 2. Seasonal variability of water characteristics in the Greenland Sea: (a) number of years*  
 547 *(1993-2016) with DC reaching its annual maximum (blue), from September of the previous year*

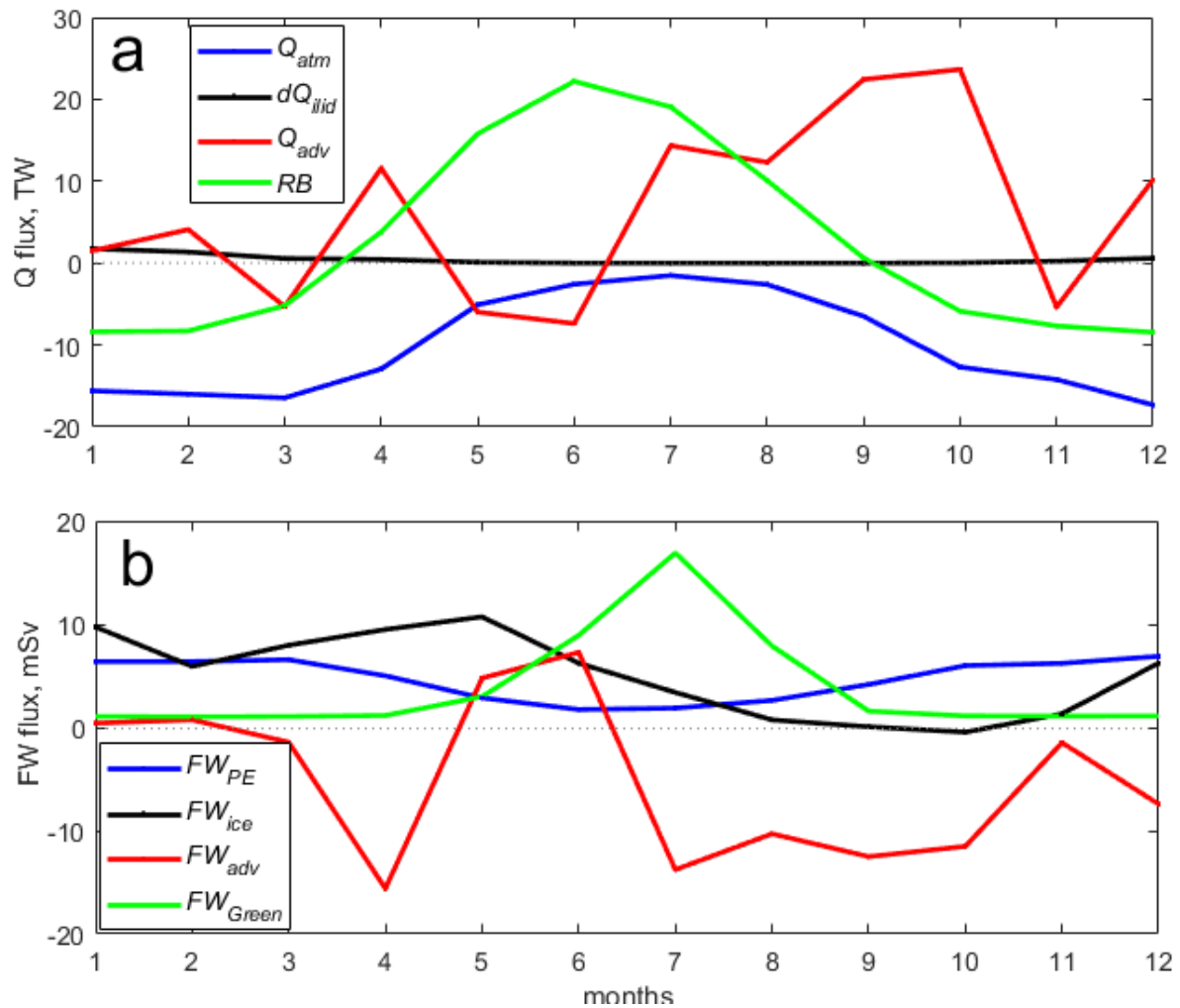


548 *to August of the current year, and percent of the area in the Greenland Sea with DC over 800*  
549 *m (black) and with DC over 1000 m (grey); (b) water T, (c) water S. Note that in panels (b) and*  
550 *(c) the amplitude of T and S variations in the upper 100-m is divided by 5 (right scale), in order*  
551 *to variability in the deeper layers becomes visible (left scale).*

552

553 In the region where DC is frequently observed (the blue trapezoid in Fig. 1), the temperature  
554 reaches its minimum in March-April in the 0-300 m layer (Fig. 2b). During the same period the  
555 temperature at 400-700 m reaches its annual maximum, i.e. the upper ocean becomes more  
556 homogenous. The complexity of the processes governing the variability of the upper ocean  
557 density is particularly evident from variations of the upper ocean salinity, which is decoupled  
558 from the salinity variation in the top 100-m layer (Fig. 2c). The maximum freshening below  
559 100 m corresponds to the time of the intensive winter vertical mixing, while the following  
560 salinification, accompanied by a temperature increase, is a result of RAW advection into the  
561 region (Rudels et al., 2002; Jeansson et al., 2008; Langehaug and Falck, 2012).

562 In the study region, the seasonal variability of the main heat fluxes to the upper ocean are of the  
563 same order of magnitude (Fig.3a). The same is true for the main freshwater fluxes (Fig. 3b).  
564 During late summer and autumn, the oceanic heat convergence in the upper 500-m layer ( $Q_{adv}$ )  
565 is positive, and at its seasonal maximum (July – November) and often exceeds  $RB$  or  $Q_{atm}$  (Fig.  
566 3a). It is during this period when the most intensive warming of the upper ocean below the  
567 MLD is observed (Fig. 2b). During the same period, the  $FW_{adv}$  stays at its most negative values  
568 and far exceeds  $FW_{PE}$  and  $FW_{ice}$  (Fig. 3b). The advective convergence of more saline water,  
569 relative to the salinity of the Greenland Sea Deep Water ( $S_{ref}$ , see Section 3.3), leads to an  
570 intensive salinification of the upper ocean below the shallow summer MLD (Fig. 2c).



571

572 *Fig. 3. Seasonal heat (TW) (a) and freshwater (mSv) (b) fluxes in the central Greenland Sea.*  
 573 *In (a):  $Q_{adv}$  is the heat flux convergence due to ocean advection;  $Q_{atm}$  is the heat flux from*  
 574 *atmosphere to the ocean;  $dQ_{illid}$  is the difference between the heat fluxes from the atmosphere*  
 575 *to the ocean when the ice-lid is artificially removed relative to those for the observed ice*  
 576 *concentrations;  $RB$  is net radiative flux ; In (b):  $FW_{adv}$  is the ocean freshwater advection,  $FW_{PE}$*   
 577 *is the precipitation minus evaporation;  $FW_{ice}$  is the freshwater flux from ice melt;  $FW_{Green}$  is*  
 578 *the freshwater flux from the Greenland ice sheet in the Greenland Sea.*

579

580 With the z-axis directed downwards, the vertical gradient of  $FW_{adv}$  in the upper 500-m layer  
 581 ( $dFW_{adv}$ , not shown) is always negative (salinity increases downwards), while the vertical  
 582 gradient of  $Q_{adv}$  in the upper 500-m layer ( $dQ_{adv}$ ) is always positive (temperature increases  
 583 downwards). This indicates a downward intensification of advection into the study region of  
 584 RAW that is warmer and more saline than the ambient water .

585 In winter, the ocean heat loss to the atmosphere ( $Q_{atm} < 0$ ) is attributed to strong negative heat  
 586 fluxes from the sea surface that far exceed the advective heat fluxes ( $Q_{adv}$ ). Similarly, the sum  
 587 of the net precipitation and the sea ice melt exceeds salt advection into the region with the  
 588 RAW. Over the study region, the seasonal variability of  $Q_{atm}$  due to the sea ice cover ( $dQ_{illid}$ )  
 589 is insignificant (Fig. 3a). For the climatological mean over the study period,  $dQ_{illid}$  is important  
 590 only along the westernmost part of the region (Supplement 7.3). Greenland freshwater  
 591 discharge into the Greenland Sea ( $FW_{Green}$ ) reveals a pronounced summer peak, but in autumn  
 592 or winter it does not affect the freshwater balance (Fig. 3b).

593 To summarize, the air-sea fluxes govern the upper ocean winter heat and freshwater balance,  
594 while advective fluxes control the upper ocean density variations before the beginning of the  
595 DC season. Both processes may be important for the interannual variability of the DC intensity  
596 (Fig. 1b).

597 Furthermore, based on Figures 2 and 3, we define the DC year (from May of the previous year  
598 to April of the current year), which is split into the preconditioning season (from May to  
599 December of the previous year, further referred as pre-DC season) and the DC season (January  
600 to April of the current year).

601

## 602 **4.2 Interannual variability of the DC intensity**

603

604 In this section we discuss the interannual variability of DC intensity in the Greenland Sea  
605 deduced from two algorithms: *MMLD* (Bashmachnikov et al., 2019) and  $S_{800}$  (Fedorov and  
606 Bashmachnikov, 2020, see also Section 3.1). The Pearson correlation coefficient between  
607 *MMLD* and  $S_{800}$  is 0.70 and the Spearman correlation is 0.85; the latter is higher due to the  
608 non-linear dependence between the parameters (Supplement 1, Fig. S1). The *MMLD* metric is  
609 more sensitive to variations of the intensity of DC for the winter with weak convection, whereas  
610 the  $S_{800}$  is more sensitive in the winter with intense DC (Figs. 4a, S1).

611 The *MMLD* increases from about 1000 m in the late 1990s to about 2000 m at the end of the  
612 2000s. Since then, a stabilisation and some decrease of the *MMLD* has been observed (Fig. 4a).  
613 This is consistent with the variations of  $S_{800}$ . Our results differ from the *MMLD* variability  
614 derived exclusively from the vertical Argo profiles (Table 1, Latarius and Quadfase, 2016), but  
615 this is due to an insufficient number of Argo profiles in the study region (see Fedorov and  
616 Bashmachnikov, 2020). The low DC in the early 1990s (Fig. 4a) agrees well with the low DC  
617 intensity in the 1980s-1990s, derived using various proxy indices (Schlosser et al., 1991;  
618 Meincke et al., 1992; Alekseev et al., 2001). The indices also suggest the intensification of the  
619 DC during the late 2000s - early 2010s (Bashmachnikov et al., 2019). Therefore, several  
620 independent metrics suggest robustness of the detected long-term tendencies in the DC intensity  
621 (Figs. 1b and 4).

622 Next we analyse the relation between the intensity of DC and the upper ocean density. We  
623 consider three factors impacting the ocean density ( $\rho$ ) at a given location: local changes of the  
624 upper ocean temperature ( $\rho_T = \rho_{ref} \alpha T(t)$ ), local changes of the upper ocean salinity (  
625  $\rho_S = \rho_{ref} \beta S(t)$ ), and changes caused by the upwards Ekman suction driven by the cyclonic  
626 circulation in the Greenland Sea. A relationship between a doming of isopycnals in the central  
627 Greenland Sea and cyclonic vorticity of the Greenland Gyre driven by the cyclonic winds has  
628 been demonstrated in previous studies (e.g., Malmberg and Jonsson, 1997; Rossby et al., 2009;  
629 Dukhovskoy et al., 2017). We expect the *MMLD* (and  $S_{800}$ ) to increase with an increase of  $\rho_S$   
630 , of  $\rho_T$  and of the mean relative vorticity in the study region ( $\omega$ ).

631 The interannual variability of the upper ocean density is further split into the autumn density  
632 (mean over September-December), i.e. accumulated during the pre-DC season, and that at the  
633 end of the cold season (April), mostly accounting for the density evolution during the DC  
634 season. Besides looking into the interannual variability (Fig. 4a-b), we also analyze the 3-year  
635 means (including the current and the two preceding years, Fig. 4c-d). This smoothing reduces  
636 the possible errors in the annual *MMLD* ( $S_{800}$ ) values, as well as taking into account some  
637 preconditioning of the DC intensity during preceding years (Wadhams et al., 2004).

638 The correlation coefficients of  $\omega$  with the *MMLD* and with  $S_{800}$  does not exceed 0.10-0.25 and  
639 are not significant at 0.05 significance level, for interannual, as well as for the 3-year smoothed  
640 results.

641 The correlation coefficient between the *MMLD* and  $\rho$  for April reaches 0.7-0.8 for the  
642 unsmoothed (Fig. 4b) and 0.9 for the 3-year smoothed values (Fig. 4d). The correlation  
643 coefficients between  $S_{800}$  and  $\rho$  in the upper 500-m layer in April reaches 0.6 for the  
644 unsmoothed and 0.8 for the 3-year smoothed values. The correlation coefficient between the  
645 *MMLD* ( $S_{800}$ ) and the mean  $\rho$  for the pre-DC season (Fig. 4c) are not significant (from 0.2 to  
646 0.3 for the unsmoothed and from 0.4 to 0.5 for the 3-year smoothed values).

647 From Figure 4(b-d) we see that, the intensification of DC from the 1990s to the late 2010s  
648 coincides with an increase in the winter  $\rho_s$  (and  $\rho$ ), while the tendency of  $\rho_T$  contradicts the  
649 observed intensification of the DC (note the reverse y-scale in the figure). The Pearson and  
650 Spearman correlation coefficients between the *MMLD* and  $\rho_s$  are equally high for the DC  
651 season of the current year, as well as for the end of the pre-DC season (0.6 to 0.7 for the annual  
652 values and 0.8 for the 3-year means). Correlations with  $S_{800}$  are slightly lower, yet significant.  
653 The correlations of the *MMLD* ( $S_{800}$ ) with  $\rho_T$  have the opposite sign at the end of the pre-DC  
654 season (-0.3 to -0.8) and are not significant (-0.1 to 0.1) in winter. Also the linear trends of the  
655 regional mean winter temperature increase during the study period from 0.5 to 1°C and the  
656 salinity – from 34.85 to 34.94. The resulting regional mean  $\rho_T$  decreases by 0.02 kg m<sup>-1</sup> and  
657  $\rho_s$  increases by 0.07 kg m<sup>-1</sup>. Therefore, these are the salinity variations that determine the  
658 change in the upper ocean density fields during winter.

659 To investigate sources of the higher frequency DC variability, we remove the quadratic trends  
660 and consider only the non-smoothed interannual variations. For the pre-DC season, the  
661 correlation coefficients of the *MMLD* ( $S_{800}$ ) with  $\rho_s$ ,  $\rho_T$  and  $\rho$  are then not significant (0.1-  
662 0.2). For the DC season, the correlation coefficients of the *MMLD* ( $S_{800}$ ) with  $\rho_s$  (and with  $\rho$   
663 ) remain significant (0.4-0.5). This means that the upper ocean salinity remains an important  
664 factor for the interannual variability of the DC intensity at high frequency.

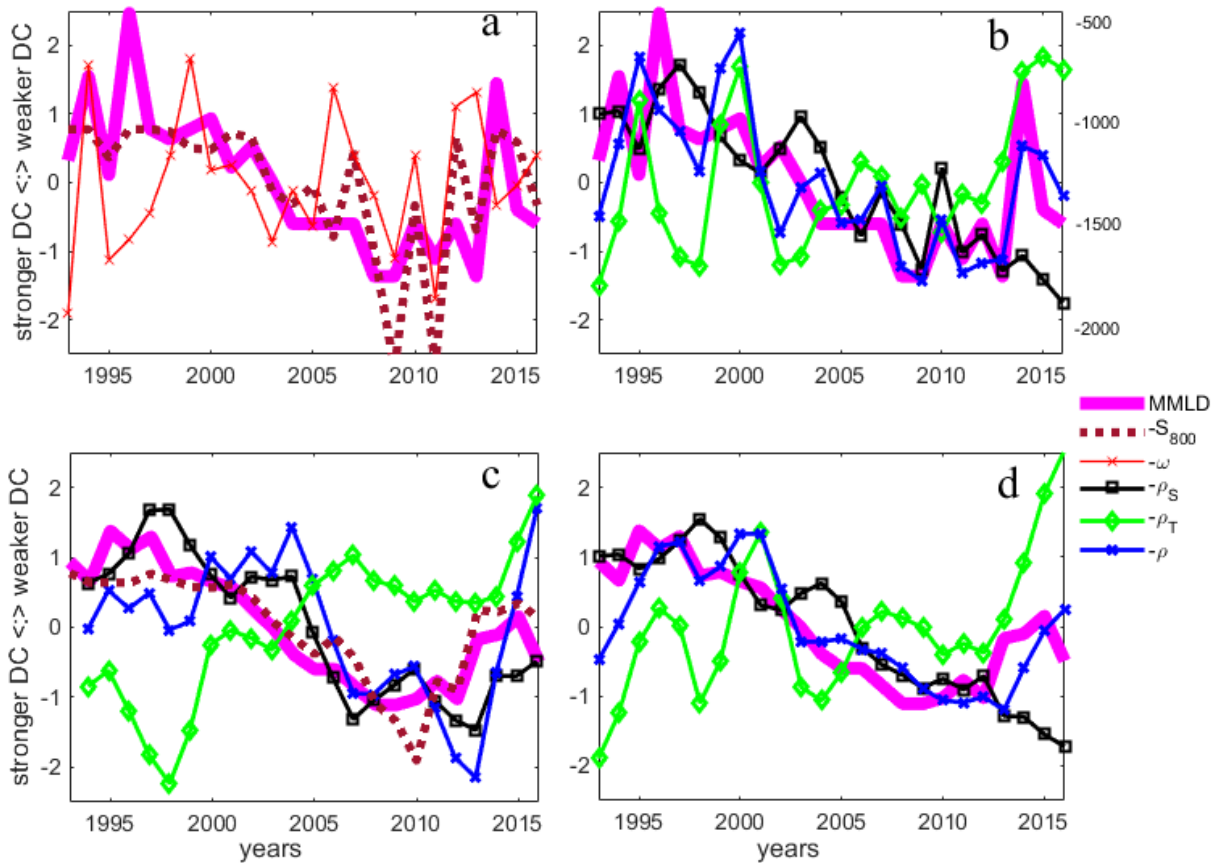
665 To summarize, we conclude that the interannual variability in the upper ocean salinity (before  
666 and during the DC season) has shaped the interannual, and, in particular, the inter-decadal,  
667 variations of the DC intensity in the Greenland Sea since 1993. However, at the end of the study  
668 period, some decrease of the DC intensity from 2013 to 2015 cannot be explained by variations  
669 of  $\rho_s$ , but corresponds to a dominating decrease of the  $\rho_T$  (Fig. 4 b-d). Thus, during this latter  
670 period, the interannual DC variability can be significantly affected by anomalous heat fluxes.

671 The unexpected negative correlation of  $\rho_T$  with *MMLD* during the warm season results from a  
672 high negative interannual correlation of  $\rho_T$  with  $\rho_s$  (-0.7). In winter there is some decoupling  
673 of the temperature and salinity interannual variations (correlation coefficient decreases to -0.6),  
674 which goes along with the drop of the  $\rho_T$  correlation with *MMLD*.

675 The difference between the summer to winter transition in the spatial distribution of the upper  
676 ocean temperature and salinity are demonstrated in Figure 5. At the start of the mixing in  
677 autumn (October), the tongue of the relatively warm and salty RAW projects into the study  
678 region. This penetration becomes deeper during the 2000s (Fig. 5 a-b). However, already at the  
679 beginning of the DC season (in January), the upper ocean temperature anomalies disappear or  
680 are strongly reduced, while the salinity anomalies continue propagating into the DC region (Fig.  
681 5 c-d). Quantitatively, the long-term effect can be estimated as the linear tendencies of the mean  
682 distance between chosen isohalines/isotherms and the western boundary of the study region (the

683 nearest point at the 2000 m isobath along the continental slope). The winter distance for the  
 684 34.9 isohaline decreased by about 35% during the study period (from 450 in 1993 to less than  
 685 300 km in 2016), whereas that of the 2°C isotherm approaches the shelf break only by about  
 686 15% (from 470 in 1993 km to 400 km in 2016), and that of the position of 1°C isotherm  
 687 practically did not change (at around 350 km from the western boundary).

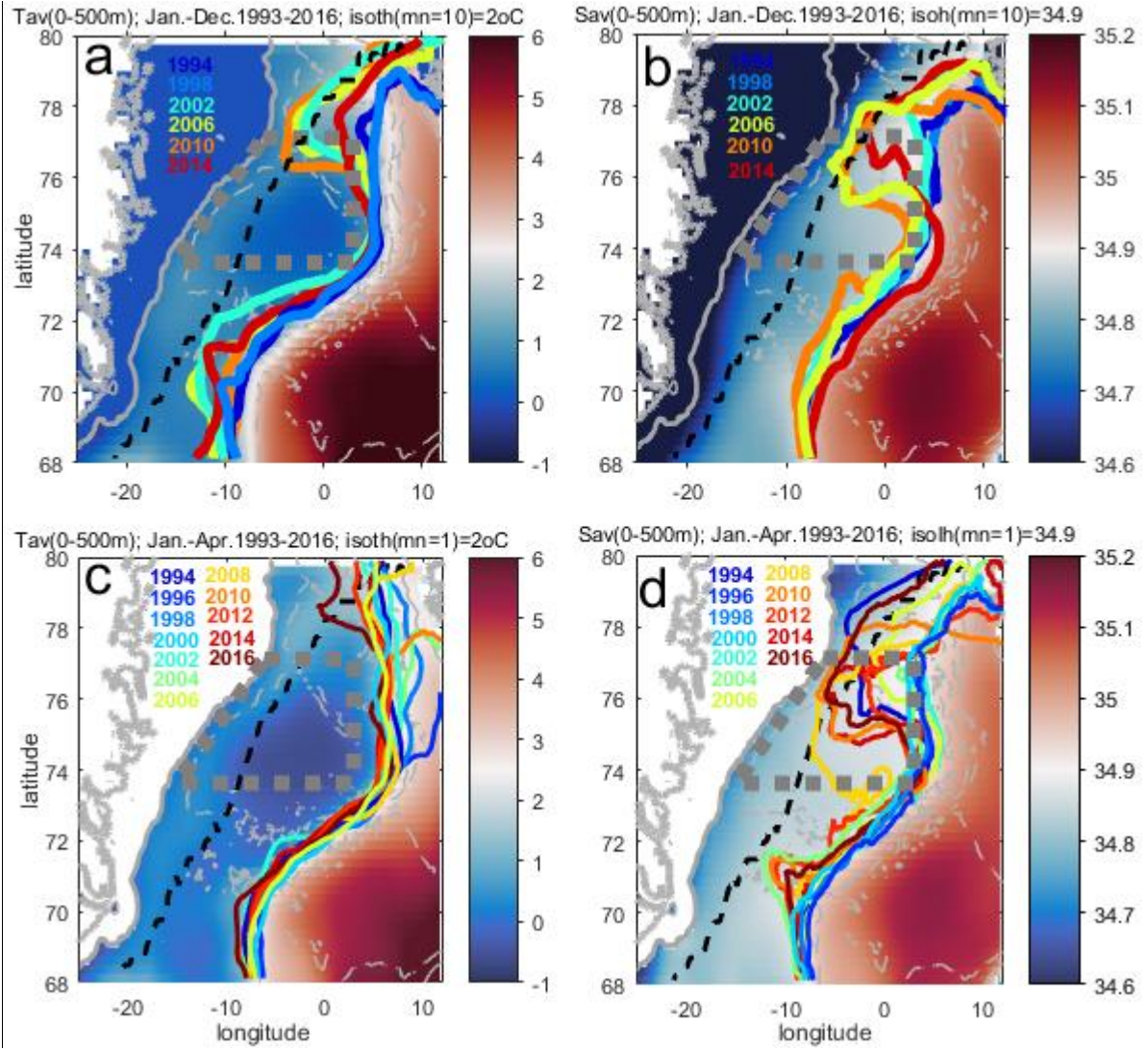
688 In summary, the analysis of this section shows that the interannual variability of the *MMLD* is  
 689 controlled by the interannual variation of salinity. The mean value of the latter reflects the  
 690 combined effect of several freshwater fluxes into and out of the study region. Figure 5(b,d)  
 691 suggests that the interannual variability in salinity might be related to the variability in the  
 692 intensity of oceanic advection. On the other hand, the excess of the advected heat, accumulated  
 693 during the warm season, is effectively removed already by the beginning of the DC season: the  
 694 more heat is accumulated during autumn, the stronger is the ocean heat release during winter.  
 695 In fact, in the beginning of the DC season, the *RB* and  $Q_{atm}$  stay strongly negative already for  
 696 three months, while the convergence of heat advection drops nearly to zero (Fig. 3a). The  
 697 interannual variability of the heat fluxes is analysed in the next Section.  
 698



699

700 *Fig. 4. Interannual variability of the normalised maximum mixed layer depth (MMLD), the*  
 701 *areas with MLD over 800 m ( $-S_{800}$ ), the normalised mean relative vorticity in the central*  
 702 *Greenland Sea during the DC season ( $\omega$ ), the mean water density of the upper 500 m ( $\rho =$*   
 703  *$\rho_0(\beta S - \alpha T)$ ), the density variability related to changes of ocean salinity ( $\rho_S = \rho_0\beta S$ ) and to*  
 704 *that of ocean temperature ( $\rho_T = -\rho_0\alpha T$ ).  $S_{800}$ ,  $\omega$  and water density are taken with the opposite*  
 705 *sign for better visibility. The data are averaged over the study region and normalized by*  
 706 *subtracting the respective mean and dividing on the respective standard deviation. Water*  
 707 *density in panels (b, d) is given for April, while in panel (c) it is averaged over the pre-DC*  
 708 *season. Panels (a, b) present unsmoothed values and panels (c, d) – the 3-year sliding means*  
 709 *over the current year and two preceding years.*

710



711

712 *Fig. 5. Time-mean temperature (°C, panels a,c) and salinity (panels b,d) averaged over the*  
 713 *upper 500-m layer (ARMOR3D data-set). Upper panels – T was averaged over the whole*  
 714 *period of 1993-2016 and lower panels – over the DC season (January to April) only. The 2°C*  
 715 *isotherm (panels a, c) and the 34.9 isohaline (panels b, d) are shown for October (upper panels)*  
 716 *and January (lower panels) for selected years (see legend in the figures). The*  
 717 *isotherm/isohalines are computed from temperature and salinity distributions, averaged over*  
 718 *the upper 500-m layer. The thick grey dashed contour indicates the study region. The black*  
 719 *dashed line is the mean winter edge of sea ice (PIOMAS data-set). Thin grey lines are the 500-*  
 720 *m and 2500-m isobaths.*

721

### 722 4.3. Heat fluxes

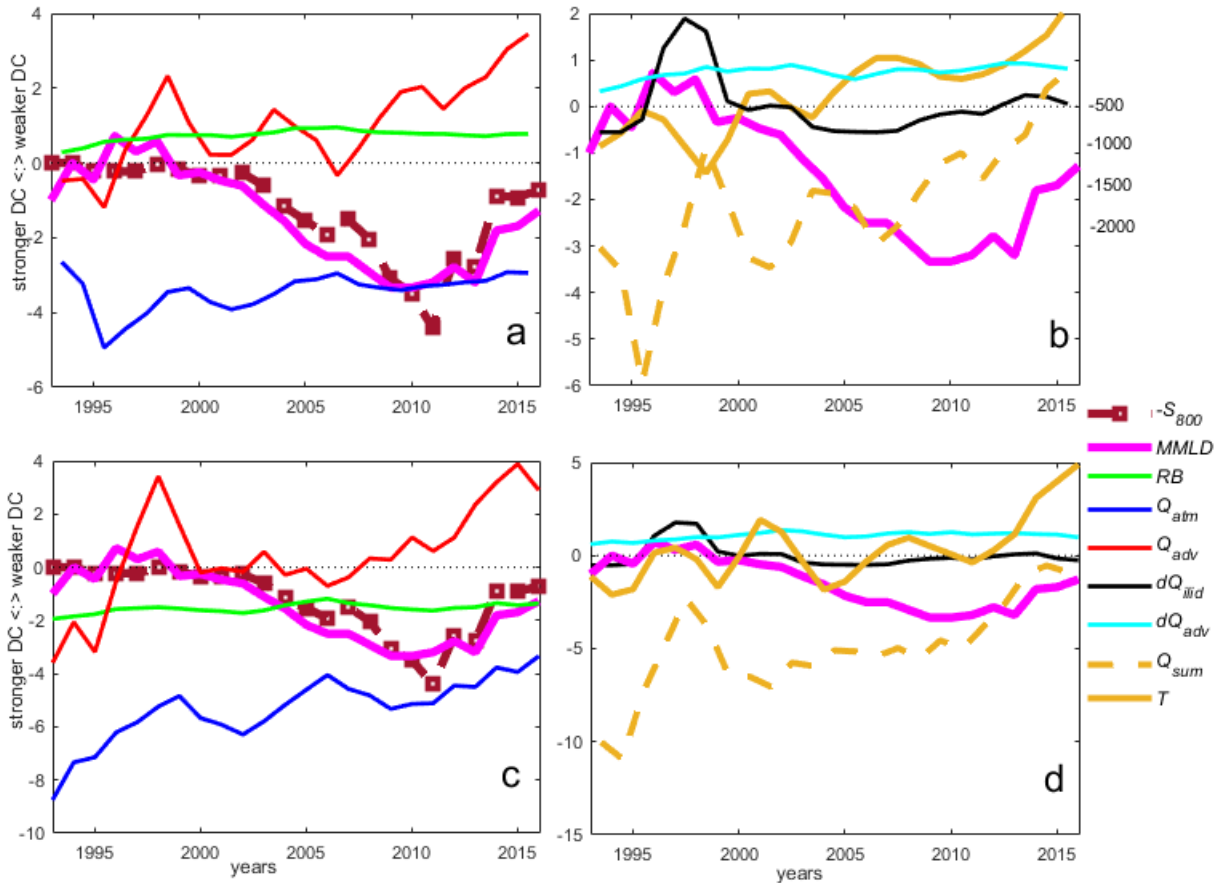
723

724 In this Section we investigate the interannual variability of the dominant heat and freshwater  
 725 fluxes, which may affect the DC intensity. The heat fluxes considered are (Fig. 6, Table 2): net  
 726 radiative flux ( $RB$ ), net air-sea heat exchange ( $Q_{atm}$ ) and the convergence of the heat fluxes in  
 727 the upper ocean ( $Q_{adv}$ ).

$$728 \frac{dQ}{dt} = RB + Q_{atm} + Q_{adv} + Q_{resid} \quad (7)$$

729 For the ice-covered grid cells, deduced from the NSIDC sea ice concentration data, we assume  
 730  $Q_{atm}=0$ . The term  $Q_{adv}$ , represents the bulk warming or cooling of the upper 500-m layer due

731 to convergence of the oceanic heat transport. The horizontal heat flux associated with mesoscale  
 732 eddies is relatively small in the region, less than 1 TW (from our preliminary analysis not  
 733 presented here), compared to 3-6 TW coming with the advective transport. The advective flux  
 734 is referenced to water temperature of the Greenland Sea Intermediate/Deep Water ( $T_{ref}$ , Section  
 735 3.2). Thus, the negative values favour a possible thermal instability of the water column. The  
 736 vertical diffusive or convective flux, as well as the horizontal eddy heat flux form the residual  
 737 term ( $Q_{resid}$ ).  
 738



739

740 *Fig. 6. Interannual variability of mean heat fluxes (TW): (a-b) at the end of the pre-DC season*  
 741 *(August-December), (c-d) during the DC season (January to April).  $Q_{atm}$  is the sensible plus*  
 742 *latent heat fluxes to the ocean,  $dQ_{iiid}$  – the effect of ice lid on the ocean-atmosphere heat*  
 743 *exchange, RB– the radiation balance,  $Q_{adv}$  –the convergence of oceanic heat advection,  $dQ_{adv}$  –*  
 744 *the mean vertical gradient of  $Q_{adv}$  (see text for details).  $Q_{sum}$  is the sum of  $Q_{atm}$ , RB and  $Q_{adv}$*   
 745 *(right panels). All fluxes are normalized by the standard deviation of  $Q_{atm}$  for the pre-DC*  
 746 *season; positive values favour vertical stability in the upper ocean.  $T$  is the mean temperature*  
 747 *in the upper 500-m layer (relative units, right panels). Positive fluxes lead to stabilization of*  
 748 *the upper part of the water column, decreasing the DC intensity. The DC intensity is*  
 749 *represented with the MMLD and  $S_{800}$  (taken with the opposite signs, relative units). The right*  
 750 *scale in panel (b) presents the MMLD in meters.*

751

752 Table 2. Heat fluxes (TW), mean values and standard deviations (std). Positive values of the  
753 variables lead to stabilization of the water column in the upper ocean. Note that, as in Fig. 6,  
754 higher values of  $MMLD$  or  $S_{800}$  signify a weaker DC intensity. Thus, positive correlations in  
755 the table means that the heat input into the ocean flux decreases the DC intensity. Grey cells  
756 mark the dominating fluxes with high interannual variability or with a significant correlation.  
757 The significant correlations were estimated using the effective degrees of freedom computed as  
758  $N_{ef}=(1-r)\cdot N$  (Thomson and Emery, 2014), where  $r$  is the correlation coefficient and  $N$  is the  
759 number of years. CV is the coefficient of variation which is the standard deviation (std)  
760 normalised by the mean value. The pre-DC season is from June to December, the DC season is  
761 from January to April. Statistics are obtained from the 3-year sliding averages of the seasonal  
762 means. See Table 4 in Supplement 7 for the corresponding density fluxes.

fluxes	mean $\pm$ std, monthly means	mean $\pm$ std pre-DC season means (3year smoothed)	mean $\pm$ std DC season means (3 year smoothed)	CV DC season (%)	Correl. with $MMLD$ ( $S_{800}$ ), pre- DC/DC seasons
$RB$ (to the ocean)	2.3 $\pm$ 11.2	4.0 $\pm$ 0.7	-4.6 $\pm$ 0.5	10%	-0.6/-0.4 (-0.5/-0.2)
$Q_{atm}$ (to the ocean)	-10.3 $\pm$ 7.6	-10.2 $\pm$ 1.5	-15.8 $\pm$ 3.7	22%	-0.5/-0.5 (-0.3/-0.4)
$Q_{adv}$ (0-500 m)	4.1 $\pm$ 12.9	3.2 $\pm$ 3.5	1.5 $\pm$ 5.6	1040%	-0.4/-0.1 (-0.3/-0.2)
$Q_{adv1}$ (500-1000 m)	2.3 $\pm$ 4.4	1.9 $\pm$ 1.3	0.5 $\pm$ 2.4	480%	0.2/-0.1 (0,0/0.0)
$Q_{adv2}$ (0-1000 m)	6.4 $\pm$ 16.8	5.1 $\pm$ 4.8	2.0 $\pm$ 8.0	400%	-0.3/-0.1 (0,2/0.0)
$dQ_{adv} =$ $dQ_{adv}/dz$ [up-low]	0.8 $\pm$ 0.7	0.8 $\pm$ 0.1	1.2 $\pm$ 0.2	16%	-0.2/0.2 (0.0/0.0)
$dQ_{ilid}$	0.4 $\pm$ 1.7	0.4 $\pm$ 0.5	1.0 $\pm$ 1.3	130%	0.5/0.5 (0.4/0.3)

763

764



765 For the time-averaged fluxes, the upper ocean heat loss to the atmosphere ( $Q_{atm}$ ) clearly  
766 dominates the upper ocean heat balance (Table 2). The oceanic heat is released to the  
767 atmosphere all year round, being particularly strong in winter (Figs. 3a and 6a,c). In the climatic  
768 annual mean,  $Q_{adv}$  in the upper 500-m layer, the second largest term in the right-hand side of  
769 Eq.(7), is twice the heat coming from  $RB$  (though  $RB$  strongly exceeds  $Q_{adv}$  during the DC  
770 season). The  $Q_{adv}$  and  $RB$  in their annual means oppose  $Q_{atm}$  and favour a decrease of the DC  
771 intensity. Together these two heat fluxes compensate about 60% of  $Q_{atm}$ , while if we account  
772 for the heat convergence by ocean advection in the upper 1000 m this is up to 90%. As  $MMLD$   
773 exceeds 1000 m for 75% of the winters, this deeper layer should rather be considered for  
774 estimating the heat balance in the study region. The situation radically changes during the DC  
775 season, when both  $RB$  and  $Q_{atm}$  destabilise the water column and strongly exceed  $Q_{adv}$ .

776 The high importance of  $Q_{atm}$  for the seasonal variability of DC in the Greenland Sea, makes  
777 many researchers consider  $Q_{atm}$  as the main driver for the DC interannual variability (Jones  
778 and Marshall, 1993; Bailey et al, 2005; Falina and Sarafanov, 2015; Moore et al., 2015; Yang  
779 et al, 2016). However, the standard deviation (and the coefficient of variation) of the interannual  
780 variability of  $Q_{adv}$  exceeds that of  $Q_{atm}$  almost by a factor of two in winter and by a factor of  
781 three in summer (Table 2). These ratios further increase, if the oceanic heat flux convergence  
782 is integrated down to 1000 m. This suggests that, the interannual variability of  $Q_{adv}$  may have  
783 a higher importance for the variability of the upper ocean stratification on the interannual time  
784 scales than that of  $Q_{atm}$ .

785 Since 1993, both  $Q_{atm}$  and  $Q_{adv}$  show positive trends, which result in an overall increase of  
786  $Q_{sum}$  over the time period from 1993 to present (Fig. 6b,d). This is consistent with the increase  
787 of the upper ocean temperature in the study region (Fig. 6b,d). This long-term temperature trend  
788 is less pronounced in winter (there is practically no trend, except during 5 years at the end of  
789 the study period, Fig. 6d). We assume that, in winter, large  $Q_{atm}$  and  $RB$  effectively abate  
790 interannual variations of  $Q_{adv}$  (see Fig. 5c and Supplement 7.4).

791 In addition to  $Q_{adv}$ , accounting for a possible thermal convective instability below the upper  
792 500-m layer, we also estimate the effect of the convergence of oceanic advective heat fluxes on  
793 the static stability of the upper 500-m layer ( $dQ_{adv}$ ). The  $dQ_{adv}$  is defined as  
794  $\partial Q_{adv}/\partial z$  averaged over the upper 500-m layer. Positive values of  $dQ_{adv}$  suggest stronger  
795 warming in the upper part of the layer (due to the horizontal heat advection) relative to the  
796 lower one. Always positive values of  $dQ_{adv}$  signify that the ocean heat advection stabilizes the  
797 upper 500-m of the water column all year round (Table 2, Figs. 6b,d). However, the coefficient  
798 of variation of  $dQ_{adv}$  is low, suggesting a small relative interannual variability of this parameter  
799 and a minor role of this effect in the interannual variability of DC.

800 The correlation of most of the heat fluxes with the  $MMLD$  ( $S_{800}$ ) are predominantly negative.  
801 Therefore, an increase of the DC intensity during the study period coincides with more heat  
802 absorbed by the upper ocean (Table 2), which is counterintuitive. For an explanation we direct  
803 the reader to Supplement 7.4 and discussion below.

804 The hypothesis of Moore et al (2015) on the possible variability of DC intensity due to the  
805 modification of  $Q_{atm}$  by the ice cover in the central Greenland Sea, is examined by introducing  
806 an additional variable  $dQ_{iild}$ . To single out the effect of the ice-lid,  $dQ_{iild}$  is computed as the  
807 difference between the possible latent and sensible heat fluxes over the sea ice covered areas,  
808 computed as if the sea ice is absent, and the previously estimated  $Q_{atm}$ , which takes into account  
809 a real ice cover. The positive values of  $dQ_{iild}$  account for the suppression of the DC by the ice  
810 cover. On average, the effect of ice cover ( $dQ_{iild}$ ) is small, compared to other terms of the heat  
811 balance (Table 2), and it does not explain the long-term tendencies in the DC intensity (Fig.  
812 6b,d). However, episodically  $dQ_{iild}$  might become important. Thus, during the winters of  
813 1996/1997 and 1997/1998 (Fig. 6), the anomalously weak DC corresponds to the anomalously

814 big Oden ice tongue projecting far into the central Greenland Sea (Comiso et al., 2001; Germe  
 815 et al., 2011). The interannual variability of the Odden ice tongue is linked to the wind direction,  
 816 mostly intensified during the negative North Atlantic Oscillation (NAO) phase (Germe et al.,  
 817 2011). The long-term tendencies in  $dQ_{iid}$  may also be shaped by the intensity of the oceanic  
 818 heat advection with RAW, which becomes weaker at the negative NAO phase (Selyuzhenok et  
 819 al., 2020), though we did not find a clear indication of this link within the study period.

820 To conclude, all heat fluxes, except  $dQ_{iid}$ , are weakly or inversely correlated with the *MMLD*  
 821 ( $S_{800}$ ). A long-term increase of the heat input into the study region, which goes in parallel with  
 822 an increase of the upper ocean temperature, contradicts the observed intensification of the DC  
 823 during the 2000s (Fig. 6). This counterintuitive “reaction” of the *MMLD* results from its  
 824 dependence on the freshwater fluxes (see Section 4.2), while the main freshwater fluxes are  
 825 inversely correlated with the heat fluxes. For example, the major source of the interannual  
 826 variability of the upper ocean heat content,  $Q_{adv}$ , is inversely correlated with the  $FW_{adv}$  (-0.54),  
 827 i.e. the oceanic heat and salt transport in the region increases/decreases simultaneously (see also  
 828 Supplement 7.4). The freshwater fluxes are discussed in the next section.

829

#### 830 **4.4. Freshwater fluxes**

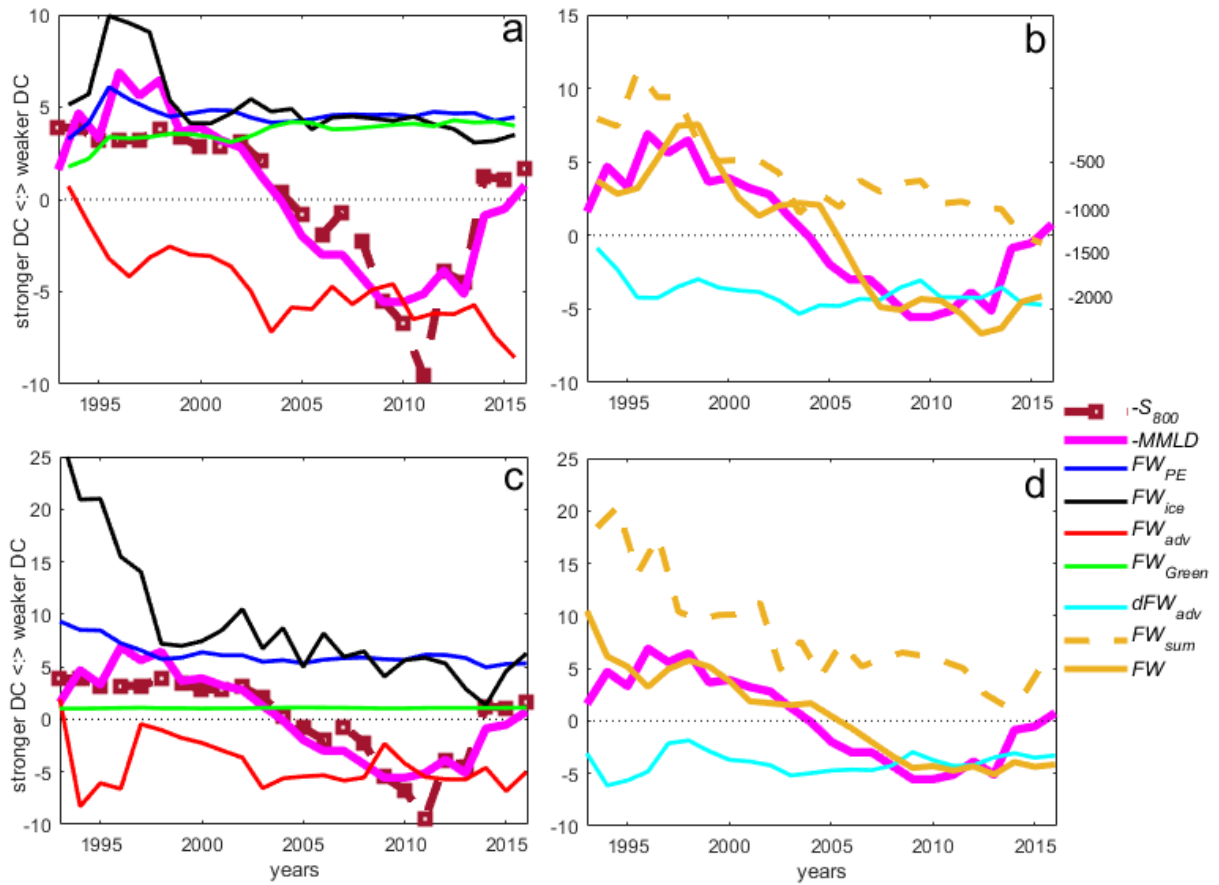
831

832 Components of the Greenland Sea freshwater budget are net precipitation ( $FW_{PE}$ ), net sea ice  
 833 melt ( $FW_{ice}$ ) and convergence of the freshwater advection in the upper ocean ( $FW_{adv}$ ):

$$834 \frac{dFW}{dt} = FW_{PE} + FW_{ice} + FW_{adv} + FW_{resid}. \quad (8)$$

835 The first three terms on the right-hand side of Eq. (8) are approximately of the same order of  
 836 magnitude (Fig. 7, Table 3). The convergence of advective freshwater fluxes between 500 and  
 837 1000-m is negligibly small compared to  $FW_{adv}$  in the upper 500-m layer. The freshwater from  
 838 the Greenland Ice Sheet ( $FW_{Green}$ ) is listed in Table 3 for reference. It does not affect the central  
 839 areas of the study region, as all the meltwater is advected out of the sea by the EGC  
 840 (Dukhovskoy et al., 2019). Thus,  $FW_{Green}$  is not included in the following analysis.

841 One can easily see (Table 3) that positive  $FW_{PE}$  and  $FW_{ice}$  are not balanced by the negative  
 842  $FW_{adv}$ , neither in the annual nor in the seasonal means. Therefore, unlike the residual heat flux,  
 843  $FW_{resid}$  has the same order of magnitude as each of the terms in right-hand side of Eq. (8) (on  
 844 average 5 mSv, ranging from 0 to 10 mSv). The  $FW_{resid}$  includes the vertical freshwater  
 845 exchange due to convection or vertical mixing and the deep water outflow below 1000 m, as  
 846 well as the eddy transport. These fluxes are largely uncertain. In particular, the vertical mixing  
 847 during the DC episodes effectively redistributes the freshwater over the water column  
 848 (Dukhovskoy et al., 2019). The freshwater further outflows from the study region at 1000-2000  
 849 m as the Greenland Sea Deep Water (see, for example, Jochumsen et al., 2012; Buckley and  
 850 Marshall, 2016; Kovalevsky and Bashmachnikov, 2020). Available estimates suggest that the  
 851 total freshwater outflow from the Greenland Sea may exceed 100 mSv (Vage et al., 2013;  
 852 Chafik and Rossby, 2019). Even though 95% of the outflow belongs to the upper ocean (Vage  
 853 et al., 2013), the remaining 5 mSv at depth are sufficient to close the balance.



854

855 *Fig. 7. Interannual variability of mean freshwater fluxes (mSv): (a-b) by the beginning of the*  
 856 *DC season (August-December), (c-d) during the DC season (January to April).  $FW_{PE}$  is the*  
 857 *precipitation minus evaporation,  $FW_{ice}$  – the freshwater from ice melt/freezing,  $FW_{adv}$ –the*  
 858 *convergence of oceanic freshwater advection,  $FW_{Green}$  – the freshwater from melt of Greenland*  
 859 *ice cap in the Greenland Sea,  $dFW_{adv}$  – the mean vertical gradient of  $FW_{adv}$  (see text for details).*  
 860  *$FW_{sum}$  is the sum of  $FW_{PE}$ ,  $FW_{ice}$  and  $FW_{adv}$  (right panels). All fluxes are normalized by the*  
 861 *standard deviation of  $FW_{PE}$  for the pre-DC season; positive values favour vertical stability in*  
 862 *the upper ocean. The regional mean salinity anomaly ( $FW$ , relative units, higher values means*  
 863 *a fresher water) is presented in the right panels. Positive fluxes lead to stabilization of the upper*  
 864 *part of the water column, decreasing the DC intensity. The DC intensity is represented with*  
 865 *MMLD and  $S_{800}$  (taken with the opposite signs, relative units).*

866

867

868 Table 3. Freshwater fluxes ( $\text{mSv}=10^3 \text{ m}^3 \text{ s}^{-1}$ ), mean values and standard deviations (std).  
869 Positive values lead to stabilization of the water column in the upper ocean. Note that, as in Fig.  
870 7, higher values of  $MMLD$  or  $S_{800}$  signify a weaker DC intensity. Thus, positive correlations in  
871 the table means that the freshwater input into the ocean decreases the DC intensity. Grey cells  
872 mark the dominating fluxes with high interannual variability or the significant correlations. The  
873 significant correlations were estimated using the effective degrees of freedom (see Table 2).  
874 The pre-DC season is from June to December, the DC season is from January to April. Statistics  
875 are obtained from the 3-year sliding averages of the seasonal means. When multiplied by the  
876 factor of 3, the freshwater fluxes (in  $\text{mSv}$ ) have the same effect on water density as the heat  
877 fluxes (in TW) from Table 2. See Table 4 in Supplement 7 for the corresponding density fluxes.

types of fluxes	mean $\pm$ std, monthly means	mean $\pm$ std pre-DC season means (3year smoothed)	mean $\pm$ std DC season means (3 year smoothed)	CV DC season (%)	Correl. with $MMLD$ ( $S_{800}$ ), pre-DC/DC seasons
$FW_{Green}$	$3.8 \pm 4.9$	$3.7 \pm 0.5$	$1.1 \pm 0.0$	5%	-0.7/-0.4 (-0.6/-0.2)
$FW_{PE}$	$4.7 \pm 2.3$	$4.6 \pm 0.5$	$6.2 \pm 1.1$	18%	0.3/0.4 (0.1/0.4)
$FW_{ice}$	$5.1 \pm 8.6$	$5.1 \pm 1.9$	$9.0 \pm 6.3$	70%	<b>0.7/0.5</b> (0.4/0.5)
$FW_{adv}$ (0-500 m)	$-5.1 \pm 9.2$	$-4.5 \pm 2.3$	$-4.4 \pm 2.4$	55%	<b>0.6/0.3</b> (0.5/0.2)
$FW_{adv1}$ (500-1000 m)	$0.04 \pm 1.1$	$0.1 \pm 0.4$	$0.50 \pm 0.50$	100%	0.2/0.3 (0.2/0.3)
$FW_{adv2}$ (0-1000 m)	$-5.1 \pm 9.9$	$-4.4 \pm 2.5$	$-3.9 \pm 2.7$	70%	<b>0.6/0.3</b> (0.5/0.3)
$dFW_{adv} = dFW_{adv}/dz[\text{up-low}]$	$-1.4 \pm 1.4$	$-1.3 \pm 0.3$	$-1.3 \pm 0.4$	31%	0.2/0.1 (0.1/0.0)

878

879

880 The interannual variability of the net freshwater flux is dominated by the  $FW_{adv}$  and  $FW_{ice}$ ;  
881 the variability of each of these fluxes exceeds two to six times that of  $FW_{PE}$  (Table 3).

882 High positive correlations of  $FW_{ice}$  and  $FW_{adv}$  with the  $MMLD$  (Table 3) suggest an expected  
883 decrease of the DC intensity with a higher freshwater input. However, these two freshwater  
884 fluxes are not independent. We found a positive correlation of  $FW_{ice}$  with the oceanic heat  
885 inflow to the region in the upper 100-m (the correlation coefficient is 0.45). A previously  
886 derived coupling of an increase of the ice volume and RAW inflows into the Greenland Sea  
887 favours a stronger ice melt in the study region during these episodes (Selyuzhenok et al., 2020,  
888 see also Fig. 7a,c). Further, a stronger RAW advection also destabilises the upper water column  
889 and uplifts deeper warm RAW water to the ocean surface which increases the ice melt  
890 (Selyuzhenok et al., 2020; see also Section 4.3 and Supplements 7.5-7.6).

891 In spite of an increase in the ice melt, the annual mean salinity in the DC region has been  
892 increasing since 1993 (Fig. 4c,d, note the reverse vertical axis in the figure). An increase of  
893 water salinity in the DC region could be attributed to a stronger advection of RAW (Fig. 5c,d).  
894 Negative all the year round, the absolute value of  $FW_{adv}$  starts exceeding  $FW_{ice}$  (in the annual  
895 mean) after the beginning of the 2000s (Fig. 7a,c). The decreasing effect of the ice melt on the  
896 DC intensity during the 2000s is also due to a westwards retreat of the marginal ice zone,  
897 towards the EGC, with an increase of the sea-surface in the Greenland Sea (Selyuzhenok et al.,  
898 2020; see also Fig. 6b). With the EGC, a stronger outflow of the sea ice meltwater from the  
899 study region is observed (Fig. S2e). As a result, the joint decrease of  $FW_{adv}$  and  $FW_{ice}$  during  
900 the 2000s (Fig. 7a,c) leads to the positive salinity trend in the study region and a stronger DC  
901 intensity (Fig. 4c,d).

902 To summarize, oceanic advection of salt with the RAW appears to be the most important factor  
903 in controlling the long-term interannual variability of DC intensity in the Greenland Sea during  
904 the study period (see also Fig. 5). A relatively small effect of heat advection compared to the  
905 freshwater (salt) advection in the overall upper ocean density advection into the study region is  
906 discussed in Supplement 7.7. A synergy of the extent of the ice cover and of the upper ocean  
907 RAW advection may also be responsible for an episodic year-to-year variation in the DC  
908 intensity (via variability  $FW_{ice}$  and  $dQ_{iild}$ ). However, overall  $FW_{ice}$  is concentrated in the  
909 western part of the DC region and does not affect the areas of the most frequent DC  
910 development (Fig. S2e).

911

#### 912 **4.5 The transient forcing of extratropical cyclones and polar lows**

913

914 Besides the mean heat release from the ocean to atmosphere, the extreme heat release, which  
915 may be linked to cyclonic activity, can be a factor in the interannual variability of DC. In  
916 cyclones the vertical heat fluxes from the ocean can grow several times compared to the climatic  
917 means and cyclones can trigger fast DC development (Kovalevsky et al., 2020). Over the course  
918 of the 24-year study period, 325 long lived cyclones covering at least 20% of the DC area that  
919 translated over the region were identified (Hodges 1995, 1999; Hoskins and Hodges 2002). For  
920 every cyclone within the study region, the sensible and latent heat fluxes to the atmosphere  
921 were estimated using the Coupled Ocean–Atmosphere Response Experiment algorithm  
922 (COARE 3.5; Fairall et al., 2003). The resulting mean and integral heat flux in the cyclones  
923 inside the DC region (as well as in its sub-region with the maximum DC frequency – Fig. 1a)  
924 were recorded.

925 The extreme vertical heat winter fluxes in the cyclones reached 400-500 W m<sup>-2</sup>, compared to  
926 about 100 W m<sup>-2</sup> of the winter regional average. However, the mean winter heat fluxes over all  
927 cyclones of 115 W m<sup>-2</sup> was close to the regional mean and only in about half of the recorded

928 cyclones the regional mean values were exceeded. The absence of a statistically significant  
929 increase of mean heat fluxes in a cyclone has been noted previously for the North Atlantic  
930 (Rudeva and Gulev, 2011).

931 To explore any relation with the DC intensity, the air-sea heat fluxes in the cyclones were  
932 integrated in time from the beginning of November of the previous year until the month of the  
933 maximum *MMLD* event. The sensitivity tests showed that the choice of the starting month for  
934 the integration within the pre-DC season (August to December) had almost no impact on the  
935 results. Another calculation was performed in the same way, but the heat fluxes were integrated  
936 only over those cells, where combined sensible and the latent heat fluxes exceeded the  
937 corresponding monthly mean value. Correlation between the interannual variability of  
938 integrated heat fluxes and of *MMLD* did not exceeded 0.3-0.4 (at maximum being of marginal  
939 significance). Similar values are obtained when considering only cyclones within the smaller  
940 region of the most frequent DC (Fig. 1a). To better assess the influence of cyclones with  
941 extreme heat fluxes on DC intensity, we computed monthly mean and monthly maximum heat  
942 fluxes in the cyclones for both, values integrated over the areas of the cyclones and the not  
943 integrated ones. Next, mean and maximum values over the period of integration were correlated  
944 with the interannual variability of *MMLD*. The resulting correlations were also low, with about  
945 0.4 for the case when mean values are used and about 0.3 when using maximum values. Overall,  
946 this indicates only a weak dependence of the interannual DC intensity on variations in cyclone-  
947 induced ocean-atmosphere heat exchange.

948 The role of mesoscale atmospheric patterns on the DC intensity, however, requires further  
949 investigation. In particular, in some case studies extremely high heat fluxes were observed in  
950 the transition zones between cyclones and anticyclones (Lui et al., 1997). In addition, polar  
951 lows, which are short-lived intense mesoscale cyclones, are also observed in the DC region  
952 (Rasmussen and Turner, 2003). To assess their possible influence on the DC intensity we used  
953 a satellite-derived polar low list available for 1995-2009 (Smirnova et al., 2015). The analysis  
954 considered polar lows that occurred from November to the month of the maximum *MMLD*  
955 event. Over the 14-year period, a total of 56 polar lows that covered at least 20% of the DC  
956 region area were identified. The number of events might be insufficient for deriving a  
957 meaningful statistical relationship between the air-sea heat fluxes in the polar lows and the DC  
958 intensity. Therefore, the identified polar lows were combined with the data set of extratropical  
959 cyclones to deduce the relationship between the air-sea fluxes and the DC intensity. This  
960 approach, however, did not result in higher correlation (compared to the array of extratropical  
961 cyclones only presented in the previous paragraph). The mean heat fluxes in polar lows of 122  
962  $\text{W m}^{-2}$  were close to the regional mean values, although slightly higher than in extratropical  
963 cyclones. Only in 30 cases, the mean fluxes exceed the monthly mean values. It should be noted  
964 that polar lows are poorly resolved in ERA-Interim leading to substantial negative bias in the  
965 maximum wind speeds in the cyclones (e.g., Smirnova and Golubkin, 2017), which apparently  
966 results in underestimated air-sea heat fluxes. Condron and Renfrew (2013) found substantial  
967 influence of polar mesocyclones on DC in the Nordic seas using model experiments forced with  
968 atmospheric reanalysis wind fields corrected by implementing a parameterization of Rankine  
969 vortices to better represent polar mesocyclones. However, their number of artificially  
970 parameterized polar mesocyclones in the North Atlantic (about 2000 per year) far exceeds the  
971 annual mean polar low numbers found in satellite-based studies (e.g., less than 50 in Golubkin  
972 et al. (2021) for a slightly larger area). Overall, given the small number of polar lows over the  
973 DC region (about 4 per season, as has been derived from the available data-sets), we assume  
974 their negligible impact on the interannual variability of the DC intensity.

975 Cyclones may additionally affect the DC intensity via  $FW_{PE}$  or ice advection by wind. We  
976 found that the interannual variations of  $FW_{PE}$  in the cyclones were small, compared to other  
977 parameters of the freshwater balance (Table 3) and did not to have a significant effect on the

978 DC intensity. There are also practically no correlations with the DC intensity (below 0.2) of the  
979 number of cyclones, or of the total time when the cyclones were observed over the DC region.  
980 Therefore, in spite of several understudied effects, we assume the overall small effect of  
981 cyclones on the interannual variability the intensity of DC in the Greenland Sea.

982

## 983 **5. Summary and Discussion**

984

985 Various mechanisms have been suggested to govern the interannual variability of the intensity  
986 of DC in the Greenland Sea such as the cyclonic circulation in the central Greenland Sea (Clarke  
987 and Gascard, 1983), upper ocean cooling associated with intense air-sea heat fluxes (Marshall  
988 and Schott, 1999; Moore et al., 2015; Yang et al, 2016), presence of sea ice reducing the air-  
989 sea heat exchange (Mysak et al., 1990; Moore et al., 2015; Vage et al., 2018), the oceanic  
990 buoyancy advection into the central Greenland Sea (Johannessen et al. 1991; Alekseev et al.,  
991 2001; Zang et al., 2004; Dickson et al., 2008; Glessmer et al., 2014; Lauvset et al., 2018;  
992 Brakstad et al., 2019), the sea ice and the Greenland Ice Sheet melt (Dukhovskoy et al., 2016).  
993 Two main problems in understanding the major mechanisms driving the interannual variability  
994 of DC in the Greenland Sea can be highlighted.

995 The first problem is the choice of a robust metric that realistically quantifies the interannual  
996 variability of the DC. A low number of available in situ vertical profiles may result in wrong  
997 interannual tendencies in the intensity of DC (Fedorov and Bashmachnikov, 2020). In Fedorov  
998 and Bashmachnikov (2020) it has been demonstrated that the number of in situ vertical profiles  
999 in the Greenland Sea is sufficient for the estimation of interannual variability of the *MMLD*  
1000 with at least 25% accuracy (250 m for *MMLD*= 1000 m) for 85% of the years since 1993. In  
1001 this study we use the ARMOR dataset, which benefits from combining individual in situ  
1002 profiles with satellite data (see Section 2.1). This increases the robustness of the final gridded  
1003 fields. Compared to GLORYS and SODA, ARMOR shows a shallower maximum convection  
1004 depth (Table 1). This is presumably due to insufficient in situ data for deep layers replaced by  
1005 climatological hydrographic fields below 1500 m in the ARMOR dataset. Nevertheless, the  
1006 tendency in interannual variability of the *MMLD* in the Greenland Sea since 1993, derived from  
1007 the *MMLD* of ARMOR, is reproduced in the ocean reanalysis products (SODA, GLORYS), as  
1008 well as various complementary indices: the integral density (Bashmachnikov et al., 2019) and  
1009 the deep water temperature (Alekseev et al., 2001). In this study, the robustness of these  
1010 tendencies is additionally supported by  $S_{800}$  metrics, which are not affected by possible biases  
1011 in the deep ocean hydrography in ARMOR (the correlation between the  $S_{800}$  and the *MMLD* is  
1012 0.7 on monthly, as well as on interannual time scales). Various data sets and metrics of the DC  
1013 intensity show that the tendency for DC intensification from the 1990s to the end of the 2000s  
1014 and its further stabilization during the 2010s, are robust and can be used for analysis of the  
1015 related mechanisms.

1016 The long-term tendencies in the *MMLD* and  $S_{800}$  are governed by the variability of the upper  
1017 ocean (0-500 m) density (including that before the DC season) in the central Greenland Sea  
1018 (Fig. 4). In the subsurface layers, upward-doming isopycnal surfaces driven by the cyclonic  
1019 circulation in the Greenland Sea are considered as an important pre-convection condition that  
1020 determines the intensity of the deep convection in the following winter. However, this study  
1021 did not find any notable links between the interannual variability of the isopycnal depths in the  
1022 central Greenland Sea and the intensity of the DC during the study period (Section 4.2).

1023 Another problem is the strong association between the interannual variability of various heat  
1024 and freshwater fluxes, each of which may govern the interannual variability of the DC intensity.  
1025 The interannual variability of the upper ocean temperature or salinity reflects possible  
1026 imbalance of the heat or freshwater fluxes. We found that salinity plays the leading role in the

1027 interannual variability of the upper ocean density and the DC intensity (Section 4.2), whereas  
1028 the interannual variability of the upper ocean temperature is by far less important.

1029 The leading role of salinity, advected into the Greenland Sea with the RAW, in modifying the  
1030 density of the upper Greenland Sea has been noted in several studies (Johannessen et al., 1991;  
1031 Alekseev et al., 2001; Marnela et al., 2013; Glessmer et al., 2014; Deshayes et al., 2014; Boning  
1032 et al., 2016; Lauvset et al., 2018). There are two reasons for this. First, we found an effective  
1033 damping of the variability of the oceanic heat transport, the flux with the largest amplitude of  
1034 interannual variations among the heat fluxes in the study region. The magnitude of the oceanic  
1035 heat flux variability is strongly abated before it reaches the convective sites in the Greenland  
1036 Sea, reducing its impact on the DC. Second, the ratio  $\frac{\beta_s}{\alpha_t}$  in the subpolar regions is five times  
1037 that in the tropics. This demonstrates a relatively large effect of water salinity on the variability  
1038 of water density in the subpolar areas (see also Ferreira et al., 2018). Therefore, among the  
1039 number of interlinked fluxes, the mechanisms of the DC variability should be primarily  
1040 governed by the freshwater fluxes (see Table 4). The buoyancy fluxes are considered not only  
1041 within the DC season, but also accumulated during the preceding warm period.

1042 Among the main freshwater fluxes ( $FW_{PE}$ ,  $FW_{adv}$ ,  $FW_{ice}$  and  $FW_{Green}$ ), interannual variations  
1043 of the oceanic freshwater advection ( $FW_{adv}$ ) and of the ice melt ( $FW_{ice}$ ), are found to be the  
1044 most important for the interannual variability of the DC intensity in the Greenland Sea (Section  
1045 4.4). In the upper 500-m layer, advection of salt increases towards the sea-surface, which leads  
1046 to a decrease of stability of the water column. The negative  $FW_{adv}$ , on average, leads to a  
1047 salinification of the upper ocean, while the positive  $FW_{ice}$  – to its freshening (Figs. 5, 7 and  
1048 S2e). The tendency for salinification of the upper ocean in the central Greenland Sea during the  
1049 2000s (Fig. 4b,d) corresponds to a tendency for  $FW_{adv}$  to become more negative and to a  
1050 decrease of  $FW_{ice}$  in the study region over the 24 year period of the study (Fig. 7a,c). This study  
1051 develops further the results by Johannessen et al. (1991), Alekseev et al. (2001), Dickson et al.  
1052 (2008), Chatterjee et al. (2018), where the role of RAW in forming the salinity of the upper  
1053 Greenland Sea was highlighted. Here we showed the role of RAW in shaping the long-term  
1054 interannual variability of DC through the analysis of the variability of the major heat and  
1055 freshwater fluxes in the region. The intensity of the RAW inflow into the region is regulated by  
1056 water transport, as well as by the thermohaline water properties in the WSC (Chatterjee et al.,  
1057 2018), while its effect on the variability of  $FW_{adv}$  (and  $Q_{adv}$ ) in the study region through the  
1058 RAW recirculation, as well as the degree of RAW modification along the recirculation branches  
1059 with the Polar Water still remains to be understood.

1060 We also found that during the years of intensive DC, ice meltwater from the Greenland Ice  
1061 Sheet ( $FW_{Green}$ ) also increases (Table 2). The correlation coefficients between the variables  
1062 are high (0.7), although the Greenland ice melt water only weakly affects its central areas  
1063 (Dukhovskoy et al., 2019). We suggest that this link can be induced by a more intensive warm  
1064 and salty RAW advection in the shelf of Greenland. Entering the Greenland shelf below the  
1065 Polar water, the stronger heat flux accelerates the melt of Greenland glaciers (Johannessen et  
1066 al., 2011, 2013).

1067 The yearly main heat fluxes ( $RB$ ,  $Q_{atm}$ ,  $Q_{adv}$ ), forming the variability in water temperature in  
1068 the DC region, on average are in an approximate balance. Contrary to what has been suggested  
1069 in a number of other studies, the interannual variability of the oceanic heat release to the  
1070 atmosphere appears to be far less important for the interannual variability of the heat balance  
1071 than  $Q_{adv}$ , even during the DC season. Thus, our results show that the interannual variation of  
1072  $Q_{atm}$  are significantly smaller than those of  $Q_{adv}$ , in spite of  $Q_{adv}$  (even in its autumn extreme)  
1073 that forms only about 30% of  $Q_{atm}$ .

1074 The two fluxes in the study region are linked as the correlations between winter  $|Q_{atm}|$  and  
1075  $|Q_{adv}|$  varies from -0.6 (detrended) to -0.8 (original). The heat, advected by the ocean, is



1076 effectively released to the atmosphere by way of the RAW to the DC region. From one side,  
1077 this decreases the effect of  $Q_{adv}$  on the upper ocean density in the study region. In fact, the  
1078 winter variability of upper 500-m water density, advected across the northern boundary into the  
1079 study region, is a function of water salinity (the correlation coefficient is 0.77) and is very  
1080 weakly linked to water temperature (the correlation coefficient is -0.12) (Fig. S5 in Supplement  
1081 7.7). From the other side,  $Q_{adv}$  affects the interannual variability of  $Q_{atm}$  over the study region.  
1082 There is a clear tendency for the air temperature and humidity to increase in time. The increase  
1083 is particularly strong over the pathway of the RAW, in particular north and east of the study  
1084 region (see Fig. S3a,c in Supplement 7.4). The warmer more humid air is further spread over  
1085 the study region by the northerly winds (Fig. S3b), which decreases the heat release by the  
1086 ocean (Fig. S3d). As a result of such a link, the increasing  $Q_{adv}$  leads to a decrease of  $Q_{atm}$  in  
1087 the areas of the most frequent DC development since 1993. The tendencies in both fluxes result  
1088 in an increase of the upper ocean temperature in the areas of the DC development (Fig. 6).  
1089 However, temperature does not play the leading role in the long-term variability of the DC  
1090 intensity during the study period (Fig. 4).

1091 The ice cover may have a double effect on the DC intensity – through baring the ocean-  
1092 atmospheric exchange ( $dQ_{ilid}$ ) and through contributing to the freshwater balance of the  
1093 melting/freezing ice ( $FW_{ice}$ ). The  $FW_{ice}$  is not only one of the largest terms in the freshwater  
1094 balance of the central Greenland Sea, it also strongly correlates with the DC intensity. However,  
1095 the direct effect of  $FW_{ice}$  is mostly limited to the western part of the region (Fig. S2d). In the  
1096 eastern area of the most frequent development of the DC, the mean effect of  $FW_{ice}$  decreases  
1097 by an order of magnitude. This freshwater is concentrated at the very sea-surface and the way  
1098 it spreads over the central Greenland Sea is not well understood.

1099 On the contrary, during the study period, the effect of  $dQ_{ilid}$ , on average, is small (Table 2).  
1100 However, during some winters,  $dQ_{ilid}$  may decrease the ocean heat flux to the atmosphere by  
1101 as much as 30-50% (Table 2, Fig. 6). Since 1993, during the 24 years of the study period, this  
1102 happened for only two winters (of 1996/1997 and of 1997/1998), but it might happen more  
1103 frequently before 1993 with the development more often of the Oden ice tongue (Comiso et  
1104 al., 2001; Germe et al., 2011). On the other hand, both  $dQ_{ilid}$  and  $FW_{ice}$  are partly shaped by  
1105  $Q_{adv}$  and  $Q_{atm}$  and cannot be considered fully independent variables.

1106 The annual mean  $Q_{atm}$ ,  $Q_{adv}$  are strongly correlated with  $RB$  (0.7-0.8). Besides a stronger heat  
1107 release by the ocean surface ( $Q_{atm}$  and  $RB$ ) over the core of the RAW along the EGC (a larger  
1108  $Q_{adv}$ ), all three parameters may depend on a third factor. The oceanic advection in the Nordic  
1109 Seas intensifies with an intensification of the cyclonic atmospheric circulation around the  
1110 Icelandic minimum during the positive NAO phase (Yashayaev and Seidov, 2015; Chatterjee  
1111 et al., 2018; Selyuzhenok et al., 2020). Thus, the high correlation of ocean-atmosphere heat  
1112 exchange with the radiative heat fluxes (clouds) and with the intensity of ocean heat/freshwater  
1113 advection may all be a result of the intensification of the regional cyclonic wind pattern.

1114 The observed increase in the RAW advection, is consistent with the AMOC intensification in  
1115 the North Atlantic during the 1990s, followed by a certain AMOC slowdown in the 2010s  
1116 (Rahmstorf et al., 2015; Chen and Tung, 2018). However, we lack observations to verify this  
1117 link as the period since 2004, covered by RAPID observations, only shows a short period of  
1118 relatively stable AMOC intensity (Volkov et al., 2020). The possible link between the  
1119 convection and the RAW transport intensities suggests a possible positive feedback between  
1120 the AMOC on variability of the DC intensity in the Greenland Sea, previously described for the  
1121 Subpolar Gyre, i.e. Labrador and Irminger seas (Levermann and Born, 2007; Bower and von  
1122 Appen, 2008; Born et al., 2013). The intensified AMOC leads to a stronger RAW inflow in the  
1123 Nordic Seas, which increases the water salinity in the central Greenland Sea. The further  
1124 increase of the convection intensity presumably increases the dense water outflow through the  
1125 Denmark and the Faroe-Shetland straits. The possible existence of this feedback, though acting

1126 at much larger time scales, which includes convection in the Greenland Sea, has been derived  
1127 in some model studies (see, for example, Renold et al., 2010). At the time scales discussed in  
1128 this study, this hypothetical feedback can be abated and masked by numerous intermediate and  
1129 external effects. First, observed increase in salinity in the central Greenland Sea is counteracted  
1130 by the increasing upper ocean temperature (Brakstad et al., 2019). Although, the effect on water  
1131 density of the latter increase was smaller than that of salinity, as discussed above. Second, the  
1132 Greenland Sea Water formed during convection forms only a certain fraction of the AMOC  
1133 water outflow across the sills (see, for example, Hansen and Osterhus 2000; Våge et al., 2013;  
1134 Saberi et al., 2020). Third, recirculation of thermohaline anomalies masks the external  
1135 thermohaline forcing at decadal time scales (Eldvik et al., 2009). Finally, there are other  
1136 processes, besides DC, that regulate the AMOC intensity in the North Atlantic (see, for  
1137 example, a review in Buckley and Marshall, 2016). Further studies are needed to evaluate the  
1138 efficiency of this hypothetical feedback.

1139

## 1140 **6. Conclusions**

1141

1142 The main result of our study is that, during the most recent 24 years, the interannual variability  
1143 in the intensity of DC in the Greenland Sea has been governed by variations of the upper ocean  
1144 salinity. The latter is primarily regulated by oceanic salinity advection of the Re-circulating  
1145 Atlantic Water, accumulated since the end of the previous DC season and, to a lesser extent, by  
1146 winter freshwater fluxes from the melting ice. The variation of the ocean heat release to the  
1147 atmosphere due to its barring by the ice cover becomes important episodically, for the winters  
1148 with anomalously large and persistent Odden ice tongue (as during the winter of 1997).  
1149 Therefore, ocean advection has multiple effects on the intensity of deep convection in the  
1150 Greenland Sea (see also Kovalevsky and Bashmachnikov, 2020).

1151 Therefore, depending on the time scales different combinations of major factors govern the DC.  
1152 The climatic location with the most frequent and intense DC in the central Greenland Sea is a  
1153 result of a combined effect of the isopycnal rise and intensity of the winter heat loss of the upper  
1154 ocean. In this study we find that the long-term interannual variations of the DC intensity, at  
1155 least during the study period, are primarily linked to the ocean advection, in particular to the  
1156 freshwater advection. The synoptic and seasonal variability of the DC intensity should be  
1157 strongly influenced by the ocean heat release to the atmosphere, as noted before (Visbeck et al.,  
1158 1996; Kovalevsky et al., 2020), however this was out of the scope of this study.

1159

## 1160 **7. The Supplement**

1161

### 1162 7.1 Notations used in the text

1163

1164 *MMLD\** and *MMLD* – the maximum mixed layer depth and the normalized values of *MMLD\**,  
1165 respectively

1166  $S_{800}^*$  and  $S_{800}$  – the area over which the DC exceeds 800 m and the normalized values of  $S_{800}^*$ ,  
1167 respectively

1168 *RB* – the radiation balance, which is net shortwave (solar) and net longwave radiative fluxes

1169  $Q_{atm}$  – the sum of sensible and latent heat fluxes to the ocean

- 1170  $dQ_{lida}$  – the difference between the turbulent heat fluxes over the ocean with no sea-ice and  
 1171 over the ocean with the observed ice cover ( $Q_{atm}$ )
- 1172  $Q_{adv}$  – the heat convergence by oceanic advection in the layer 0-500 m
- 1173  $Q_{adv1}$  – the heat convergence by oceanic advection in the layer 500-1000 m
- 1174  $Q_{adv2}$  – the heat convergence by oceanic advection in the layer 0-1000 m
- 1175  $dQ_{adv} = dQ_{adv}/dz$  – the vertical gradient of  $Q_{adv}$  in the upper 500-m layer (up-low)
- 1176  $FW_{PE}$  – the precipitation minus evaporation
- 1177  $FW_{ice}$  – the freshwater flux from the sea ice
- 1178  $FW_{Green}$  – the freshwater flux from the Greenland Ice Sheet in the Greenland Sea (between  
 1179 73°N and the Fram Strait)
- 1180  $FW_{adv}$  – the freshwater convergence by oceanic advection in the layer 0-500 m
- 1181  $FW_{adv1}$  – the freshwater convergence by oceanic advection in the layer 500-1000 m
- 1182  $FW_{adv2}$  – the freshwater convergence by oceanic advection in the layer 0--1000 m
- 1183  $dFW_{adv} = dFW_{adv}/dz$  – the vertical gradient of  $FW_{adv}$  in the upper 500-m layer (up-low)
- 1184  $\alpha = 0.37 \cdot 10^{-4} \text{ } ^\circ\text{C}^{-1}$  – the coefficients of the thermal expansion
- 1185  $\beta = 7.74 \cdot 10^{-4}$  – the coefficients of the salt contraction
- 1186 All fluxes above are positive when heat (freshwater) is directed into the study region.

1187

## 1188 7.2 Comparison of ARMOR results with GLORYS and SODA ocean reanalyses

1189

1190 Figure S1 presents the dependence between the  $MMLD^*$  and  $S_{800}^*$ , derived from the data  
 1191 assimilating ocean general circulation models GLORYS and SODA. GLORYS has 1/12°  
 1192 spatial resolution, and the daily fields were averaged to monthly values. The reanalysis is based  
 1193 on LIM2 EVP NEMO 3.1, with an active ice block. SODA has 1/2° spatial grid and monthly-  
 1194 mean fields. The reanalysis is based on MOM5 ocean model and SIS1 active ice model. We  
 1195 used the SODA version, forced by ERA-Interim atmospheric reanalysis. Both ocean models  
 1196 assimilate satellite information for sea-surface temperature and salinity, as well as vertical  
 1197 temperature and salinity profiles. SODA additionally assimilates data from ocean moorings,  
 1198 while GLORYS assimilates the absolute dynamic topography from the satellite altimetry.

1199 Both models show a higher maximum MLD of about 2500-3000 m (Fig. S1), compared to 1500  
 1200 m in ARMOR, which is due to a weaker stratification and a higher variability of the low-  
 1201 stratified Greenland Sea Deep Water in the model results. However, the interannual and inter-  
 1202 monthly variations of the  $MMLD^*$  (and of  $S_{800}^*$ ) in the models present similar long-term  
 1203 tendencies for the DC intensification from mid-1990s to the end of 2000s, as in ARMOR. The  
 1204 correlation coefficient for the monthly  $MMLD^*$  and for the monthly  $S_{800}^*$  over the 96 winter  
 1205 months are: ARMOR- GLORYS 0.50 and 0.76, ARMOR-SODA 0.31 and 0.15, GLORYS-  
 1206 SODA 0.42 and 0.37, respectively. Using K-mean cluster analysis the data were split into 3  
 1207 clusters with moderate, intermediate and high DC intensity (Fig. S1). For GLORYS more than  
 1208 65% of the monthly points in  $MMLD^*$ -  $S_{800}^*$  space belong to the same clusters, as for ARMOR

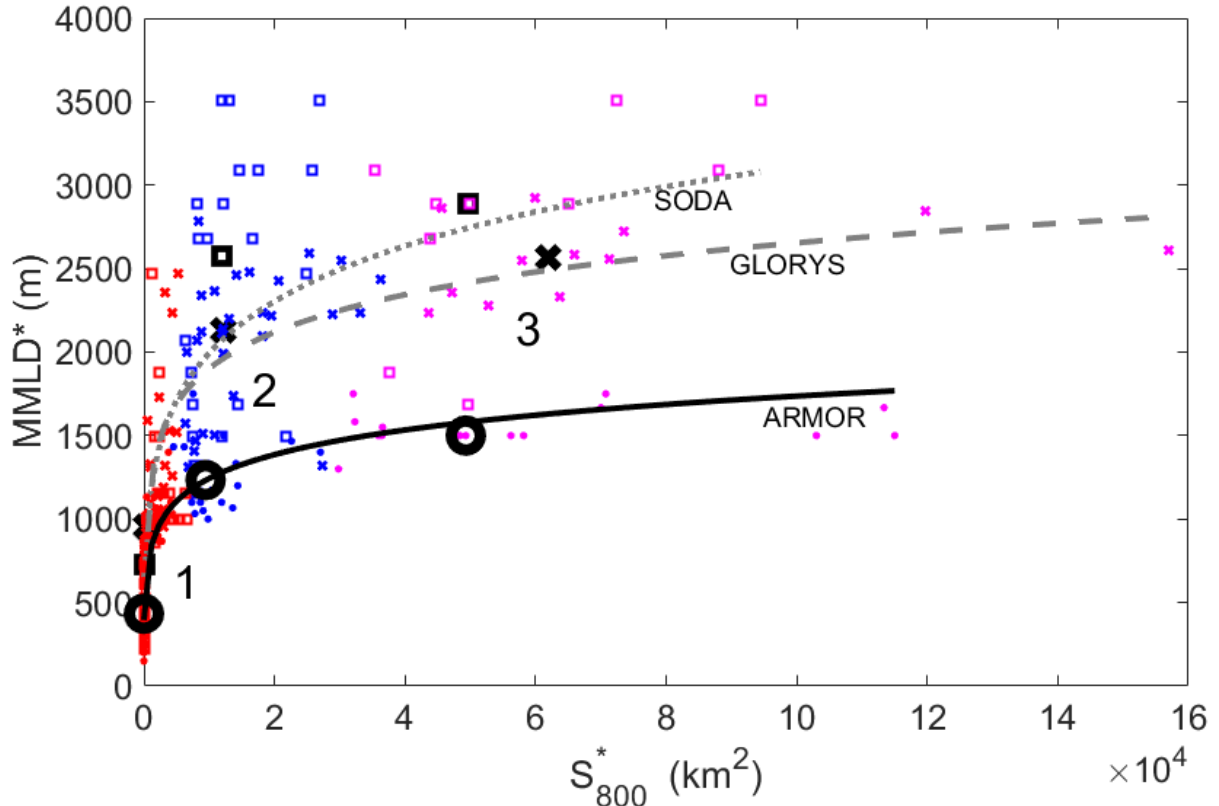
1209 data. The results show that ARMOR and GLORYS show very similar interannual and inter-  
 1210 monthly variations, although the details of the both differ from those in SODA.

1211 All data-sets show the similar logarithmic dependence between  $S_{800}^*$  and  $MMLD^*$ , differing  
 1212 mostly in the amplitude parameters:

1213 ARMOR:  $MMLD^* = 44.5 * (\ln(S_{800}^* + 72.8))^{3/2}; R^2=0.47;$

1214 GLORYS:  $MMLD^* = 67.9 * (\ln(S_{800}^* + 84.7))^{3/2}; R^2=0.53;$

1215 SODA:  $MMLD^* = 71.7 * (\ln(S_{800}^* + 41.2))^{3/2}; R^2=0.48;$



1216

1217 *Figure S1. Cluster analysis for monthly maximum mixed layer depth ( $MMLD^*$ ) and the square*  
 1218 *of the area with MLD over 800 m ( $S_{800}^*$ ): ARMOR3D – dots, GLORYS – crosses and SODA –*  
 1219 *squares. Cluster 1 – red, cluster 2 – blue, cluster 3 – magenta. The logarithmic approximations*  
 1220 *are overlaid. The cluster centroids for each of the data-set are marked with the corresponding*  
 1221 *marker.*

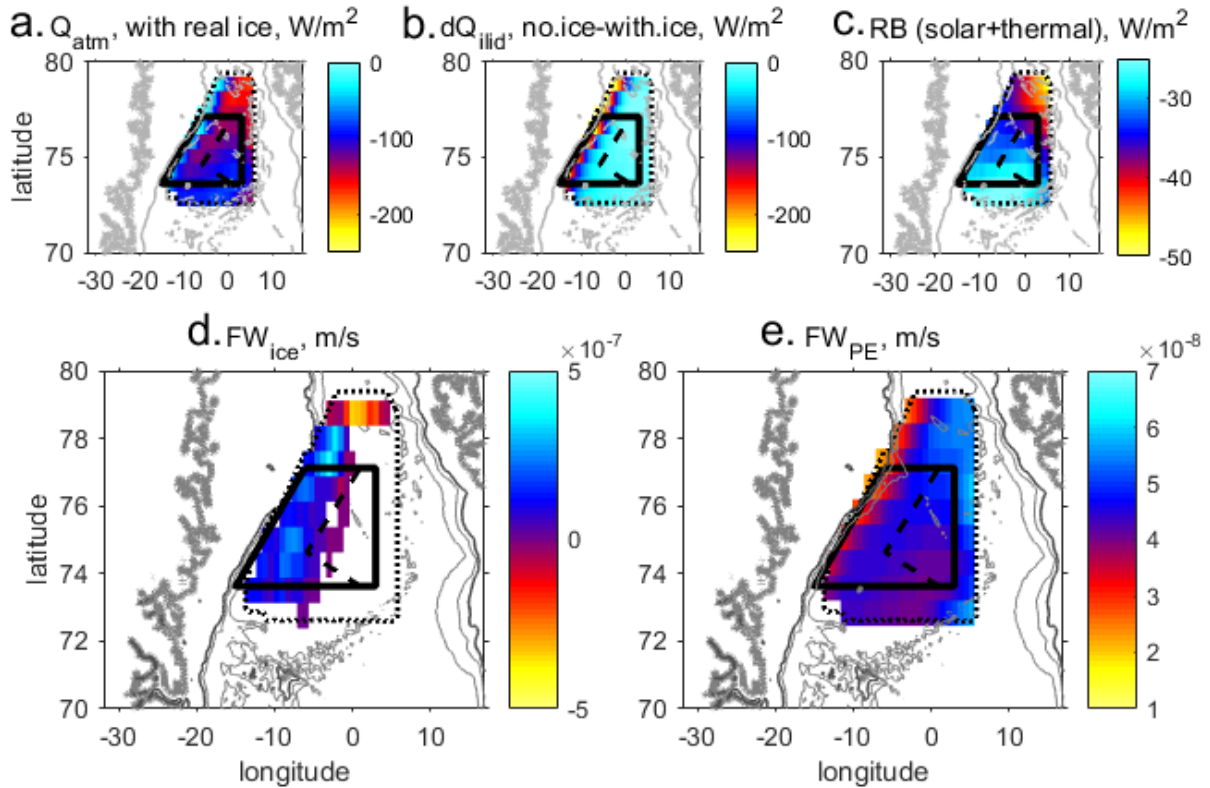
1222

### 1223 7.3 Spatial distributions of sea-surface fluxes in the Greenland Sea

1224

1225 The mean spatial distributions of heat and freshwater fluxes through the sea-surface, averaged  
 1226 over all the DC seasons (January to April), show an increase of the sensible and latent heat  
 1227 fluxes ( $|Q_{atm}|$ ) in the north of the region and seawards of the Greenland shelf (Fig. S2a),  
 1228 supporting the previously suggested link between the intensity of  $Q_{atm}$  and the presence of the  
 1229 warmer Recirculating Atlantic Water. The effect of the ice lid in shaping the heat fluxes to the  
 1230 atmosphere ( $dQ_{iuid}$ ) for an average winter is concentrated along the Greenland shelf and only  
 1231 marginally affecting the DC region (Fig. S2b). However, for some years, an anomalous ice  
 1232 extent (Odden ice tongue) may affect the DC intensity. The winter  $RB$  is negative, dominated  
 1233 by the long-wave radiation from the ocean surface (Fig. S2c). Similar to  $|Q_{atm}|$ , it increases  
 1234 north-eastwards, towards the warmer water and away from the typical DC areas.

1235 The freshwater from ice melt ( $FW_{ice}$ ) is observed only in the western part of the DC region and  
 1236 is mostly positive even during winter (Fig. S2d). Together with  $dQ_{liid}$ , it should inhibit DC in  
 1237 the western part of the DC region. This explains why the DC is most often observed in the  
 1238 central and eastern parts of the Greenland Basin. However, it is not clear to what degree  $FW_{ice}$   
 1239 influences the eastern areas with the most frequent DC.  $FW_{PE}$  is positive over the whole region  
 1240 (Fig. S2e, precipitation exceeds evaporation). Although its peak values at all grid-points are  
 1241 negligibly small compared to  $FW_{ice}$ , when averaged over the whole region, the inputs of both  
 1242 fluxes in the freshwater balance are of the same order of magnitude (Figs. 3b, 7).



1243

1244 *Fig. S2. The spatial distributions of heat fluxes (a-c,  $W m^{-2}$ , positive – to the ocean) and of*  
 1245 *freshwater fluxes (d-e,  $m s^{-1}$ , positive – to the ocean), averaged over the DC season (January*  
 1246 *to April) of the study period: a) sensible and latent heat fluxes with realistic ice cover from*  
 1247 *NSIDC; b) the same as (a), but with ice cover artificially removed; c) heat flux from the*  
 1248 *radiation balance (short and long wave); d) the freshwater flux from melting/forming sea ice;*  
 1249 *e) the freshwater input from precipitation minus evaporation. The positive fluxes lead to an*  
 1250 *increase of the upper ocean stratification. Black solid quadrangles mark the study region,*  
 1251 *where the DC was observed, dashed line limit from the west the region with the most frequent*  
 1252 *DC events. Grey lines are 500-m and 2500-m isobaths.*

1253

#### 1254 7.4 On the inverse dependence of the MMLD with the RB and $Q_{atm}$

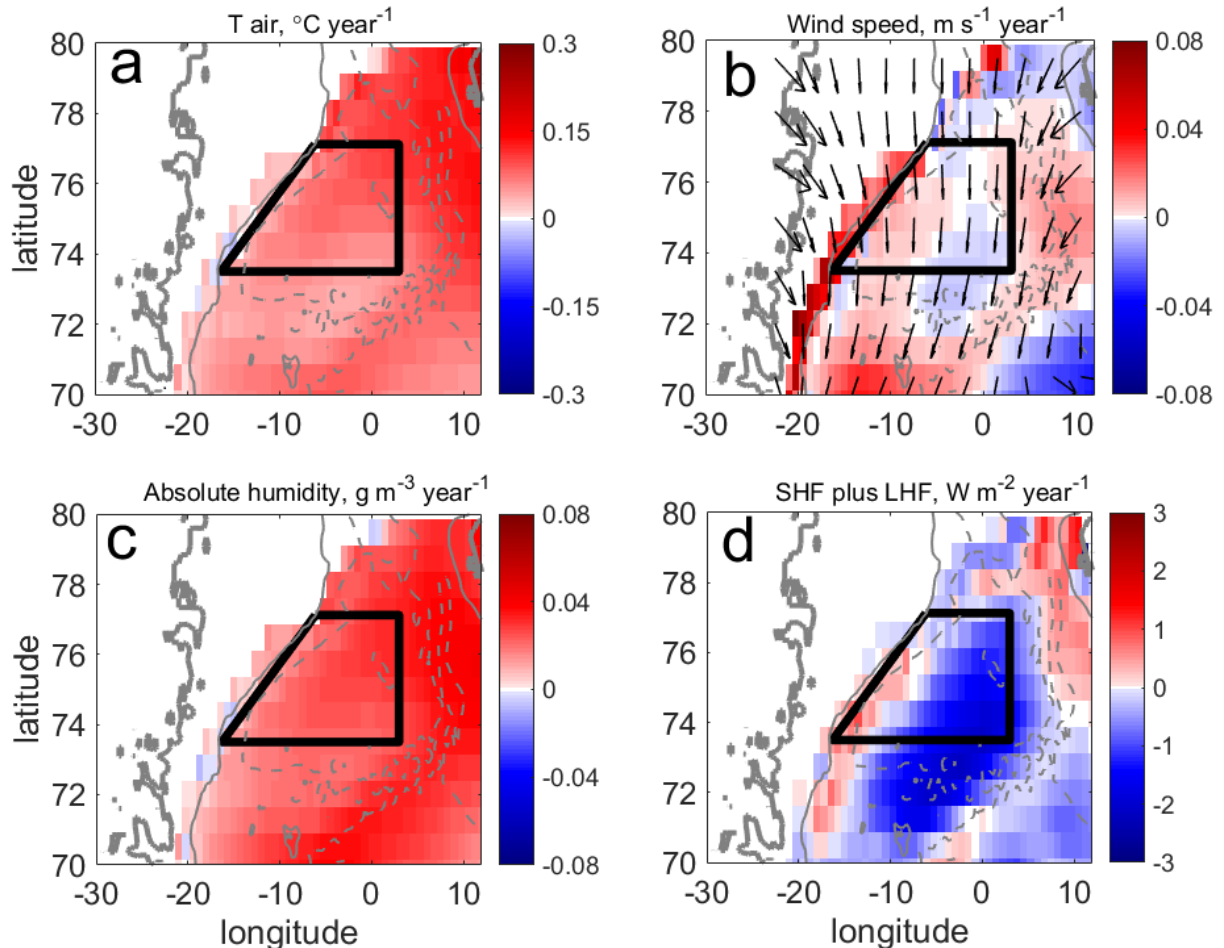
1255

1256 Correlations of  $Q_{atm}$  and RB with the MMLD are negative and significant, which is  
 1257 counterintuitive. We suppose that these correlations are induced and linked to the positive  
 1258 correlation of  $Q_{atm}$  with  $Q_{adv}$ .

1259 The negative interannual correlations of the MMLD with  $Q_{atm}$  can be, at least partly, induced  
 1260 by the interannual variability of  $Q_{adv}$ . Winter correlations between  $Q_{atm}$  and  $Q_{adv}$  are positive  
 1261 and significant (0.6-0.7). The decadal linear variations of  $Q_{atm}$  decrease (in their absolute  
 1262 value) together with an increase of  $Q_{adv}$ , mostly explain their correlation with the MMLD (Fig.

1263 6a,c). In the region of interest, a relatively modest increase of the air temperature and humidity,  
 1264 together with a certain decrease of the wind speed, compensates the SST increase and leads to  
 1265 a winter decrease of the area-mean  $|Q_{atm}|$  (Fig. S3). The same trends are observed in the annual  
 1266 means (not shown). In the study region, the air temperature increases not only due to the heat  
 1267 flux from the ocean, but also due to a decrease of the northerly winds (Fig. S3b), as well as due  
 1268 to a much stronger upwind air warming in the Fram Strait (Fig. S3a), which, at least partly, is  
 1269 supposed to be a result of the RAW warming west of Spitsbergen.

1270 The negative interannual correlations of the  $MMLD$  with the weakly varying  $RB$  is induced by  
 1271 the high correlation of  $RB$  with  $Q_{atm}$  (0.7-0.8). The latter correlation is presumably a result of  
 1272 a conjunction of wind speed (affecting sensible and latent heat fluxes) with cloud cover  
 1273 (affecting short and long-wave radiation balances).



1274 *Fig. S3. Winter (January to April) linear trends (1993-2016) in: (a) the air temperature ( $^{\circ}\text{C}$*   
 1275 *year $^{-1}$ ); (b) the wind speed ( $\text{m s}^{-1}$  year $^{-1}$ ) with the mean winter wind vectors overlaid; (c) the*  
 1276 *absolute humidity ( $\text{kg m}^{-3}$  year $^{-1}$ ); (d) absolute value of the sum of sensible and latent heat fluxes*  
 1277 *( $\text{W m}^{-2}$  year $^{-1}$ , positive is from the ocean);. Black solid quadrangles mark the study region with*  
 1278 *the most frequent DC events. Grey lines are 500-m and 2500-m isobaths.*  
 1279

1280

### 1281 7.5 On the dependence of the $FW_{ice}$ on $Q_{adv}$ and $dFW_{adv}$

1282

1283 The positive and significant correlation of  $FW_{ice}$  with the ocean heat advection in the upper  
 1284 100-m in the sea (0.45) is explained as follows. Most of the sea ice in the Greenland Sea is  
 1285 advected from the Arctic. Nearly all this ice melts in the Greenland Sea, as the ice volume  
 1286 leaving the Greenland Sea through the Denmark Strait is only 10% of that coming through the

1287 Fram Strait (in all seasons). The  $FW_{ice}$  depends on the sea ice volume entering through the  
1288 Fram Strait and on the amount of heat locally transmitted to the ice by the ocean and the  
1289 atmosphere. The first factor is a function of the wind speed and direction (Germe et al., 2011).  
1290 The long-term variations of the second factor primarily depends on the intensity of the oceanic  
1291 heat advection (Selyuzhenok et al., 2020). In Selyuzhenok et al. (2020) it has been also noted,  
1292 that increasing ice transport through the Fram Strait is observed together with an increase in the  
1293 oceanic heat advection into the Greenland Sea with the RAW from the WSC (see also Fig. 5).

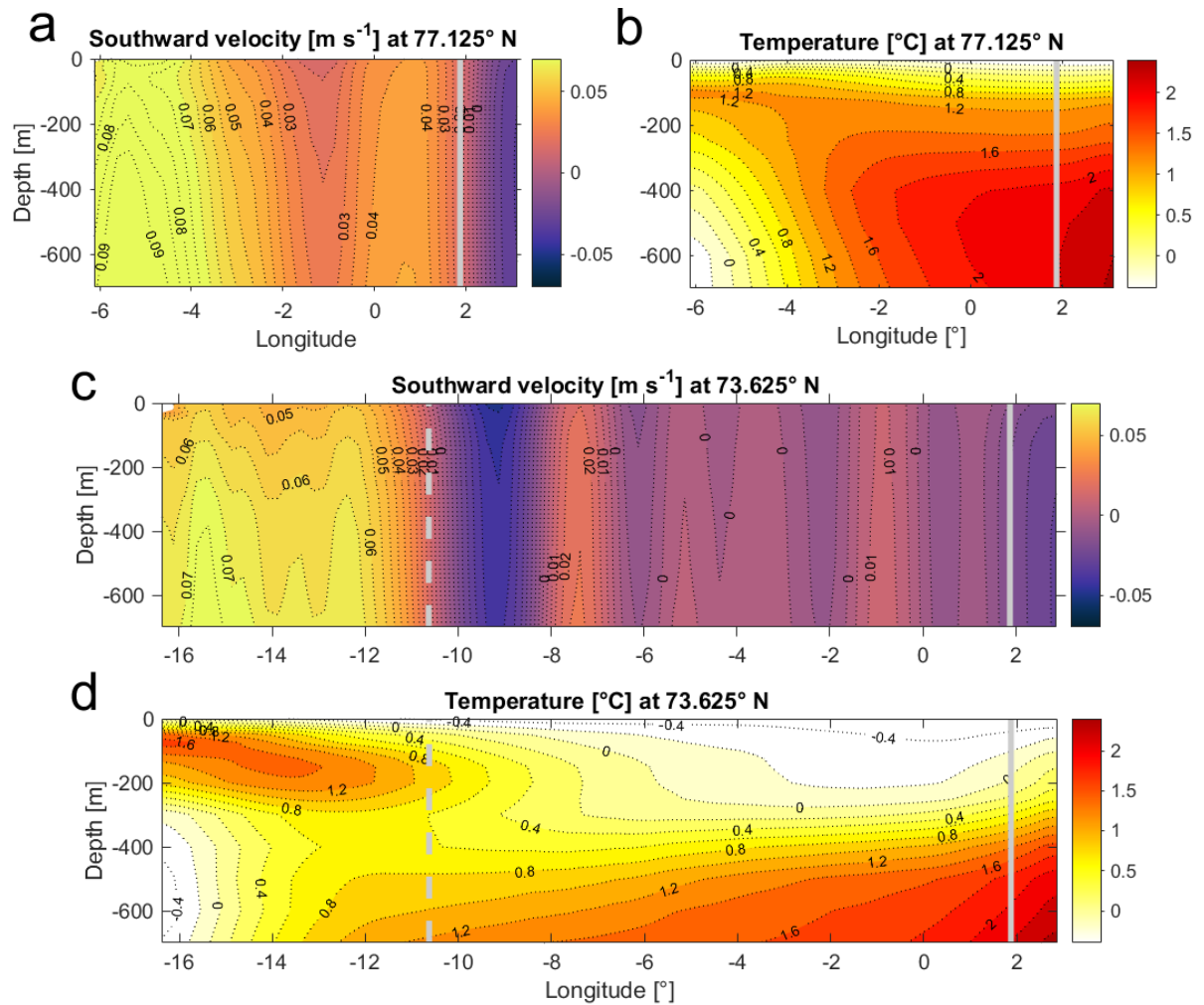
1294 Winter  $FW_{ice}$  is also positively correlated with the degree of instability of the upper part of the  
1295 water column ( $dFW_{adv}$ ) with the correlation coefficient of 0.50. This can be explained as  
1296 follows. The vertical gradient of the  $FW_{adv}$  in the upper 500-m layer ( $dFW_{adv}$ ) is always  
1297 negative (Figs. 3 and 7), i.e. the convergence of the oceanic freshwater advection also  
1298 destabilizes the upper 500 m of the water column. Already when entering the study region,  
1299  $Q_{atm}$  continues to effectively remove the sea-surface heat from the ocean, intensifying the  
1300 vertical mixing. Therefore, an increase  $FW_{adv}$  corresponds to an increase in the haline vertical  
1301 mixing which uplifts warm Atlantic water from below and intensifies the sea ice melt (see also  
1302 Selyuzhenok et al., 2020).

1303

#### 1304 7.6 Northern and southern sections of the study region

1305

1306 The northern and the southern boundaries of the study region are selected to limit the area with  
1307 the most frequent DC development (Fig. 1). The western boundary of the section passes along  
1308 the Greenland shelf-break. The topographically trapped southwards shelf-break branch of the  
1309 EGC is seen in the left parts of Figs. 1 and S4 (a,c). The eastern boundary is limited by the  
1310 northwards Norwegian Atlantic Front Current (Fig. 1 and grey solid lines in Fig.S4). In the  
1311 western parts of the northern and the southern sections (50-200 m), the southwards flowing  
1312 warmer Atlantic water, coming from the recirculation in the Fram Strait is seen (Fig. S4). The  
1313 southern section shows numerous northwards recirculations bring water from the coastally  
1314 trapped current into the DC region. The oceanic advection of heat ( $Q_{adv}$ ) and freshwater  
1315 ( $FW_{adv}$ ) is computed along these sections.



1316

1317 *Fig. S4. Time-mean southwards current velocity ( $m s^{-1}$ , panels a, c) and water temperature ( $^{\circ}C$ ,*  
 1318 *panels b, d) across the northern (a-b) and the southern (c-d) sections, limiting the study region.*  
 1319 *The dashed grey lines mark the time-mean eastern limit of the EGC and of the Atlantic water*  
 1320 *recirculation (for the northwards section this is also the eastern edge of the section). The solid*  
 1321 *grey lines mark the eastern edges of the sections.*

1322

1323 7.7 A relative importance of the heat and freshwater fluxes in the density flux into the Greenland  
 1324 Sea

1325

1326 The month-to-month water density advection in the study region (Fig. S5) shows a pronounced  
 1327 inverse dependence with the oceanic freshwater flux (with the correlation coefficient of -0.77),  
 1328 while it is practically independent of the oceanic heat flux (the correlation coefficient is -0.12).  
 1329 The  $Q_{adv}$  weakly influences the upper ocean density as it is effectively removed by  $Q_{atm}$   
 1330 already in the northern part of the region and goes to the sea ice melt (5 mSv of the melted ice  
 1331 corresponds to extraction of 1.5 TW of heat).

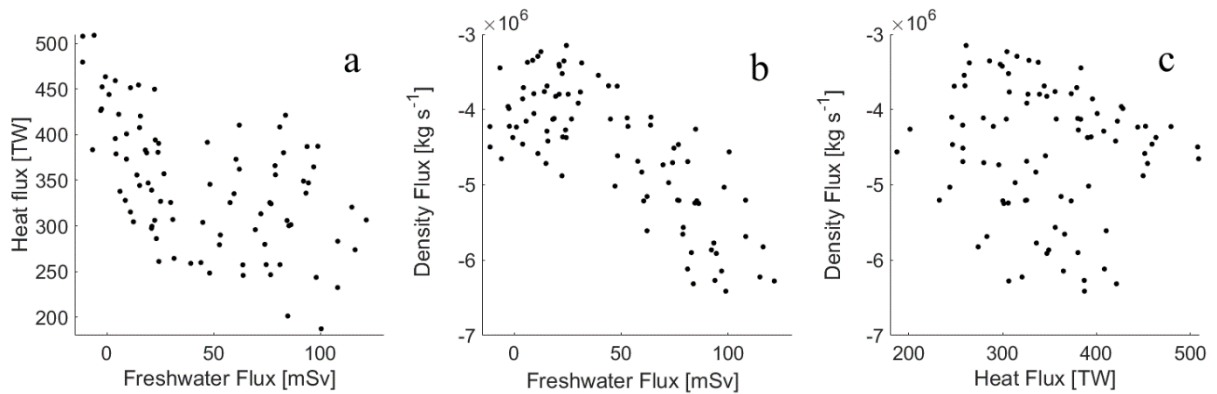
1332 A negative (though insignificant) correlation of  $Q_{adv}$  with the DC intensity, derived in Section  
 1333 4.3, therefore results from an increase of upper ocean density when a larger portion of the RAW  
 1334 (warmer, but what is more important – more saline) enters the study region.

1335



1336 Table 4 provides the budgets of the density fluxes, formed by the corresponding heat fluxes  
 1337 (Table 2) and freshwater fluxes (Table 3). The results show an overall higher effect of salinity  
 1338 of the variability of density fluxes into the upper Greenland Sea.

1339



1340

1341 *Fig. S5. Scatter diagrams of the oceanic advective fluxes through 77.1°N, averaged over the*  
 1342 *upper 500-m layer and accumulated since August of the previous year to the months in the DC*  
 1343 *season (January-April): (a) the heat advection versus the freshwater advection, (b) the density*  
 1344 *advection versus the freshwater advection, (c) the density advection versus the heat advection.*

1345

1346 Table 4. Upper ocean mean water density fluxes and their standard deviations at interannual  
 1347 time scales ( $\times 10^3 \text{ kg m}^{-3} \text{ s}^{-1}$ ) estimated from heat fluxes ( $DF_{RB}$  – from the radiation balance,  
 1348  $DF_{atm}$  – from the ocean-atmosphere heat exchange,  $DF_{T,adv}$  – from the oceanic heat advection in  
 1349 the upper 500m layer) and from freshwater fluxes ( $DF_{PE}$  – from the precipitation minus  
 1350 evaporation,  $DF_{ice}$  – from the ice melt minus ice formation at the sea-surface,  $DF_{S,adv}$  – from the  
 1351 oceanic freshwater advection in the upper 500m layer). See Tables 2 and 3 and Eqs.3-6. The  
 1352 global means are computed from the 3-year smoothed seasonal means for the pre-DC season  
 1353 (June to December) and the DC season (January to April). The fluxes are to the ocean, positive  
 1354 values means a water density increase.

From heat fluxes	$DF_T$ , pre-DC season	$DF_T$ , DC season	From freshwater fluxes	$DF_S$ , pre-DC season	$DF_S$ , DC season
$DF_{RB}$ (to the ocean)	$-37 \pm 6$	$42 \pm 5$	$DF_{PE}$	$-124 \pm 14$	$-167 \pm 30$
$DF_{atm}$ (to the ocean)	$94 \pm 14$	$146 \pm 34$	$DF_{ice}$	$-138 \pm 51$	$-243 \pm 170$
$DF_{T,adv}(0-500 \text{ m})$	$-30 \pm 32$	$-14 \pm 52$	$DF_{S,adv}(0-500 \text{ m})$	$122 \pm 62$	$119 \pm 65$
$DF_{RB} + DF_{atm} + DF_{adv}$	$28 \pm 53$	$174 \pm 90$	$DF_{PE} + DF_{ice} + DF$	$-140 \pm 127$	$-292 \pm 265$

1355

1356 **Acknowledgement:** The research was funded by Saint Petersburg State University (project  
 1357 N 75295423). D.S. Dukhovskoy was funded by the DOE (award DE-SC0014378).

1358

### 1359 References

- 1360 1. Alekseev G.V., Ivanov V.V., Korablev A.A. 1994. Interannual variability of the  
 1361 thermohaline structure in the convective gyre of the Greenland Sea. The Polar Oceans and Their  
 1362 Role in Shaping the Global Environment. Geophys. Monogr. Ser. 85, 485-496. AGU,  
 1363 Washington. doi:10.1029/GM085p0485.  
 1364 2. Alekseev, G.V., Bogorodskiy, P.V., Nagurny, A.P. 1989. Thermohaline structure of  
 1365 waters in the area with cyclonic circulation and upwelling. Structure and variability of  
 1366 largescale processes in the Norwegian zone of intensive ocean-atmosphere interactions (eds.  
 1367 Nikolayev, Yu.V., Alekseev, G.V.). Hydrometeoizdat., Leningrad. 37-43. (In Russian)

- 1368 3. Alekseev, G.V., Johannessen, O.M., Kovalevsky, D. V. 2001. On development of  
1369 convective motions under the influence of local density perturbations on the sea surface.  
1370 Izvestiya RAS. Atmospheric and ocean physics. 37 (3), 368-377. (In Russian)
- 1371 4. Alekseev, G. V., Johannessen, O. M., Korablev, A. A., Ivanov, V. V., Kovalevsky, D.  
1372 V. 2001. Interannual variability in water masses in the Greenland Sea and adjacent areas. Polar  
1373 Research. 20 (2), 201-208. <https://doi.org/10.1111/j.1751-8369.2001.tb00057.x>.
- 1374 5. Androsov, A., Rubino, A., Romeiser, R., Sein, D. V. 2005. Open-ocean convection in  
1375 the Greenland Sea: preconditioning through a mesoscale chimney and detectability in SAR  
1376 imagery studied with a hierarchy of nested numerical models. Meteorologische Zeitschrift. 14  
1377 (6), 693-702. <https://doi.org/10.1127/0941-2948/2005/0078>.
- 1378 6. Arbic, B. K., Scott, R. B., Chelton, D. B., Richman, J. G., Shriver, J. F. 2012. Effects of  
1379 stencil width on surface ocean geostrophic velocity and vorticity estimation from gridded  
1380 satellite altimeter data. J. Geophys. Res. 117, C03029. doi:10.1029/2011JC007367.
- 1381 7. Arthur, D., Vassilvitskii, S. 2007. k-means++: the advantages of careful seeding.  
1382 Proceedings of the Eighteenth Annual ACM-SIAM Symposium on Discrete Algorithms. 1027–  
1383 1035.
- 1384 8. Aubert, O., Le Bars, M., Le Gal, P., Marcus, P. S. 2012. The universal aspect ratio of  
1385 vortices in rotating stratified flows: experiments and observations. Journal of Fluid Mechanics,  
1386 706, 34-45. <https://doi.org/10.1017/jfm.2012.176>.
- 1387 9. Azetsu-Scott, K., Jones, E. P., Gershey, R. M. 2005. Distribution and ventilation of  
1388 water masses in the Labrador Sea inferred from CFCs and carbon tetrachloride. Marine  
1389 chemistry, 94 (1), 55-66. <https://doi.org/10.1016/j.marchem.2004.07.015>.
- 1390 10. Bamber, J., den Broeke, M., Ettema, J., Lenaerts, J., Rignot, E. 2012. Recent large  
1391 increases in freshwater fluxes from Greenland into the North Atlantic. Geophys. Res. Lett. 39,  
1392 L19501, doi:10.1029/2012GL052552.
- 1393 11. Bamber J.L., Tedstone, A.J., King, M.D., Howat, I.M., Enderlin, E.M., van den Broeke,  
1394 M.R., Noel, B. 2018. Land ice freshwater budget of the Arctic and North Atlantic Oceans: 1.  
1395 Data, methods, and results. Journal of Geophysical Research: Oceans, 123 (3), 1827-1837
- 1396 12. Bashmachnikov, I. L., Fedorov, A. M., Vesman, A. V., Belonenko, T. V., Koldunov, A.  
1397 V., Dukhovskoy, D. S. 2018. Thermohaline convection in the subpolar seas of the North  
1398 Atlantic from satellite and in situ observations. Part 1: Localization of the deep convection sites.  
1399 Sovremennye Problemy Distantionnogo Zondirovaniya Zemli iz Kosmosa. 15 (7), 184–  
1400 194. doi: [10.21046/2070-7401-2018-15-7-184-194](https://doi.org/10.21046/2070-7401-2018-15-7-184-194). (In Russian)
- 1401 13. Bashmachnikov, I. L., Fedorov, A. M., Vesman, A. V., Belonenko, T. V., Dukhovskoy,  
1402 D. S. 2019. Thermohaline convection in the subpolar seas of the North Atlantic from satellite  
1403 and in situ observations. Part 2: indices of intensity of deep convection. Sovremennye Problemy  
1404 Distantionnogo Zondirovaniya Zemli iz Kosmosa. 16 (1), 191–201. doi: [10.21046/2070-7401-  
1405 2019-16-1-191-201](https://doi.org/10.21046/2070-7401-2019-16-1-191-201). (In Russian)
- 1406 14. Bashmachnikov, I., Nascimento A., Neves F., Calheiros T., Koldunov N.V., 2015a.  
1407 Distribution of Intermediate Water Masses in the Subtropical Northeast Atlantic. Ocean  
1408 Science. 11, 803-827. doi:10.5194/os-11-803-2015.
- 1409 15. Bashmachnikov, I., Neves F., Calheiros T., Carton X., 2015b. Properties and pathways  
1410 of Mediterranean water eddies in the Atlantic. Progress in Oceanography. 137A, 149-172.  
1411 doi:10.1016/j.pocean.2015.06.001.
- 1412 16. Bashmachnikov, I., Sokolovskiy M.A., Belonenko T.V., Volkov D.L., Isachsen P.E.  
1413 Carton X. 2017. On the vertical structure and stability of the Lofoten vortex in the Norwegian  
1414 Sea. Deep-Sea Research I. 128, 1-27 <https://doi.org/10.1016/j.dsr.2017.08.001>
- 1415 17. Bashmachnikov, I.L., Volkov, D.L., Yurova, A.Yu., Bobylev L.P., 2016a. Interannual  
1416 variability of oceanic heat fluxes in the Atlantic Sector of the Arctic Ocean, U Arctic Congress,  
1417 12-16 of September. St.Petersburg, Russia
- 1418 18. Berry, D. I., Kent, E. C. 2009. A new air–sea interaction gridded dataset from ICOADS  
1419 with uncertainty estimates. Bulletin of the American Meteorological Society, 90(5), 645-656.

- 1420 19. Beszczynska-Möller A., von Appen W.-J., Fahrbach E. 2015. Physical oceanography  
1421 and current meter data from moorings F1-F14 and F15/F16 in the Fram Strait, 1997-2012.  
1422 PANGAEA. doi:10.1594/PANGAEA.150016.
- 1423 20. Beszczynska-Möller, A., Fahrbach E., Schauer U., Hansen E. 2012. Variability in  
1424 Atlantic water temperature and transport at the entrance to the Arctic Ocean, 1997–2010. ICES  
1425 Journal of Marine Science. 69 (5), 852–863. <https://doi.org/10.1093/icesjms/fss056>.
- 1426 21. Björk, G., Gustafsson, B. G., Stigebr and t, A. 2001. Upper layer circulation of the  
1427 Nordic seas as inferred from the spatial distribution of heat and freshwater content and potential  
1428 energy. Polar research. 20 (2), 161-168. <https://doi.org/10.1111/j.1751-8369.2001.tb00052.x>.
- 1429 22. Boning, C. W., Behrens, E., Biastoch, A., Getzlaff, K., Bamber, J. L. 2016. Emerging  
1430 impact of Greenland meltwater on deepwater formation in the North Atlantic Ocean. Nature  
1431 Geoscience. volume 9, pages 523–527.
- 1432 23. Bonisch, G., Blindheim, J., Bullister, J. L., Schlosser, P. Wallace, D. W. R. 1997. Long-  
1433 term trends of temperature, salinity, density and transient tracers in the central Greenland Sea.  
1434 J. Geophys. Res. 102(C8), 18553– 18571. doi:10.1029/97JC00740.
- 1435 24. Born, A., Stocker, T. F., Raible, C. C., Levermann, A. 2013. Is the Atlantic subpolar  
1436 gyre bistable in comprehensive coupled climate models? Climate dynamics. 40(11-12). 2993-  
1437 3007.
- 1438 25. Box, J. E., Bromwich, D. H., Bai, L. S. 2004. Greenland ice sheet surface mass balance  
1439 1991–2000: Application of Polar MM5 mesoscale model and in situ data. Journal of  
1440 Geophysical Research: Atmospheres. 109, D16105. doi:10.1029/2003JD004451.
- 1441 26. Bower A. S., von Appen W. J. 2008. Interannual variability in the pathways of the North  
1442 Atlantic Current over the Mid-Atlantic Ridge and the impact of topography, Journal of Physical  
1443 Oceanography. 38(1).104-120
- 1444 27. Broecker, W. S., 1987. The biggest chill. Natural History 97 (2): pp. 74-82
- 1445 28. Broecker, W. S., 1991. The great ocean conveyor. Oceanography, 4(2), 79-89.
- 1446 29. Brakstad, A., Våge, K., Håvik, L., Moore, G.W.K., 2019. Water mass transformation in  
1447 the Greenland Sea during the period 1986–2016. Journal of Physical Oceanography, 49(1),  
1448 pp.121-140.
- 1449 30. Buckley M. W., Marshall J. 2016. Observations, inferences, and mechanisms of Atlantic  
1450 Meridional Overturning Circulation variability: A review. Rev. Geophys. 54, 5-63.  
1451 doi:10.1002/2015RG000493.
- 1452 31. Budeus G., Schneider W., Krause G. 1998. Winter convective events and bottom water  
1453 warming in the Greenland Sea. J. Geophys. Res. 103 (C9), 18513– 18527.  
1454 doi:10.1029/98JC01563.
- 1455 32. Budeus G., Schneider W., Krause G. 1998. Winter convective events and bottom water  
1456 warming in the Greenland Sea. J. Geophys. Res. 103 (C9), 18513– 18527.  
1457 doi:10.1029/98JC01563.
- 1458 33. Chafik, L., Nilsson, J., Skagseth, O., Lundberg, P. (2015). On the flow of Atlantic water  
1459 and temperature anomalies in the Nordic Seas toward the Arctic Ocean. Journal of Geophysical  
1460 Research: Oceans, 120(12), 7897-7918.
- 1461 34. Chafik, L., Rossby, T. 2019. Volume, heat, and freshwater divergences in the subpolar  
1462 North Atlantic suggest the Nordic seas as key to the state of the meridional overturning  
1463 circulation. Geophysical Research Letters, 46(9), 4799-4808.
- 1464 35. Chatterjee, S., Raj, R.P., Bertino, L., Skagseth, Ø., Ravichandran, M., Johannessen,  
1465 O.M., 2018. Role of Greenland Sea gyre circulation on Atlantic water temperature variability  
1466 in the Fram Strait. Geophysical Research Letters, 45 (16), pp.8399-8406.
- 1467 36. Chen, X., Tung, K. K. 2018. Global surface warming enhanced by weak Atlantic  
1468 overturning circulation. Nature, 559(7714), 387-391.
- 1469 37. Chu, S., Gascard, J. C. 1991. Deep convection and deep water formation in the oceans.  
1470 57. Elsevier.

- 1471 38. Clarke, R. A., J.-C. Gascard, 1983: The formation of Labrador Sea water. Part 1: Large-  
1472 scale processes. *J. Phys. Oceanogr.*, 13, 1764-1788.
- 1473 39. Clarke, A., Swift, J. H., Reid, J.C., Koltermann, K. P. 1990. The formation of the  
1474 Greenland Sea Deep Water: double diffusion or deep convection. *Deep-Sea Res.* 37, 1385-  
1475 1424. [https://doi.org/10.1016/0198-0149\(90\)90135-I](https://doi.org/10.1016/0198-0149(90)90135-I).
- 1476 40. Comiso, J. C., Wadhams, P., Pedersen, L. T., Gersten, R. A. 2001. Seasonal and  
1477 interannual variability of the Odden ice tongue and a study of environmental effects. *J.*  
1478 *Geophys. Res.* 106(C5), 9093– 9116. doi:[10.1029/2000JC000204](https://doi.org/10.1029/2000JC000204).
- 1479 41. Condron, A., Renfrew, I.A. 2013. The impact of polar mesoscale storms on northeast  
1480 Atlantic Ocean circulation. *Nature Geoscience.* 6(1), pp.34-37.
- 1481 42. Curry, R., Mauritzen, C. 2005. Dilution of the northern North Atlantic Ocean in recent  
1482 decades. *Science.* 308 (5729), 1772-1774. doi: 10.1126/science.1109477
- 1483 43. de Boyer Montégut, C., Madec, G., Fischer, A. S., Lazar, A., Iudicone, D. 2004. Mixed  
1484 layer depth over the global ocean: An examination of profile data and a profile-based  
1485 climatology. *Journal of Geophysical Research: Oceans.* 109, C12003.  
1486 doi:[10.1029/2004JC002378](https://doi.org/10.1029/2004JC002378).
- 1487 44. de Steur L., Hansen E., Gerdes R., Karcher M., Fahrbach E., Holfort J. 2009. Freshwater  
1488 fluxes in the East Greenland Current: A decade of observations. *Geophysical Research Letters.*  
1489 36 (23). L23611. doi: 10.1029/2009GL041278.
- 1490 45. Dee, D. and National Center for Atmospheric Research Staff (Eds). Last modified 11  
1491 Nov 2016. "The Climate Data Guide: ERA-Interim." [https://climatedataguide.ucar.edu/climate-](https://climatedataguide.ucar.edu/climate-data/era-interim)  
1492 [data/era-interim](https://climatedataguide.ucar.edu/climate-data/era-interim).
- 1493 46. Deshayes, J., Curry, R., Msadek, R. 2014. CMIP5 model inter-comparison of freshwater  
1494 budget and circulation in the North Atlantic. *Journal of Climate,* 27 (9), 3298-3317.  
1495 <https://doi.org/10.1175/JCLI-D-12-00700.1>
- 1496 47. Dickson, R.R., Meincke, J., Rhines, P. 2008. Arctic, Sub-arctic Ocean Fluxes: Defining  
1497 the Role of the Northern Seas in Climate. Springer, p. 736.
- 1498 48. Drange, H., Dokken, T., Furevik, T., Gerdes, R., Berger, W., Nesje, A., Østerhus, S.  
1499 2005. The Nordic seas: an overview. *American Geophysical Union.* 1-10.
- 1500 49. Drijfhout, S. 2015. Competition between global warming and an abrupt collapse of the  
1501 AMOC in Earth's energy imbalance. *Scientific reports.* 5, 14877. doi: 10.1038/srep14877
- 1502 50. Dukhovskoy, D. S., Johnson, M. A., Proshutinsky, A. 2004. Arctic decadal variability:  
1503 An auto-oscillatory system of heat and fresh water exchange. *Geophys. Res. Lett.* 31, L03302.  
1504 doi:[10.1029/2003GL019023](https://doi.org/10.1029/2003GL019023).
- 1505 51. Dukhovskoy D.S. et al. 2016. Greenland freshwater pathways in the sub-Arctic Seas  
1506 from model experiments with passive tracers. *J. Geophys. Res. Oceans.* 121. 877–907.  
1507 doi:[10.1002/2015JC011290](https://doi.org/10.1002/2015JC011290)
- 1508 52. Dukhovskoy, D. S., Bourassa, M. A., Petersen, G. N., and Steffen, J. (2017),  
1509 Comparison of the ocean surface vector winds from atmospheric reanalysis and scatterometer-  
1510 based wind products over the Nordic Seas and the northern North Atlantic and their application  
1511 for ocean modeling, *J. Geophys. Res. Oceans,* 122, 1943– 1973, doi:[10.1002/2016JC012453](https://doi.org/10.1002/2016JC012453).
- 1512 53. Dukhovskoy, D. S., Yashayaev, I., Proshutinsky, A., Bamber, J. L., Bashmachnikov, I.  
1513 L., Chassignet, E. P., et al. 2019. Role of Greenland freshwater anomaly in the recent freshening  
1514 of the subpolar North Atlantic. *Journal of Geophysical Research: Oceans.* 124, 3333–3360.  
1515 <https://doi.org/10.1029/2018JC014686>.
- 1516 54. Eldevik, T., Nilsen, J. E. Ø., Iovino, D., Olsson, K. A., Sandø, A. B., Drange, H. 2009.  
1517 Observed sources and variability of Nordic seas overflow. *Nature Geoscience,* 2(6), 406-410.
- 1518 55. Fairall, C. W., Bradley, E. F., Hare, J. E., Grachev, A. A., Edson, J. B., 2003. Bulk  
1519 parameterization of air–sea fluxes: Updates and verification for the COARE algorithm. *Journal*  
1520 *of climate,* 16(4), 571-591.

- 1521 56. Falina, A.S., Sarafanov, A.A. 2015. On the formation of the lower limb of the North  
1522 Atlantic Meridional Overturning Circulation. *Doklady. Earth Sciences*. 461 (2), 427-431. (In  
1523 Russian)
- 1524 57. Falina, A.S., Sarafanov, A.A., Dobrolyubov, S.A., Zapotyilko, V.S., Gladyshev, S.V.  
1525 2017. Convection and water stratification in the North Atlantic ocean according to  
1526 measurements in winter 2013/14. *Vestnik Moskovskogo universiteta. Ser. 5: Geografiya*. 4, 45-  
1527 54. (In Russian)
- 1528 58. Falina, A.S., Sarafanov, A.A., Sokov, A.V., 2007. On the renewal of Labrador Sea water  
1529 in the Irminger basin. *Oceanology*, 47(4), 494-499.
- 1530 59. Ferreira, D., Cessi, P., Coxall, H.K., De Boer, A., Dijkstra, H. A., Drijfhout, S. S., ...,  
1531 Wills, R.C. (2018). Atlantic-Pacific asymmetry in deep water formation. *Annual Review of*  
1532 *Earth and Planetary Sciences*, 46 (1), 327-352
- 1533 60. Fedorov, A.M., Bashmachnikov, I.L, Belonenko, T.V. 2018. Localization of areas of  
1534 deep convection in the Nordic seas, the Labrador Sea and the Irminger Sea. *Vestnik of Saint*  
1535 *Petersburg University. Earth Sciences*. 63 (3), 345–362.  
1536 <https://doi.org/10.21638/spbu07.2018.306>. (In Russian)
- 1537 61. Fedorov, A.M., Bashmachnikov, I.L. 2020. Quality assessments of the deep convection  
1538 intensity for a limited number of in-situ measurements. *Dynamics of Atmospheres and Oceans*  
1539 (submitted)
- 1540 62. Fischer J., Schott F., Visbeck M. 1995 Greenland Sea convection monitoring. In: *The*  
1541 *Nordic Seas*, Hamburg, March 7-9, 1995. p.61-64.
- 1542 63. Frolov, I.E., Gudkovich, Z.M., Karlin, V.P., Kovalev E.G., Smolyanitsky, V.M. 2007.  
1543 Scientific researches in Arctic. Volume 2. Climatic changes in the ice cover of the Eurasian  
1544 shelf seas. Nauka. Saint-Petersburg. pp. 136. (In Russian)
- 1545 64. Furevik, T., Bentsen, M., Drange, H., Johannessen, J. A., Korablev, A. 2002. Temporal  
1546 and spatial variability of the sea surface salinity in the Nordic Seas. *Journal of Geophysical*  
1547 *Research: Oceans*, 107(C12), SRF-10.
- 1548 65. Ghaffari, P., Isachsen, P. E., Nost, O. A., Weber, J. E., 2018. The influence of  
1549 topography on the stability of the Norwegian Atlantic Current off northern Norway. *Journal of*  
1550 *Physical Oceanography*, 48(11), 2761-2777.
- 1551 66. Garzoli, S. L., Matano, R. 2011. The South Atlantic and the Atlantic meridional  
1552 overturning circulation. *Deep Sea Research Part II: Topical Studies in Oceanography*. 58 (17),  
1553 1837-1847. <https://doi.org/10.1016/j.dsr2.2010.10.063>
- 1554 67. Gascard, J. C., Watson, A. J., Messias, M. J., Olsson, K. A., Johannessen, T., Simonsen,  
1555 K. 2002. Long-lived vortices as a mode of deep ventilation in the Greenland Sea. *Nature*. 416  
1556 (6880), 525-527.
- 1557 68. Gelderloos, R., Katsman, C.A., Våge, K. 2013. Detecting Labrador Sea water formation  
1558 from space. *J. Geophys. Res. C: Oceans*. 118 (4), 2074-2086. doi:[10.1002/jgrc.20176](https://doi.org/10.1002/jgrc.20176).
- 1559 69. Gerdes, R., W. Hurlin, and S. M. Griffies (2006), Sensitivity of a global ocean model to  
1560 increased run-off from Greenland, *Ocean Modell.*, 12( 3–4), 416– 435.
- 1561 70. Germe, A., Houssais, M.-N., Herbaut, C., Cassou, C. 2011. Greenland Sea sea-ice  
1562 variability over 1979–2007 and its link to the surface atmosphere. *J. Geophys. Res.* 116,  
1563 C10034. doi:[10.1029/2011JC006960](https://doi.org/10.1029/2011JC006960).
- 1564 71. Giles, K. A., Laxon, S. W., Ridout, A. L., Wingham, D. J., Bacon, S. 2012. Western  
1565 Arctic Ocean freshwater storage increased by wind-driven spin-up of the Beaufort Gyre. *Nature*  
1566 *Geoscience*. 5 (3), 194-197.
- 1567 72. Gladyshev, S. V., Gladyshev, V. S., Falina, A. S., Sarafanov, A. A. 2016. Winter  
1568 convection in the Irminger Sea in 2004–2014. *Oceanology*. 56 (3), 326-335. doi:  
1569 [10.1134/S0001437016030073](https://doi.org/10.1134/S0001437016030073).
- 1570 73. Glessmer, M. S., Eldevik, T., Våge, K., Nilsen, J. E. Ø., Behrens, E. 2014. Atlantic  
1571 origin of observed and modelled freshwater anomalies in the Nordic Seas. *Nature Geoscience*.  
1572 7 (11), 801-805.

- 1573 74. Golubkin, P., Smirnova, J., and Bobylev, L. 2021. Satellite-Derived Spatio-Temporal  
1574 Distribution and Parameters of North Atlantic Polar Lows for 2015–2017. *Atmosphere*, 12(2),  
1575 224. <https://doi.org/10.3390/atmos12020224>.
- 1576 75. GSP Group. 1990. Greenland Sea Project - a venture toward improved understanding of  
1577 the ocean's role in climate. *Eos Trans. AGU*. 71 (24), 750–756. doi:10.1029/90EO00208.
- 1578 76. Gudkovich Z.M., Nikolaeva A.Ya. 1963. Sea ice drift in the Arctic basin and its link to  
1579 ice volume in the Arctic seas of the USSR. *Trudy AARI*. 104, 210. (In Russian)
- 1580 77. Guinehut, S., Dhomps, A.L., Larnicol, G., Le Traon P.-Y. 2012. High resolution 3-D  
1581 temperature and salinity fields derived from in situ and satellite observations. *Ocean Sci.* 8,  
1582 845-857. <https://doi.org/10.5194/os-8-845-2012>.
- 1583 78. Guinehut, S., Le Traon P.-Y., Larnicol, G., Philipps, S. 2004. Combining Argo and  
1584 remote-sensing data to estimate the ocean three-dimensional temperature fields—a first  
1585 approach based on simulated observations *Journal of Marine Systems*. 46 (1–4), 85-98.  
1586 <https://doi.org/10.1016/j.jmarsys.2003.11.022>.
- 1587 79. Gulev S.K., Kattsov V.M., Solomina O.N. Global warming continues. *Herald of the*  
1588 *Russian Academy of Sciences*. 78 (1), 44–50.
- 1589 80. Gulev, S., Jung T., Ruprecht E. 2007a. Estimation of the Impact of Sampling Errors in  
1590 the VOS Observations on Air–Sea Fluxes. Part I: Uncertainties in Climate Means. *J. Climate*.  
1591 20, 279–301. <https://doi.org/10.1175/JCLI4010.1>.
- 1592 81. Gulev, S., Jung T., Ruprecht E. 2007b. Estimation of the Impact of Sampling Errors in  
1593 the VOS Observations on Air–Sea Fluxes. Part II: Impact on Trends and Interannual  
1594 Variability. *J. Climate*. 20, 302–315. <https://doi.org/10.1175/JCLI4008.1>.
- 1595 82. Hakkinen, S., and Rhines, P. B. (2009). Shifting surface currents in the northern North  
1596 Atlantic Ocean. *Journal of Geophysical Research: Oceans*, 114(C4), C04005,  
1597 doi:10.1029/2008JC004883
- 1598 83. Hansen, E., Gerland, S., Granskog, M.A., Pavlova, O., Renner, A.H.H., Haapala, J.,  
1599 Løyning, T.B. and Tschudi, M. 2013. Thinning of Arctic sea ice observed in Fram Strait: 1990–  
1600 2011. *Journal of Geophysical Research: Oceans*. 118 (10), 5202-5221. doi:10.1002/jgrc.20393.
- 1601 84. Hansen B., Osterhus S. 2000. North Atlantic –Nordic Seas Exchanges. *Progress in*  
1602 *Oceanography*, 45, 109-208.
- 1603 85. Hodges, K. I., 1995. Feature tracking on the unit sphere. *Monthly Weather*  
1604 *Review*, 123(12), 3458-3465.
- 1605 86. Hodges, K. I. (1999). Adaptive constraints for feature tracking. *Monthly Weather*  
1606 *Review*, 127(6), 1362-1373.
- 1607 87. Hodges, K. I., Lee, R. W., and Bengtsson, L., 2011. A comparison of extratropical  
1608 cyclones in recent reanalyses ERA-Interim, NASA MERRA, NCEP CFSR, and JRA-25.  
1609 *Journal of Climate*, 24(18), 4888-4906.
- 1610 88. Hoskins, B. J. and Hodges, K. I., 2002. New perspectives on the Northern Hemisphere  
1611 winter storm tracks. *Journal of the Atmospheric Sciences*, 59(6), 1041-1061.
- 1612 89. Herrmann, M., Bouffard, J., Béranger, K. 2009. Monitoring open-ocean deep  
1613 convection from space. *Geophys. Res. Lett.* 36, L03606. doi:10.1029/2008GL036422.
- 1614 90. Jeansson, E., Jutterström, S., Rudels, B., Anderson, L.G., Olsson, K.A., Jones, E.P.,  
1615 Smethie Jr, W.M. and Swift, J.H., 2008. Sources to the East Greenland Current and its  
1616 contribution to the Denmark Strait Overflow. *Progress in Oceanography*, 78(1), 12-28.
- 1617 91. Jochumsen, K., Quadfasel D., Valdimarsson H., Jonsson S. 2012. Variability of the  
1618 Denmark Strait overflow: Moored time series from 1996–2011. *J. Geophys. Res.* 117. C12003.  
1619 doi:10.1029/2012JC008244.
- 1620 92. Johannessen, O.M., Johannessen J.A., Svendsen E., Shuchmann R.A., Campbell W.J.,  
1621 Josberger E. 1987. Ice-Edge Eddies in the Fram Strait Marginal Ice Zone. *Science*. 236, 427 –  
1622 429. doi: 10.1126/science.236.4800.427.

- 1623 93. Johannessen, O. M., Sandven, S., Johannessen, J. A. 1991. Eddy-related winter  
1624 convection in the Boreas Basin. Elsevier Oceanography Series. 57, 87-105.  
1625 [https://doi.org/10.1016/S0422-9894\(08\)70062-X](https://doi.org/10.1016/S0422-9894(08)70062-X).
- 1626 94. Johannessen, O. M., Lygre, K., Eldevik, T. 2005. Convective chimneys and plumes in  
1627 the Northern Greenland Sea. The Nordic Seas: An Integrated Perspective. 251-272. doi:  
1628 10.1029/xxxxgmxx.
- 1629 95. Johannessen, O. M., Korablev, A., Miles, V., Miles, M. W., Solberg, K. E. (2011).  
1630 Interaction between the warm subsurface Atlantic water in the Sermilik Fjord and Helheim  
1631 glacier in southeast Greenland. Surveys in geophysics, 32(4-5), 387-398
- 1632 96. Johannessen, O. M., M. Babiker, M. W. Miles, 2013: Unprecedented retreat in a 50-  
1633 year observational record for Petermann Glacier, North Greenland, Atmos. Oceanic Sci.  
1634 Lett., 6, 259–265, doi:10.3878/j.issn.1674-2834.13.0021
- 1635 97. Johannessen, O.M., S.I. Kuzmina, L.P. Bobylev, M.W. Miles. 2016. Surface air  
1636 temperature variability and trends in the Arctic: new amplification assessment and  
1637 regionalization. Tellus A. 68, 28234. <http://dx.doi.org/10.3402/tellusa.v68.28234>.
- 1638 98. Johnson, H.L., Cessi, P., Marshall, D.P., Schloesser, F., Spall, M.A. 2019. Recent  
1639 contributions of theory to our understanding of the Atlantic Meridional Overturning  
1640 Circulation. Journal of Geophysical Research: Oceans, 124(8), 5376-5399.
- 1641 99. Jones, H., Marshall, J. 1993. Convection with rotation in a neutral ocean: A study of  
1642 open-ocean deep convection. Journal of Physical Oceanography, 23(6), 1009-1039.
- 1643 100. Jonsson, S., 1991. Seasonal and interannual variability of wind stress curl over the  
1644 Nordic Seas. Journal of Geophysical Research: Oceans, 96(C2), pp.2649-2659.
- 1645 101. Jonsson S., Valdimarsson H. 2012. Water mass transport variability to the North  
1646 Icelandic shelf, 1994–2010. ICES Journal of Marine Science. 69 (5), 809–815.  
1647 <https://doi.org/10.1093/icesjms/fss024>.
- 1648 102. Josey S. A., Marsh R. Surface freshwater flux variability and recent freshening of the  
1649 North Atlantic in the eastern subpolar gyre. J. Geophys. Res. 110, C05008.  
1650 doi:10.1029/2004JC002521.
- 1651 103. Kara A.B., Rochford P.A., Hurlburt H.E. 2003. Mixed layer depth variability over the  
1652 global ocean. J. Geophys. Res. 108, 3079. doi:10.1029/2000JC000736, C3.
- 1653 104. Kawasaki, T., Hasumi, H. 2014. Effect of freshwater from the West Greenland Current  
1654 on the winter deep convection in the Labrador Sea. Ocean Modelling. 75, 51-64.  
1655 <https://doi.org/10.1016/j.ocemod.2014.01.003>.
- 1656 105. Khatiwala S., Schlosser P., Visbeck M. 2002. Rates and mechanisms of water mass  
1657 transformation in the Labrador Sea as inferred from tracer observations. Journal of Physical  
1658 Oceanography. 32 (2), 666-686. [https://doi.org/10.1175/1520-0485\(2002\)032<0666:RAMOWM>2.0.CO;2](https://doi.org/10.1175/1520-0485(2002)032<0666:RAMOWM>2.0.CO;2)
- 1659 106. Killworth, P. D. 1983. Deep convection in the world ocean. Reviews of Geophysics. 21  
1660 (1), 1-26.
- 1661 107. Koenigk T., Mikolajewicz U., Haak H., Jungclaus J. 2007. Arctic freshwater export in  
1662 the 20th and 21st centuries. J. Geophys. Res. 112, G04S41. doi:10.1029/2006JG000274.
- 1663 108. Köhl, A., Serra, N. (2014). Causes of decadal changes of the freshwater content in the  
1664 Arctic Ocean. Journal of Climate, 27 (9), 3461-3475. <https://doi.org/10.1175/JCLI-D-13-00389.1>.
- 1665 109. Koszalka I., LaCasce, J.H., Andersson, M., Orvik, K.A., Mauritzen, C., 2011. Surface  
1666 circulation in the Nordic Seas from clustered drifters. Deep-Sea Research I. 58. P. 468-485.  
1667 doi:10.1016/j.dsr.2011.01.007.
- 1668 110. Korablev, A.A., 2001. Water structure and variability of oceanographic parameters in  
1669 the Norwegian and Greenland Seas. PhD thesis, Saint-Petersburg. (In Russian)
- 1670 111. Kovalevsky D.V., 2002. Analysis and modelling of the deep convection in the  
1671 Greenland Sea. PhD thesis, Saint-Petersburg. (In Russian)
- 1672
- 1673

- 1674 112. Kovalevsky D.V., Bashmachnikov I.L., 2019. Nonlinear dynamics of deep open-ocean  
 1675 convection: an analytical approach. In: “Nonlinear Dynamics, Chaos, and Complexity II:  
 1676 memory of Valentin Afraimovich (1945-2018)”, Springer (accepted)
- 1677 113. Kovalevsky D.V., Bashmachnikov, I.L., 2020. An analytical model of open-ocean deep  
 1678 convection with multiple steady states, *Ocean Modelling*, 154, 101680, 1-18, doi:  
 1679 10.1016/j.ocemod.2020.101680
- 1680 114. Kovalevsky D.V., Bashmachnikov, I.L., Alekseev, G.V. 2020. Formation and decay of  
 1681 a deep convective chimney, *Ocean Modelling*, 148, 101583,  
 1682 <https://doi.org/10.1016/j.ocemod.2020.101583>
- 1683 115. Kwok, R., Cunningham, G.F. and Pang, S.S., 2004. Fram Strait sea ice outflow. *Journal*  
 1684 *of Geophysical Research: Oceans*. 109, C01009, doi:10.1029/2003JC001785.
- 1685 116. Langehaug, H.R., Falck, E., 2012. Changes in the properties and distribution of the  
 1686 intermediate and deep waters in the Fram Strait. *Progress in Oceanography*, 96(1), pp.57-76.
- 1687 117. Lappo S. S. 1984. On the mechanisms of the northwards heat advection across the  
 1688 equator in the Atlantic Ocean. *Investigations of the process of ocean-atmosphere interactions*,  
 1689 Moscow, 125-129 (in Russian).
- 1690 118. Larnicol, G., Guinehut, S., Rio, M. H., Drevillon, M., Faugere, Y., Nicolas, G. 2006.  
 1691 The global observed ocean products of the French Mercator project. *Proceedings of the*  
 1692 *Symposium on 15 Years of Progress in Radar Altimetry*, 13–18 March 2006, Venice, Italy.
- 1693 119. Lauvset, S.K., Brakstad, A., Våge, K., Olsen, A., Jeansson, E., Mork, K.A., 2018.  
 1694 Continued warming, salinification and oxygenation of the Greenland Sea gyre. *Tellus A:*  
 1695 *Dynamic Meteorology and Oceanography*, 70(1), pp.1-9.
- 1696 120. Latarius, K., Quadfasel, D. 2016. Water mass transformation in the deep basins of the  
 1697 Nordic Seas: Analyses of heat and freshwater budgets. *Deep Sea Research. Part I:*  
 1698 *Oceanographic Research Papers*. 114, 23-42. <https://doi.org/10.1016/j.dsr.2016.04.012>.
- 1699 121. Lecomte, O., Fichet, T., Vancoppenolle, M., Domine, F., Massonnet, F., Mathiot, P.,  
 1700 ..., Barriat, P. Y. 2013. On the formulation of snow thermal conductivity in large-scale sea ice  
 1701 models. *Journal of Advances in Modeling Earth Systems*, 5(3), 542-557.
- 1702 122. Lenaerts, J. T. M., Bars D. Le, van Kampenhout L., Vizcaino M., Enderlin E. M., van  
 1703 den Broeke M. R. 2015. Representing Greenland ice sheet freshwater fluxes in climate models.  
 1704 *Geophys. Res. Lett.* 42, 6373–6381. doi:10.1002/2015GL064738.
- 1705 123. Levermann, A., Born, A. 2007. Bistability of the Atlantic subpolar gyre in a coarse-  
 1706 resolution climate model, *Geophysical Research Letters*. 34(24). L24605.  
 1707 doi:10.1029/2007GL031732.
- 1708 124. Lien, V. S., Vikebø, F. B., Skagseth, O. (2013). One mechanism contributing to co-  
 1709 variability of the Atlantic inflow branches to the Arctic. *Nature Communications*, 4(1), 1-6.
- 1710 125. Liu, C. H., Wakimoto, R. M., Roux, F. (1997). Observations of mesoscale circulations  
 1711 within extratropical cyclones over the North Atlantic Ocean during ERICA. *Monthly weather*  
 1712 *review*, 125(3), 341-364.
- 1713 126. Lockwood, J. G. 2001. Abrupt and sudden climatic transitions and fluctuations: a  
 1714 review. *International Journal of Climatology*. 21 (9), 1153-1179. doi:10.1002/joc.630.
- 1715 127. Lozier, M.S., Li, F., Bacon, S., Bahr, F., Bower, A.S., Cunningham, S.A., De Jong,  
 1716 M.F., De Steur, L., Deyoung, B., Fischer, J. and Gary, S.F., 2019. A sea change in our view of  
 1717 overturning in the subpolar North Atlantic. *Science*, 363(6426),516-521.
- 1718 128. Lumpkin, R., Speer, K. 2007. Global ocean meridional overturning. *J. Phys. Oceanogr.*  
 1719 37 (10), 2550–2562. <https://doi.org/10.1175/JPO3130.1>
- 1720 129. Luo, H., Castelao, R. M., Rennermalm, A. K., Tedesco, M., Bracco, A., Yager, P. L.,  
 1721 Mote, T. L. 2016. Oceanic transport of surface meltwater from the southern Greenland ice sheet.  
 1722 *Nature Geoscience*. 9, 528–532.
- 1723 130. Malmberg, S.-A. 1983. Hydrographic investigations in the Iceland and Greenland Seas  
 1724 in late winter 1971 - "Deep Water Project", *J6kull*. 33, 133-140.



- 1725 131. Malmberg, S.A., Jonsson, S., 1997. Timing of deep convection in the Greenland and  
1726 Iceland Seas. *ICES Journal of Marine Science*, 54(3), pp.300-309.
- 1727 132. Marnela, M., Rudels, B., Houssais, M.N., Beszczynska-Möller, A., Eriksson, P.B.,  
1728 2013. Recirculation in the Fram Strait and transports of water in and north of the Fram Strait  
1729 derived from CTD data. *Ocean Science*. 9, 499–519. doi:10.5194/os-9-499-2013.
- 1730 133. Marshall, J., Schott, F. 1999. Open-ocean convection: Observations, theory, and models.  
1731 *Reviews of Geophysics*, 37 (1), 1-64. <https://doi.org/10.1029/98RG02739>.
- 1732 134. Maslowski, W., Kinney, J.C., Jakacki, J. 2008. On the importance of freshwater fluxes  
1733 from the Arctic Ocean into the North Atlantic: the Nordic Seas versus Canadian Arctic  
1734 Archipelago. Poster.
- 1735 135. Meincke, J., Jonsson, S., Swift, J. H. 1992. Variability of convective conditions in the  
1736 Greenland Sea. *ICES Mar. Sci. Symp.*195, 32–39.
- 1737 136. Meincke, J., Rudels, B., Friedrich, H.J., 1997. The Arctic Ocean–Nordic Seas  
1738 thermohaline system. *ICES Journal of Marine Science*, 54(3), pp.283-299.
- 1739 137. Mironov E.U., Sea-ice conditions in the Greenland and Barents seas and their long-term  
1740 predictions, 2004, St.Petersburg, AARI, 1-320 (In Russian).
- 1741 138. Moore, G. W. K., Våge, K., Pickart, R. S., Renfrew, I. A. 2015. Decreasing intensity of  
1742 open-ocean convection in the Greenland and Iceland seas. *Nature Climate Change*. 5, 877–882.
- 1743 139. Moretsky V.N., Popov A.V. 1989. Water masses of the Norwegian and the Greenland  
1744 seas and the principle types of vertical water structure in the region. Structure and variability of  
1745 largescale processes in the Norwegian zone of intensive ocean-atmosphere interactions (eds.  
1746 Nikolayev, Yu.V., Alekseev, G.V.). Hydrometeoizdat., Leningrad. 18-27. (In Russian)
- 1747 140. Mulet, S., Rio, M.H., Mignot, A., Guinehut, S., Morrow, R., 2012. A new estimate of  
1748 the global 3D geostrophic ocean circulation based on satellite data and in-situ measurements.  
1749 *Deep Sea Research II*, 77, 70-81.
- 1750 141. Muller, F. L., Wekerle, C., Dettmering, D., Passaro, M., Bosch, W., Seitz, F. (2019).  
1751 Dynamic ocean topography of the northern Nordic seas: a comparison between satellite  
1752 altimetry and ocean modelling. *The Cryosphere*, 13 (2).
- 1753 142. Myers P. G., Josey S. A., Wheler B., Kulan N. 2007. Interdecadal variability in Labrador  
1754 Sea precipitation minus evaporation and salinity. *Progress in Oceanography*. 73 (3-4), 341-357.  
1755 <https://doi.org/10.1016/j.pocean.2006.06.003>
- 1756 143. Mysak, L. A., Manak, D. K., Marsden, R. F. 1990. Sea ice anomalies observed in the  
1757 Greenland and Labrador Seas during 1901–1984 and their relation to an interdecadal Arctic  
1758 climate cycle. *Climate Dynamics*. 5 (2), 111-133.
- 1759 144. Nagurny. A. P. Popov, A. V. 1985. Intensive upwelling of deep and bottom waters and  
1760 their formation at the surface in the region of the Greenland Hollow. *Meteorologiyai*  
1761 *Gidrologiya*. 7, 71-75. (In Russian)
- 1762 145. Nansen F. 1912. Das Bodenwasser und die Abkühlung des Meeres. *Int. Rev. Hydrobiol.*  
1763 5, 1–42.
- 1764 146. Nikolayev, Yu.V., Alekseev, G.V. (eds.) 1989. Structure and variability of largescale  
1765 processes in the Norwegian zone of intensive ocean-atmosphere interactions.  
1766 Hydrometeoizdat., Leningrad. pp.124. (In Russian)
- 1767 147. Nurser, A.J.G., Bacon, S., 2014. The Rossby radius in the Arctic Ocean. *Ocean Science*,  
1768 10(6), pp.967-975.
- 1769 148. Paluszkiwicz, T., Romea, R. D. 1997. A one-dimensional model for the  
1770 parameterization of deep convection in the ocean. *Dynamics of Atmospheres and Oceans*,  
1771 26(2), 95–130. [https://doi.org/10.1016/S0377-0265\(96\)00482-4](https://doi.org/10.1016/S0377-0265(96)00482-4)
- 1772 149. Peterson B. J., McClell J., Curry R., Holmes R. M., Walsh J. E., Aagaard K. 2006.  
1773 Trajectory shifts in the Arctic and subarctic freshwater cycle. *Science*. 313 (5790), 1061-1066.  
1774 doi: 10.1126/science.1122593.
- 1775 150. Piechura, J., Walczowski, W. (2009). Warming of the West Spitsbergen Current and sea  
1776 ice north of Svalbard. *Oceanologia*, 51(2), 147–164. <https://doi.org/10.5697/oc.51-2.147>

- 1777 151. Pickart, R.S., Torres, D.J., Clarke, R.A. 2002. Hydrography of the Labrador Sea during  
1778 active convection. *J. Phys. Oceanogr.* 32, 428–457. [https://doi.org/10.1175/1520-](https://doi.org/10.1175/1520-0485(2002)032<0428:HOTLSD>2.0.CO;2)  
1779 0485(2002)032<0428:HOTLSD>2.0.CO;2
- 1780 152. Proshutinsky, A., Dukhovskoy, D., Timmermans, M. L., Krishfield, R., Bamber, J. L.  
1781 2015. Arctic circulation regimes. *Phil. Trans. R. Soc. A.* 373 (2015),  
1782 20140160. <https://doi.org/10.1098/rsta.2014.0160>
- 1783 153. Rabe, B., Dodd, P. A., Hansen, E., Falck, E., Schauer, U., Mackensen, A., ... Cox, K.  
1784 2013. Liquid export of Arctic freshwater components through the Fram Strait 1998–2011.  
1785 *Ocean Science.* 9 (1), 91-109. doi:10.5194/os-9-91-2013
- 1786 154. Rahmstorf, S., Box, J. E., Feulner, G., Mann, M. E., Robinson, A., Rutherford, S.,  
1787 Schaffernicht, E. J. 2015. Exceptional twentieth-century slowdown in Atlantic Ocean  
1788 overturning circulation. *Nat. Clim. Change.* 5(5), 475–480. doi:10.1038/nclimate2554.
- 1789 155. Raj, R. P., Nilsen, J. Ø., Johannessen, J. A., Furevik, T., Andersen, O. B., Bertino, L.  
1790 (2018). Quantifying Atlantic Water transport to the Nordic Seas by remote sensing. *Remote*  
1791 *Sensing of Environment,* 216, 758-769.
- 1792 156. Rasmussen, E., Turner, J. 2003. *Polar Lows: Mesoscale Weather Systems in the Polar*  
1793 *Regions.* Cambridge University Press. 612 pp.
- 1794 157. Renold, M., Raible, C. C., Yoshimori, M., and Stocker, T. F. 2010. Simulated  
1795 resumption of the North Atlantic meridional overturning circulation—Slow basin-wide  
1796 advection and abrupt local convection. *Quaternary Science Reviews,* 29(1-2), 101-112.
- 1797 158. Rhein, M. 1996. Convection in the Greenland Sea, 1982–1993. *Journal of Geophysical*  
1798 *Research: Oceans.* 101 (C8), 18183-18192. doi:10.1029/96JC01295.
- 1799 159. Rhein, M., Kieke, D., Hüttl-Kabus, S., Roessler, A., Mertens, C., Meissner, R., ...  
1800 Yashayaev, I. 2011. Deep water formation, the subpolar gyre, and the meridional overturning  
1801 circulation in the subpolar North Atlantic. *Deep Sea Research Part II: Topical Studies in*  
1802 *Oceanography,* 58 (17), 1819-1832. <https://doi.org/10.1016/j.dsr2.2010.10.061>.
- 1803 160. Ricker, R., Girard-Arduin, F., Krumpfen, T. and Lique, C. (2018). Satellite-derived sea  
1804 ice export and its impact on Arctic ice mass balance. *The Cryosphere,* 12(9), pp.3017-3032.
- 1805 161. Ronski S., Budeus G., 2005. Time series of winter convection in the Greenland Sea,  
1806 *Journal of Geophysical Research: Oceans,* 110, C04015, doi:10.1029/2004JC002318.
- 1807 162. Rosmorduc, V., Hernandez, F. 2003. Two altimetric satellites minimum are needed for  
1808 ocean observation and forecasting. *AVISO Newsletter.* 9, 12-14.
- 1809 163. Rossby, T., Ozhigin, V., Ivshin, V. and Bacon, S., 2009. An isopycnal view of the  
1810 Nordic Seas hydrography with focus on properties of the Lofoten Basin. *Deep Sea Research*  
1811 *Part I: Oceanographic Research Papers,* 56(11), pp.1955-1971.
- 1812 164. Rudels, B., Fahrbach, E., Meincke, J., Budéus, G. and Eriksson, P., 2002. The East  
1813 Greenland Current and its contribution to the Denmark Strait overflow. *ICES Journal of Marine*  
1814 *Science,* 59(6), pp.1133-1154.
- 1815 165. Rudeva, I., Gulev, S. K. (2011). Composite analysis of North Atlantic extratropical  
1816 cyclones in NCEP–NCAR reanalysis data. *Monthly weather review,* 139(5), 1419-1446.
- 1817 166. Saberi A., Haine T. W., Gelderloos R., Femke de Jong M., Furey H., Bower A. 2020.  
1818 Lagrangian Perspective on the Origins of Denmark Strait Overflow. *Journal of Physical*  
1819 *Oceanography,* 50(8), 2393-2414
- 1820 167. Schauer, U., Beszczynska-Möller, A., Walczowski, W., Fahrbach, E., Piechura, J.,  
1821 Hansen, E., 2008. Variation of measured heat flow through the Fram Strait between 1997–2006.  
1822 In: Dickson, R.R., Meincke, J., Rhines, P. (Eds.), *Arctic–Subarctic Ocean Fluxes.* Springer,  
1823 Dordrecht, pp. 65–85.
- 1824 168. Schlosser, P., Bonisch, G., Rhein, M., Bayer, R. 1991. Reduction of deep water  
1825 formation in the Greenland Sea during the 1980s: Evidence from tracer data. *Science.* 251  
1826 (4997), 1054-1056.

- 1827 169. Schweiger, A., Lindsay, R., Zhang, J., Steele, M., Stern, H., and Kwok, R. 2011.  
 1828 Uncertainty in modeled Arctic sea ice volume. *J. Geophys. Res.* 116, C00D06.  
 1829 doi:10.1029/2011JC007084.
- 1830 170. Selivanova, Yu.V., Tilinina, N. D., Gulev, S. K., Dobrolubov, S. A. 2016. An Impact  
 1831 of Sea Ice Cover on the Ocean–Atmosphere Turbulent Heat Fluxes in the Arctic.  
 1832 *Okeanologiya*. 56 (1), 18–22. doi: 10.7868/S0030157416010184. (In Russian)
- 1833 171. Selyuzhenok, V., Bashmachnikov, I, Ricker, R., Vesman, A., Bobylev, L., 2020. Sea  
 1834 ice volume variability and water temperature in the Greenland Sea. *The Cryosphere*, 14, 1–19,  
 1835 <https://doi.org/10.5194/tc-14-477-2020>
- 1836 172. Serreze, M. C., Barrett, A. P., Slater, A. G., Woodgate, R. A., Aagaard, K., Lammers,  
 1837 R. B., ... Lee, C. M. 2006. The large-scale freshwater cycle of the Arctic. *Journal of Geophysical*  
 1838 *Research: Oceans*. 111, C11010. doi:10.1029/2005JC003424.
- 1839 173. Smirnova, J.E., Golubkin, P.A., Bobylev, L.P., Zabolotskikh, E.V., Chapron, B.. 2015.  
 1840 Polar low climatology over the Nordic and Barents seas based on satellite passive microwave  
 1841 data. *Geophysical Research Letters*. 42(13), pp.5603-5609.
- 1842 174. Smirnova, J., Golubkin, P. 2017. Comparing polar lows in atmospheric reanalyses:  
 1843 Arctic System Reanalysis versus ERA-Interim. *Monthly Weather Review*. 145(6), pp.2375-  
 1844 2383.
- 1845 175. Somavilla, R. 2019. Draining and upwelling of Greenland Sea deep waters. *Journal of*  
 1846 *Geophysical Research: Oceans*, 124, 2842– 2860. <https://doi.org/10.1029/2018JC014249>
- 1847 176. Srokosz, M., Baringer, M., Bryden, H., Cunningham, S., Delworth, T., Lozier, S., ...,  
 1848 Sutton, R. (2012). Past, present, and future changes in the Atlantic meridional overturning  
 1849 circulation. *Bulletin of the American Meteorological Society*, 93(11), 1663-1676.
- 1850 177. Shalina, E. V., & Sandven, S. (2018). Snow depth on Arctic sea ice from historical in  
 1851 situ data. *The Cryosphere*, 12(6), 1867-1886.
- 1852 178. Stommel, H. 1958. The abyssal circulation. *Deep Sea Research*, 5, 80–82.
- 1853 179. Swingedouw, D., Rodehacke, C.B., Olsen, S.M., Menary, M., Gao, Y., Mikolajewicz,  
 1854 U., Mignot, J., 2014. Impact of Greenland ice sheet melting on the Atlantic overturning: A  
 1855 multi-model assessment. *Climate Dynamics*. 44 (11–12), 3261–3279. doi 10.1007/s00382-014-  
 1856 2270-x
- 1857 180. Thomson, R.E., Emery, W.J. 2014. *Data analysis methods in physical oceanography*.  
 1858 Third edition, Elsevier, Amsterdam, 1-716.
- 1859 181. Tilinina, N.D., Gulev, S.K. and Gavrikov, A.V., 2016. Formation of extreme surface  
 1860 turbulent heat fluxes from the ocean to the atmosphere in the North Atlantic. *Oceanology*,  
 1861 56(1),1-5.
- 1862 182. Timmermann, R., Beckmann, A. 2004. Parameterization of vertical mixing in the  
 1863 Weddell Sea. *Ocean Modelling*, 6(1), 83–100. [https://doi.org/10.1016/S1463-5003\(02\)00061-6](https://doi.org/10.1016/S1463-5003(02)00061-6)
- 1864 6
- 1865 183. Trodahl, M. Isachsen, P.E. 2018. Topographic Influence on Baroclinic Instability and  
 1866 the Mesoscale Eddy Field in the Northern North Atlantic Ocean and the Nordic Seas. *J. Phys.*  
 1867 *Oceanogr.* 48, 2593–2607. <https://doi.org/10.1175/JPO-D-17-0220.1>.
- 1868 184. Våge, K., Pickart, R. S., Spall, M. A., Moore, G. W. K., Valdimarsson, H., Torres, D.  
 1869 J., ..., Nilsen, J. E. Ø. 2013. Revised circulation scheme north of the Denmark Strait. *Deep Sea*  
 1870 *Research Part I: Oceanographic Research Papers*, 79, 20-39.
- 1871 185. Våge, K., Papritz, L., Håvik, L., Spall, M.A. and Moore, G.W.K., 2018. Ocean  
 1872 convection linked to the recent ice edge retreat along east Greenland. *Nature communications*,  
 1873 9(1), p.1287
- 1874 186. Walczowski, W. 2014. Atlantic Water in the Nordic Seas: Properties, Variability,  
 1875 Climatic Importance, *GeoPlanet Earth Planet. Sci.*, 13, doi:10.1007/978-3-319-01279-7.
- 1876 187. Verbrugge, N., Mulet, S., Guinehut, S., 2017. Quality Information Document for Global  
 1877 Ocean Observation-based Products, GLOBAL\_ANALYSIS\_PHYS\_001\_020.

- 1878 188. Vesman, A. V., Bashmachnikov, I. L., Golubkin, P. A., Raj, R. P. 2020. The coherence  
1879 of the oceanic heat transport through the Nordic seas: oceanic heat budget and interannual  
1880 variability. *Ocean Science Discussions*, 1-24.
- 1881 189. Vessey, A.F., Hodges, K.I., Shaffrey, L.C., Day, J.J. 2020. An inter-comparison of  
1882 Arctic synoptic scale storms between four global reanalysis datasets. *Climate Dynamics*. 54,  
1883 2777–2795.
- 1884 190. Vinje T., Finnekasa O. 1986. The ice transport through the Fram strait. *Norsk*  
1885 *Polarinstitutt*, Oslo. 186 (40).
- 1886 191. Visbeck, M., Marshall, J., Jones, H. 1996. Dynamics of Isolated Convective Regions in  
1887 the Ocean. *Journal of Physical Oceanography*, 26, 1721–1734.  
1888 [https://journals.ametsoc.org/view/journals/phoc/26/9/1520-](https://journals.ametsoc.org/view/journals/phoc/26/9/1520-0485_1996_026_1721_doicri_2_0_co_2.xml)  
1889 [0485\\_1996\\_026\\_1721\\_doicri\\_2\\_0\\_co\\_2.xml](https://journals.ametsoc.org/view/journals/phoc/26/9/1520-0485_1996_026_1721_doicri_2_0_co_2.xml)
- 1890 192. Volkov, D.L., Meinen, C. S., Schmid, C., Moat, B., Lankhorst, M., Dong, S., ..., Goni,  
1891 G. 2020. Atlantic meridional overturning circulation and associated heat transport. In: Blunden,  
1892 J.; Arndt, D. S., (eds.) *State of the climate in 2019*. *Bulletin of the American Meteorological*  
1893 *Society*, 101(8), 159-163, doi: 10.1175/BAMS-D-20-0105.1
- 1894 193. von Appen, W. J., Wekerle, C., Hehemann, L., Schourup-Kristensen, V., Konrad, C.,  
1895 Iversen, M. H. (2018). Observations of a submesoscale cyclonic filament in the marginal ice  
1896 zone. *Geophysical Research Letters*, 45(12), 6141-6149.
- 1897 194. Wadhams, P., Budéus, G., Wilkinson, J. P., Løyning, T., Pavlov, V. (2004). The multi-  
1898 year development of long-lived convective chimneys in the Greenland Sea. *Geophysical*  
1899 *research letters*, 31(6), L06306, doi:10.1029/2003GL019017.
- 1900 195. Whitehead J.A. (2000): Stratified convection with multiple states. *Ocean Modelling*, 2,  
1901 109-121.
- 1902 196. Yang, Q., Dixon, T. H., Myers, P. G., Bonin, J., Chambers, D., Van Den Broeke, M. R.  
1903 2016. Recent increases in Arctic freshwater flux affects Labrador Sea convection and Atlantic  
1904 overturning circulation. *Nature communications*, 7, 10525.
- 1905 197. Yashayaev, I. 2007. Hydrographic changes in the Labrador Sea, 1960–2005. *Prog.*  
1906 *Oceanogr.* 73, 242–276. <https://doi.org/10.1016/j.pocean.2007.04.015>.
- 1907 198. Yashayaev I., 2011. Deep water formation, the subpolar gyre, and the meridional  
1908 overturning circulation in the subpolar North Atlantic, *Deep Sea Res. Part II*, 58 (17), 1819-  
1909 1832
- 1910 199. Yashayaev, I., Seidov, D., 2015. The role of the Atlantic Water in multidecadal ocean  
1911 variability in the Nordic and Barents Seas. *Progress in oceanography*, 132, pp.68-127.
- 1912 200. Zhang J. L. Rothrock D. A. 2003. Modeling global sea ice with a thickness and enthalpy  
1913 distribution model in generalized curvilinear coordinates. *Monthly Weather Review*, 131, 845-  
1914 861, [https://journals.ametsoc.org/view/journals/mwre/131/5/1520-](https://journals.ametsoc.org/view/journals/mwre/131/5/1520-0493_2003_131_0845_mgsiwa_2.0.co_2.xml)  
1915 [0493\\_2003\\_131\\_0845\\_mgsiwa\\_2.0.co\\_2.xml](https://journals.ametsoc.org/view/journals/mwre/131/5/1520-0493_2003_131_0845_mgsiwa_2.0.co_2.xml) .
- 1916 201. Zolina, O., Gulev, S.K. 2003. Synoptic variability of ocean-atmosphere turbulent fluxes  
1917 associated with atmospheric cyclones. *Journal of climate*. 16, 2717-2734.  
1918 [https://journals.ametsoc.org/view/journals/clim/16/16/1520-](https://journals.ametsoc.org/view/journals/clim/16/16/1520-0442_2003_016_2717_svoof_2.0.co_2.xml)  
1919 [0442\\_2003\\_016\\_2717\\_svoof\\_2.0.co\\_2.xml](https://journals.ametsoc.org/view/journals/clim/16/16/1520-0442_2003_016_2717_svoof_2.0.co_2.xml).
- 1920 202. Zhang, J., Rothrock, D. A. 2003. Modelling global sea ice with a thickness and enthalpy  
1921 distribution model in generalized curvilinear coordinates. *Monthly Weather Review*, 131 (5),  
1922 845-861.
- 1923 203. Zhang, J., Steele, M., Rothrock, D. A., Lindsay, R. W. (2004). Increasing exchanges at  
1924 Greenland-Scotland Ridge and their links with the North Atlantic Oscillation and Arctic sea  
1925 ice. *Geophysical Research Letters*, 31(9), 1-5, doi: 10.1029/2003GL019304.